DISCRIMINATING CLEAR-SKY FROM CLOUD WITH MODIS

ALGORITHM THEORETICAL BASIS DOCUMENT (MOD35)

MODIS Cloud Mask Team

Steve Ackerman[1], Kathleen Strabala[1], Paul Menzel[1,2], Richard Frey[1], Chris Moeller[1], Liam Gumley[1], Bryan Baum[3], Crystal Schaaf[4], George Riggs[5]

[1]Cooperative Institute for Meteorological Satellite Studies, University of Wisconsin - Madison

[2]NOAA/NESDIS

[3]NASA/LaRC, Hampton, VA

[4]Phillips Lab/GPAB, Hascom Air Force

[5]Research and Data Systems Corporation, Greenbelt, MD

Version 3.2

November 1997

TABLE OF CONTENTS

1.0 Introduction

Clouds are generally characterized by higher reflectance and lower temperature than the underlying earth surface. As such, simple visible and infrared window threshold approaches offer considerable skill in cloud detection. However, there are many surface conditions when this characterization of clouds is inappropriate, most notably over snow and ice. Additionally, some cloud types such as thin cirrus, low stratus at night, and small cumulus are difficult to detect because of insufficient contrast with the surface radiance. Cloud edges cause further difficulty since the instrument field of view will not always be completely cloudy or clear.

The 36 channel Moderate Resolution Imaging Spectroradiometer (MODIS) offers the opportunity for multispectral approaches to cloud detection so that many of these concerns can be mitigated; additionally, spatial and temporal uniformity tests offer confirmation of cloudy or clear-sky conditions. This document describes the approach and algorithms for detecting clouds using MODIS observations. The algorithms have been drafted in close collaboration with members of the CERES Science Team. Section 2 gives an overview of the masking approach. The MODIS cloud screening approach includes new spectral techniques and incorporates many of the existing techniques to detect obstructed fields of view. The individual spectral tests are discussed in Section 3. Examples of how to interpret the cloud mask output are included in Section 4 along with validation plans. Appendix A includes an example FORTRAN code for reading the cloud mask.

2.0 Overview

2.1 Objective

The MODIS cloud mask will indicate whether a given view of the earth surface is unobstructed by clouds or optically thick aerosol, and whether that clear scene is contaminated by a shadow. The cloud mask will be generated at 250 and 1000 meter resolutions. Input to the cloud mask algorithm is assumed to be calibrated and navigated level 1B radiance data. Additionally, the MODIS data are assumed to meet instrument specifications so that no accommodation for

striping or poor navigation is required. The cloud mask will be determined for good data only (i.e., fields of view where data inMODIS bands 1, 2, 4, 5, 6, 7, 18, 19, 20, 22, 23, 26, 27, 29, 31, 32, and 35 have radiometric integrity). Incomplete or bad radiometric data will create holes in the cloud mask.

Several points need to be made regarding the approach to the MODIS cloud mask presented in this Algorithm Theoretical Basis Document (ATBD).

(1) The cloud mask is not the final cloud product from MODIS; several Principal Investigators have the responsibility to deliver algorithms for various additional cloud parameters, such as phase and altitude.

(2) The cloud mask ATBD assumes that calibrated, quality controlled data are the input and a cloud mask is the output. The overall template for the MODIS data processing must be planned at the project level as must the coordination of the cloud mask with the activities that will be producing calibrated level 1B data.

The snow/ice bit in the cloud mask output indicates a processing path in the current algorithm and should not be considered the final indicator of this product. This is the first step in distinguishing cloud from snow. In certain heavy aerosol loading situations (e.g., dust storms, volcanic eruptions and forest fires) particular tests may flag the aerosol laden atmosphere as cloudy. An aerosol bit has been included in the mask to indicate fields of view that are potentially contaminated with optically thick aerosol.

In the cloud mask algorithm for MODIS, there are operational constraints to consider. These constraints are driven by the need to process MODIS data in a timely fashion.

- CPU Constraint: Many algorithms must first determine if the pixel is cloudy or clear. A single cloud mask for MODIS exists to avoid duplication in the many MODIS algorithms. Thus, the cloud mask algorithm lies at the top of the data processing chain and must be versatile enough to satisfy the needs of many applications. The clear-sky determination algorithm must run in real time, limiting the use of CPU-intensive algorithms.
- Output File Size Constraint: Storage requirements are also a concern. The current cloud

mask is more than a yes/no decision The 48 bits of the mask include an indication of the likelihood that the pixel is contaminated with cloud It also includes ancillary information regarding the processing path and the results from individual tests and other useful information (e.g., thin cirrus flag). In processing applications, one need not access all the bits of the mask. An algorithm can make use of only the first 8 bits of the mask if that is appropriate The current 48 bit cloud mask requires 4.8 gigabytes of storage per day. This estimate does not include the cloud mask metadata.

- Comprehension: Because there are many users of the cloud mask, it is important that the mask not only provide enough information to be widely used but also that it be easily understood. To intelligently interpret the output from this algorithm, it is important to have the algorithm simple in concept but effective in its application.

Our approach to the MODIS cloud mask is for each pixel to provide a confidence flag that indicates how certain we are that the pixel is clear The cloud masking algorithm must operate under the following restrictions: near-real time execution, limited computer storage, and simplicity so that many users can follow the algorithm path.

2.2 Background

Development of the MODIS cloud mask algorithm benefits from previous work to characterize global cloud cover using satellite observations The International Satellite Cloud Climatology Project (ISCCP) has developed cloud detection schemes using visible and infrared window radiances. The AVHRR (Advanced Very High Resolution Radiometer) Processing scheme Over cLoud Land and Ocean (APOLLO) cloud detection algorithm uses the five visible and infrared channels of the AVHRR The NOAA Cloud Advanced Very High Resolution Radiometer (CLAVR) also uses a series of spectral and spatial variability tests to detect a cloud CO_2 slicing characterizes global high cloud cover, including thin cirrus, using infrared radiances in the carbon dioxide sensitive portion of the spectrum Additionally, spatial coherence of infrared radiances in cloudy and clear skies has been used successfully in regional cloud studies The following para-

graphs briefly summarize some of these prior approaches to cloud detection.

The ISCCP cloud masking algorithm is described by Rossow (1989), Rossow*et al.* (1989), Sèze and Rossow (1991a) and Rossow and Garder (1993). Only two channels are used in cloud detection, the narrowband visible (0.6 μm) and the infrared window (11 μm). Each observed radiance value is compared with its corresponding clear-sky composite value Clouds are detected only when they alter the radiances by more than the uncertainty in the clear values In this way the "threshold" for cloud detection is the magnitude of the uncertainty in the clear radiance estimates.

The ISCCP algorithm is based on the premise that the observed visible and infrared radiances are caused by only two types of conditions, *cloudy* and *clear*, and that the ranges of radiances and their variability associated with these two conditions do not overlap (Rossow and Garder 1993) As a result, the algorithm is based upon thresholds; a pixel is classified as cloudy only if at least one radiance value is distinct from the inferred clear value by an amount larger than the uncertainty in that clear threshold value The uncertainty can be caused both by measurement errors and by natural variability This algorithm is constructed to be cloud-conservative, minimizing false cloud detections but missing clouds that resemble clear conditions.

The ISCCP cloud-detection algorithm consists of five steps (Rossow and Garder 1993): (1) space contrast test on a single infrared image; (2) time contrast test on three consecutive infrared images at constant diurnal phase; (3) cumulation of space/time statistics for infrared and visible images; (4) construction of clear-sky composites for infrared and visible every 5 days at each diurnal phase and location; and (5) radiance threshold for infrared and visible for each pixel.

APOLLO is discussed in detail by Saunders and Kriebel (1988), Kriebel*et al.* (1989) and Gesell (1989). The scheme uses AVHRR channels 1 through 5 at full spatial resolution, nominally 1.1 km at nadir. The 5 spectral bandpasses are approximately 0.58-0.68 μm, 0.72-1.10 μm, 3.55-3.93 μm, 10.3-11.3 μm, and 11.5-12.5 μm. The technique is based on 5 threshold tests. A pixel is called cloudy if it is brighter or colder than a threshold, if the reflectance ratio of channels 2 to 1 is between 0.7 and 1.1, if the temperature difference between channel 4 and 5 is above a

threshold, and if the spatial uniformity over ocean is greater than athreshold (Kriebel and Saunders 1988). These tests distinguish between cloud free and cloudy pixels A pixel is defined as cloud free if the multispectral data have values below the threshold for each test The pixel is defined as cloud contaminated if it fails any single test, thus it is cloud conservative Two of those tests are then used with different thresholds to identify fully cloudy pixels from the cloud contaminated ones.

The NOAA CLAVR algorithm (Phase I) uses all five channels of AVHRR to derive a global cloud mask (Stowe *et al.* 1991). It examines multispectral information, channel differences, and spatial differences and then employs a series of sequential decision tree tests Cloud free, mixed (variable cloudy), and cloudy regions are identified for 2x2 global area coverage (GAC) pixel (4 km resolution) arrays. If all four pixels in the array fail all the cloud tests, then the array is labeled as cloud-free (0% cloudy). If all four pixels satisfy just one of the cloud tests, then the array is labeled as 100% cloudy. If 1 to 3 pixels satisfy a cloud test, then the array is labeled as mixed and assigned an arbitrary value of 50% cloudy. If all four pixels of a mixed or cloudy array satisfy a clear-restorer test (required for snow or ice, ocean specular reflection, and bright desert surfaces) then the pixel array is re-classified as"restored-clear" (0% cloudy). The set of cloud tests is subdivided into daytime ocean scenes, daytime land scenes, nighttime ocean scenes and nighttime land scenes.

Subsequent phases of CLAVR use dynamic thresholds predicted from the angular pattern observed from the clear-sky radiance statistics of the previous 9-day repeat cycle of the NOAA satellite for a mapped one degree equal area grid cell (Stowe *et al.* 1994). As a further modification, CLAVR will include pixel by pixel classification based upon different threshold tests to separate clear from cloud contaminated pixels and to separate cloud contaminated pixels into partial and overcast cover. Cloud contaminated pixels are radiatively"typed" as belonging to low stratus, thin cirrus, and deep convective cloud systems A fourth type indicates all other clouds, including mixed level clouds.

CO_2 slicing (Wylie *et al.* 1994) has been used to distinguish transmissive clouds from opaque

clouds and clear-sky using High resolution Infrared Radiation Sounder (HIRS) multispectral observations. With radiances around the broad CO_2 absorption band at 15 μm, clouds at various levels of the atmosphere can be detected. Radiances from near the center of the absorption band are sensitive to only upper levels while radiances from the wings of the band (away from the band center) see successively lower levels of the atmosphere. The CO_2 slicing algorithm determines both cloud level and effective cloud amount from radiative transfer principles. It is especially effective for detecting thin cirrus clouds that are often missed by simple infrared window and visible approaches. Difficulties arise when the clear minus cloudy radiance for a spectral band is less than the instrument noise.

Many algorithms have also been developed for cloud clearing of the TIROS-N Operational Vertical Sounder (TOVS). For example, the fifth version of the International TOVS Processing Package (ITPP-5), uses collocated AVHRR and HIRS/2 to cloud clear the HIRS/2 fooprints. A 3×3 retrieval box of collocated AVHRR and HIRS/2 are used to determine the warm, overall and cold scenes. A scene, or HIRS/2 field of view, is classified as cloudy if any of the following conditions are meet:

(1) The average AVHRR $BT_{3.7}$ or the warm signal exceeds the average AVHRR BT_{11} warm signal;

(2) The skin temperature as derived fom the AVHRR is more than 10°C colder than the initial guess surface temperature;

(3) The average albedo for the warm HIRS/2 footprint in either of the AVHRR solar channels is greater than 25% (day tests);

(4) The albedo in the HIRS visible channel (channel 20) is larger than 25% (day test);

(5) The average AVHRR $BT_{3.7}$ for the warm scene is more than 4°C warmer than the skin temperature as derived by the AVHRR (night test);

(6) The average HIRS/2 $BT_{3.7}$ for the warm scene is more than 4°C warmer than the skin temperature as derived by the HIRS/2 (night test); or

(7) Skin temperatures derived from the AVHRRR and HIRS/2 differ by more than 2°C.

If a HIRS/2 footprint is determined to be cloudy, further tests are executed to determine the nature of the cloud cover. Other TOVS cloud clearing approaches (Rizzi *et al.* 1994) are based on the N* approach developed by Smith (1968).

Operational GOES products by NESDIS also require cloud detection and are referred to as "cloud clearing." In this application, an array of $n \times n$ contiguous pixels is categorized as either *clear*, *cloudy* or *unusable*. The *clear* arrays are subcategoized as *truly clear* and *clear/cloudy*. In an approach similar to the ITPP-5 method, clear conditions are determined based on brightness thresholds, difference thresholds, and comparison of observations with first guess profiles.

The above algorithms are noted as they have been incorporated into current global cloud climatologies and have been run in an operational mode over long time periods, and thus faced some of the constraints of the MODIS cloud mask algorithm. Many other studies (see the reference list) of cloud detection influenced this draft of the ATBD. The MODIS cloud mask algorithm builds on this work, but it will have considerable advantage because it has multispectral information and high spatial resolution. MODIS has 250 m resolution in two of the visible channels, 500 m resolution in five visible and near-infrared channels, and 1000 m resolution in the remaining channels. Of the 36 spectral channels available, sixteen visible and infrared radiances will be used to mitigate some of the difficulties experienced by the previous algorithms.

2.3 MODIS Characteristics

The MODIS bands used in the cloud mask algorithm are identified in Table 1.

Table 1. MODIS bands used in the MODIS cloud mask algorithm.

Band	Wavelength (μm)	Used in Cloud Mask	
1 (250 m)	0.659	Y	(250 m and 1 km) clouds, shadow
2 (250 m)	0.865	Y	(250 m and 1 km) low clouds
3 (500 m)	0.470	N	
4 (500 m)	0.555	Y	snow
5 (500 m)	1.240	Y	shadow
6 (500 m)	1.640	Y	snow
7 (500 m)	2.130	Y	aerosol
8	0.415	N	
9	0.443	N	
10	0.490	N	
11	0.531	N	
12	0.565	N	
13	0.653	N	
14	0.681	N	
15	0.750	N	
16	0.865	N	
17	0.905	N	
18	0.936	Y	low cloud
19	0.940	y	shadow
20	3.750	Y	cloud
21/22	3.959	N(21)/Y(22)	window, shadow
23	4.050	Y	shadow
24	4.465	N	
25	4.515	N	
26	1.375	Y	thin cirrus
27	6.715	Y	high cloud
28	7.325	N	
29	8.550	Y	cloud
30	9.730	N	
31	11.030	Y	cloud
32	12.020	Y	cloud
33	13.335	N	
34	13.635	N	
35	13.935	Y	high cloud
36	14.235	N	

In preparation for a MODIS day-1 cloud mask product, observations from the MODIS Airborne Simulator (MAS) (King *et al.* 1996), AVHRR, and the HIRS/2 are being used to develop a

multispectral cloud mask algorithm. The AVHRR and HIRS/2 instruments fly on the NOAA polar orbiting satellite, while the MAS flies onboard NASA's high altitude ER-2 aircraft collecting 50 m resolution data across a 37 km swath. The multispectral nature of MAS (and later MODIS) enhances the cloud detection capability, especially for highly varying surface, atmospheric, and cloud characteristics present on the global scale.

A three month global data set of collocated AVHRR and HIRS/2 observations is also being used to develop and test the cloud masking algorithm globally. The real-time algorithm (Frey *et al.* 1996) collocated and analyzed the AVHRR and HIRS/2 observations and is referred to as CHAPS (Collocated HIRS/2 and AVHRR Processing Scheme). This collocated data set has the advantage of containing many IR observations that are similar to the planned MODIS channels. The CHAPS data are used to assist in setting infrared thresholds for cloudy conditions over water. AVHRR GAC scenes are also being used to gain experience with global processing and the development and use of clear-sky radiance maps.

AVHRR LAC scenes are also being used to familiarize the algorithm with handling large data sets with a 1 km spatial resolution. These LAC data are also used to gain experience with incorporating satellite observations with the 1 km land/sea files and ecosystem maps.

The basic data sets currently being used to develop the cloud mask algorithm are listed in Table 2, as well as brief descriptions of the advantages and disadvantages of each. Examples are provided later.

Table 2. Data sets used to develop the MODIS cloud mask.

Data Set	Advantages	Disadvantages
AVHRR LAC	Similar spatial resolution Readily available	5 Channels; No global coverage
AVHRR GAC	Global coverage; Readily available	5 Channels; 4 km footprint
Collocated HIRS/AVHRR	Many MODIS-like channels Collocation of smaller pixels within larger footprint	Large HIRS/2 FOV; Gaps between HIRS footprints
MAS (11 channel digitized)	High spatial resolution; Similar MODIS bandwidths	No global coverage; Only 11 channels
MAS (50 channels)	Most MODIS like data set; High spatial resolution	No global coverage

2.4 Cloud Mask Inputs and Outputs

The following paragraphs summarize the input and output of the MODIS cloud algorithm Details on the multispectral single field of view (FOV) and spatial variability algorithms are found in the algorithm description section As indicated earlier, input to the cloud mask algorithm is assumed to be calibrated and navigated level 1B radiance data in channels 1, 2, 4, 5, 6, 7, 18, 19, 20, 22, 23, 26, 27, 29, 31, 32, and 35. Incomplete or bad radiometric data will create holes in the cloud mask. Additionally, the cloud mask requires several ancillary data inputs:

- sun angle, solar and sensor azimuthal angle, and viewing angle: obtained from MOD03 (geolocation fields);
- land/water map at 1 km resolution: eventually this will come from MOD03, currently the land/water map is provided by EDC;
- topography: Digital Elevation Models at 1 km are sought that define rugged versus plateau terrain;
- ecosystems: 1 km map of ecosystems is desired; The Olson map of ecosystems at 10-minute resolution is used for global processing Over North America the 1 km ecosystem provided by Tom Loveland is used;
- level 3 snow/ice product at 1 km resolution: the MODIS snow and sea ice mask product will

be used. At launch the planned NESDIS product using the AVHRR 1.6 μm channel or the SSM/I product will be used to initialize the snow mask;

- surface temperatures (sea and land) and wind (sea) at best available resolution: these parameters will be interpolated from Data Assimilation Office (DAO) (or NMC) global data sets; and
- Clear-sky radiance composite maps from MODIS observations.

The best available ancillary data will be used for the day-1 MODIS cloud mask However, it is expected that several MODIS investigator products will improve upon these ancillary data, so an evolutionary development of the cloud mask is envisioned A stable operational mask will likely be achieved one year after launch.

The output of the MODIS cloud mask algorithm will be a 48 bit word for each field of view The mask includes information about the processing path the masking took (e.g., land or ocean) and whether a view of the surface is obstructed We recognize that a potentially large number of applications will use the cloud mask Some algorithms will be more tolerant of cloud contamination than others. For example, some algorithms may apply a correction to account for the radiative effects of a thin cloud In addition, certain algorithms may use spectral channels that are more sensitive to the presence of clouds than others.

The boundary between defining a pixel as cloudy or clear is sometimes ambiguous For example, a pixel may be partly cloudy, or a pixel may appear as cloudy in one spectral channel and appear cloud-free at a different wavelength Figure 1 shows three spectral images of a subvisual contrail taken from the MAS during the Subsonic Aircraft Contrail and CloudEffects Special Study (SUCCESS). The left most panel is a MAS image in the 0.66μm channel, a spectral channel typical of many satellites and commonly used for land surface classifications such as the NDVI. The contrail is not discernible in this image and scattering effects of the radiation may be accounted for in an appropriate atmospheric correction algorithm The right most panel is a MAS 11 μm image (dark is cold, light is warm) Evidence of a contrail lingers though it would be difficult to justify its existence without the aid of the center panel—an image obtained using the 1.88

μm channel. The 1.88 μm spectral channel is near a strong water vapor absorption band and, during the day, is extremely sensitive to the presence of high level clouds. While the contrail seems to have little impact on visible reflectances, its effect in the infrared window is enough to affect the retrievals of surface temperature. In this type of scene, the cloud mask needs to provide enough information to be useful to both visible and infrared applications. The 1.88 μm spectral channel on MAS is expected to exhibit similar characteristics to the 1.38μm spectral channel to be available on MODIS.

To allow for our imprecise measurement of the real world and to accommodate a wide variety of applications, the mask is more than a simple yes/no decision (though bit 1 alone could be used to represent a single bit cloud mask). The cloud mask includes 4 levels of 'confidence' with regard to whether a pixel is thought to be clear (bits 1 and 2)[1] as well as the results from different spectral tests. The bit structure of the cloud mask is:

[1] In this document, representations of bit fields are ordered from right to left. Bit 0, or the right-most bit, is the least significant.

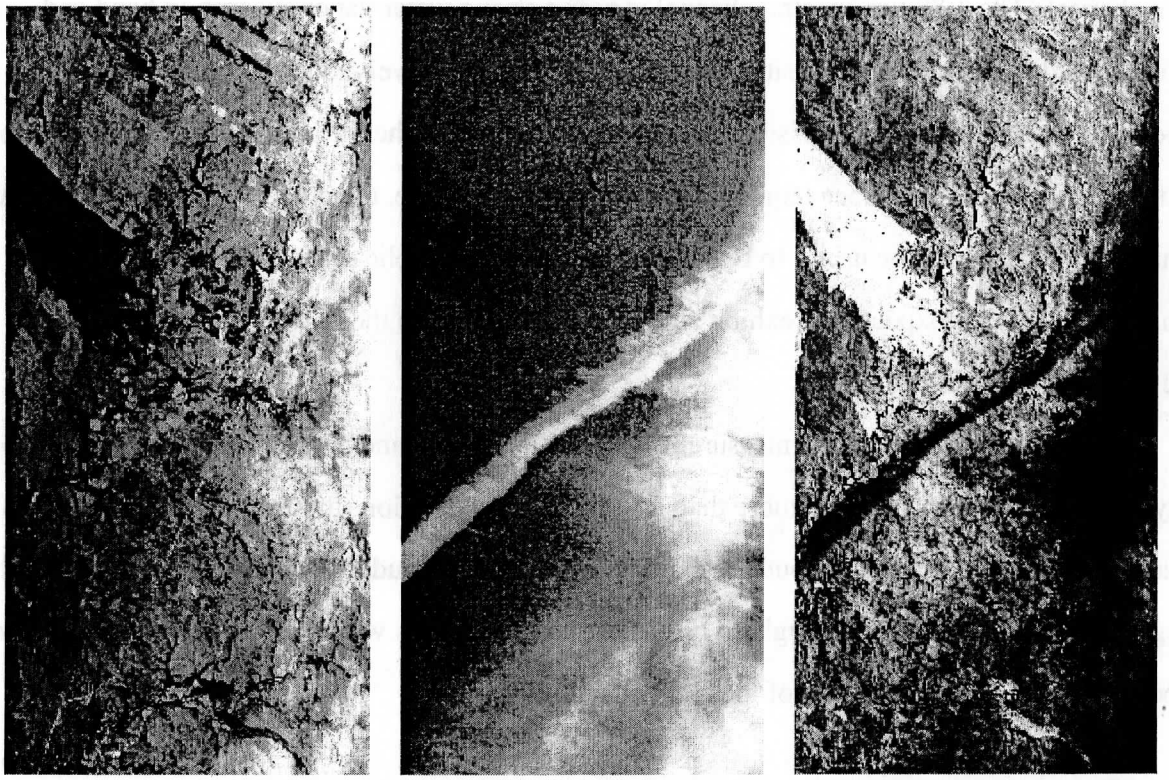

Figure 1. Three spectral images (0.66, 1.88 and 11 μm) taken from the MAS during the SUCCESS experiment (20 April 1996). In the 11 μm image, dark is cold.

Table 3. File specification for the 48-bit MODIS cloud mask. A '0' for tests 13-47 may mean the test was not run. For clear sky tests, a value of 0 indicates the presence of a cloud. Users should reference the QA data or Table 4 to determine which tests are executed.

BIT FIELD	DESCRIPTION KEY	RESULT
0	Cloud Mask Flag	0 = not determined 1 = determined
1-2	Unobstructed FOV Quality Flag	00 = cloudy 01 = probably clear 10 = confident clear 11 = high confidence clear
PROCESSING PATH FLAGS		
3	Day / Night Flag	0 = Night / 1 = Day
4	Sun glint Flag	0 = Yes / 1 = No
5	Snow / Ice Background Flag	0 = Yes/ 1 = No
6-7	Land / Water Flag	00 = Water 01 = Coastal 10 = Desert 11 = Land
ADDITIONAL INFORMATION		
8	Non-cloud obstruction Flag (heavy aerosol)	0 = Yes / 1 = No
9	Thin Cirrus Detected (solar)	0 = Yes / 1 = No
BIT FIELD	**DESCRIPTION KEY**	**RESULT**
10	Shadow Found	0 = Yes / 1 = No
11	Thin Cirrus Detected (infrared)	0 = Yes / 1 = No
12	Spare (Cloud adjacency)	(post launch)
	1-km CLOUD FLAGS	
13	Cloud Flag - simple IR Threshold Test	0 = Yes / 1 = No
14	High Cloud Flag - CO_2 Threshold Test	0 = Yes / 1 = No
15	High Cloud Flag - 6.7 μm Test	0 = Yes / 1 = No
16	High Cloud Flag - 1.38 μm Test	0 = Yes / 1 = No
17	High Cloud Flag - 3.7-12 μm Test	0 = Yes / 1 = No
18	Cloud Flag - IR Temperature Difference	0 = Yes / 1 = No
19	Cloud Flag - 3.7-11 μm Test	0 = Yes / 1 = No
20	Cloud Flag - Visible Reflectance Test	0 = Yes / 1 = No
21	Cloud Flag - Visible Ratio Test	0 = Yes / 1 = No
22	Cloud Flag - Near IR Reflectance Ratio Test	0 = Yes / 1 = No
23	Cloud Flag - 3.7-3.9 μm Test	0 = Yes / 1 = No
ADDITIONAL TESTS		

24	Cloud Flag - Temporal Consistency	0 = Yes / 1 = No
25	Cloud Flag - Spatial Variability	0 = Yes / 1 = No
26-31	Spares	
	250-m CLOUD FLAG - VISIBLE TESTS	
32	Element(1,1)	0 = Yes / 1 = No
33	Element(1,2)	0 = Yes / 1 = No
34	Element(1,3)	0 = Yes / 1 = No
35	Element(1,4)	0 = Yes / 1 = No
36	Element(2,1)	0 = Yes / 1 = No
37	Element(2,2)	0 = Yes / 1 = No
38	Element(2,3)	0 = Yes / 1 = No
39	Element(2,4)	0 = Yes / 1 = No
40	Element(3,1)	0 = Yes / 1 = No
41	Element(3,2)	0 = Yes / 1 = No
42	Element(3,3)	0 = Yes / 1 = No
43	Element(3,4)	0 = Yes / 1 = No
44	Element(4,1)	0 = Yes / 1 = No
45	Element(4,2)	0 = Yes / 1 = No
46	Element(4,3)	0 = Yes / 1 = No
47	Element(4,4)	0 = Yes / 1 = No

2.4.1 INPUT (BITS 3-7)

These input bits describe the processing path taken by the cloud mask algorithm.

BIT 3 - DAY / NIGHT FLAG

A combination of solar zenith angle and instrument mode (day or night mode) at the pixel latitude and longitude at the time of the observations is used to determine if a daytime or nighttime cloud masking algorithm should be applied Daytime algorithms, which include solar reflectance data, are constrained to solar zenith angles less than 85°. If this bit is set to 1, daytime algorithms were executed.

BIT 4 - SUN GLINT FLAG

Sun glint processing path is taken when the reflected sun angle, θ_r, lies between 0° and approximately 36°, where

$$\cos\theta_r = \sin\theta \sin\theta_0 \cos\phi + \cos\theta \cos\theta_0, \quad (1)$$

where θ_0 is the solar zenith angle, θ is the viewing zenith angle, and ϕ is the azimuthal angle. Sun glint is also a function of surface wind and sea state.

BIT 5 - SNOW / ICE BACKGROUND FLAG

Certain cloud detection tests (e.g., visible reflectance tests) are applied differently in the presence of snow or ice. This bit is set to a value of 0 when the cloud mask processing algorithm assumes that snow is present. This bit is set based on the 500 m gridded MODIS snow/ice map (MOD33 and MOD42). An abbreviated snow index (NDSI, Hall *et al.* 1995) has been incorporated into the cloud mask so that prior to full snow/ice processing the cloud mask can estimate synoptic changes in snow/ice cover from the last 24 hours. The snow/ice bit in the cloud mask will be a merging of the previous ten day snow/ice detection and the abbreviated NDSI of the current day. Post-launch, the NESDIS snow product, which makes use of the AVHRR visible and 1.6 μm channel, will be used to flag regions with snow This bit indicates a processing path and if set to 0 it should not be interpreted that snow is on the ground. Users interested in snow detection should access MODIS Level 2 Product MOD10.

BITS 6 AND 7 - LAND / WATER BACKGROUND FLAG

Bits 6 and 7 of the cloud mask output file contain information concerning the processing path taken through the algorithm. There are four possible surface type processing paths: land, water, desert, or coast. Naturally, there are times when more than one of these flags could apply to a pixel. For example, the northwest coast of the African continent could be simultaneously characterized as coast, land, and desert. In such cases, we choose to output the flag which indicates the most important characteristic for the cloud masking process. The flag precedence will be as follows: coast, desert, land or water.

Thresholds for the spectral tests are a function of surface background, land and water being the two most obvious. Therefore, each pixel will be tagged as being land or water. The 1 km United States Geological Survey (USGS) global land/water mask is currently used for this dete-

mination (available from USGS athttp://edcwww.cr.usgs.gov/landdaac/1KM/1kmhomepage.html).

Some cloud detection algorithms are also ecosystem dependent Thus, an ecosystem will be determined for each land pixel Over North America the current version of the cloud mask uses the 1 km ecosystem map of Loveland, available from EDC Global applications currently use the 10-minute resolution Olson World Ecosystem map.

As improved ancillary data bases become available, they will be incorporated into the MODIS cloud mask. The at-launch product will make use of the best available land/sea and ecosystem map with a 1 km spatial resolution We will progress to using the MODIS land cover type (MOD12) as it becomes available

2.4.2 OUTPUT (BITS 0, 1, 2 AND 8-47)

This section gives a brief description of the meaning of the output bits More discussion is given in the following sections.

BIT 0 - EXECUTION FLAG

There are conditions for which the cloud mask algorithm will not be executed For example, if all the radiance values used in the cloud masking are deemed bad, then masking cannot be undertaken. If bit 0 is set to 0, then the cloud mask algorithm was not executed. Conditions for which the cloud mask algorithm will not be executed will be set for Version 2 of the cloud mask code.

BITS 1-2 - UNOBSTRUCTED FOV QUALITY FLAG

Confidence flags convey strength of conviction in the outcome of the cloud mask algorithm tests for a given FOV. When performing spectral tests, as one approaches a threshold limit, the certainty or confidence in the outcome is reduced Therefore, a confidence flag for each individual test, based upon proximity to the threshold value, is assigned and used to work towards a final quality flag determination for the FOV. The current scheme applies a linear interpolation between

a low confidence clear threshold (0% confidence of clear) and high confidence clear threshold (100% confidence clear) for each spectral test.

The final determination is a combination of the confidences of all applied tests This determination will dictate whether additional testing (using spatial variability tests) is warranted to improve the confidence. The final cloud mask determination will be clear or cloudy with a confidence level associated with it This approach quantifies our confidence in the derived cloud mask for a given pixel For MODIS applications, spatial and temporal consistency tests will be invoked as a final check Temporal consistency compares composited clear-sky radiances with the current clear-sky single pixel results Spatial consistency checks neighboring pixel radiances (within the same ecosystem). If any consistency test fails, the confidence in the final cloud/no cloud determination is reduced.

BIT 8 - NON-CLOUD OBSTRUCTION

Smoke from forest fires, dust storms over deserts, and other aerosols that result in obstructing the FOV between the surface and the satellite may be flagged as "cloud." The aerosol obstruction bit will be set to on (a value of 0) if simple spectral tests indicate the possible presence of aerosols. This bit is not an aerosol product; rather, if the bit is set to zero, then the instrument may be viewing an aerosol laden atmosphere Aerosol testing is presented in section 3.2.3.

BIT 9 - THIN CIRRUS (NEAR-INFRARED)

MODIS includes a unique spectral channel—1.38 μm—specifically included for the detection of thin cirrus. Land and sea surface retrieval algorithms may attempt to correct the observed radiances for the effects of thin cirrus The definition of *thin* will be determined in collaboration with the MODIS Atmosphere, Land and Ocean groups. This test is discussed in Section 3.2.4. If this bit is set to 0, thin cirrus was detected using this channel.

BIT 10 - SHADOW BIT

Some land retrieval products are as sensitive to the presence of shadows as they are to con-

tamination by thin clouds The MODIS cloud masking algorithm checks for the presence of a shadow whenever bits 1 and 2 are greater than 00. Though much work remains, section 3.2.6 discusses the shadow detection algorithm If bit 10 is set to zero, a shadow was detected using spectral tests. If bits 1 and 2 are 00 (high confidence cloudy), tests will be run to discern if a shadow from a high cloud is being cast on a lower cloud In such a case is detected, this bit is set to zero.

BITS 11 - THIN CIRRUS (INFRARED)

It is likely that some IR algorithms will be insensitive to thin cirrus flagged by the MODIS 1.38 μm channel In addition, this 1.38 μm channel is not available during the night This second thin cirrus bit indicates that IR tests detect a thin cirrus cloud The results are independent of the results of bit 9. The definition of *thin* in the infrared will be determined in collaboration with the MODIS Atmosphere, Land and Ocean groups. This test is discussed in Section 3.2.5. If this bit is set to 0, thin cirrus was detected using infrared channels.

BITS 12 - SPARE BIT (POST LAUNCH CLOUD ADJACENCY BIT)

This bit was added for potential use later if additional information is required If a pixel is clear, adjacent pixels will be searched to determine if any are low confidence clear. If so, this bit will be set to 0. This algorithm will be implemented post-launch.

BITS 13 THROUGH 23 - 1 KM CLOUD MASK

These 11 bits represent the results of tests that make use of the 1 km observations. Each individual test is discussed in the next section Some tests make use of channels with a 500 m resolution; these channels are averaged up to the 1 km field of view The number of spectral tests applied is a function of the processing path. The following table lists the tests applied for each path. It is important to refer to this table (or the QA flag) when interpreting the meaning of bits 13 through 23, as a value of 0 can mean the pixel is clear, or that the test was not performed.

BITS 24 AND 25 - CONSISTENCY TESTS

These 2 bits represent the results from temporal and spatial constancy tests.

BITS 26 AND 31 - SPARE BITS

These spare bits are reserved for future tests not yet devised because we're not smart enough.

BITS 32 THROUGH 47 - 250 METER RESOLUTION FLAGS

The 250 m mask will be based on reflectance tests using only channels 1 and 2 of MODIS (see Sections 3.2.7 and 3.2.8). The 250 m cloud mask will be collocated within the 1000 m cloud mask in a fixed way; of the twenty-eight250 m pixels that can be considered located within a 1000 m pixel, the most centered sixteen will be processed for the cloud mask Of the four rows of 250 m pixels, 1 through 7 that fall into a 1000 m pixel, four rows of pixels 3 through 6 will be selected. The relationship between the sixteen 250 m fov's and the 1 km footprint in the cloud mask is defined as:

250 m beginning element number = (1km element number - 1) * 4 + 1

250 m beginning line number = (1km line number - 1) * 4 + 1

where the first line and element are 1,1. From this beginning location, the 4x4 array of lines and elements can be identified. The indexing order of the sixteen 250 m pixels in the cloud mask file is lines, elements The bit indicating that visible data was usable must be 1 for the 250 m mask to have any meaning (e.g, ignore the last 16 bits if nighttime).

It is possible to infer cloud fraction in the 1000 m field of view from the 16 visible pixels within the 1 km footprint. The cloud fraction would be the number of zeros divided by 16 This would be inadvisable in particular situations, such as over snow.

Table 4. MODIS cloud mask tests executed for a given processing path. The red check (✓) indicates that the test has been implemented on AVHRR and/or MAS data, and the blue circle (O) indicates that the test is not yet fully tested on AVHRR or MAS data.

	Daytime Ocean	Nighttime Ocean	Daytime Land	Nighttime Land	Daytime Snow/ice	Nighttime Snow/ice	Daytime Coastline	Nighttime Coastline	Daytime Desert	Nighttime Desert
BT_{11} (Bit 13)	✓	✓								
$BT_{13.9}$ (Bit 14)	✓	✓	✓	✓	✓	✓	✓	✓	✓	✓
$BT_{6.7}$ & BT_{11} - $BT_{6.7}$ (Bit 15)	O	O	O	O	✓	✓	O	O	O	O
$R_{1.38}$ (Bit 16)	✓		✓		✓		✓		O	
$BT_{3.7}$ - BT_{12} (Bit 17)				✓		✓				✓
$BT_{8.6}$ - BT_{11} & BT_{11} - BT_{12} (Bit 18)	✓	✓	✓	✓			✓	✓	O	✓
BT_{11} - $BT_{3.7}$ (Bit 19)	✓	✓	✓	✓	✓	✓	✓	✓	O	✓
$R_{0.66}$ or $R_{0.87}$ (Bit 20)	✓		✓		O		✓		O	
$R_{0.87}/R_{0.66}$ (Bit 21)	✓		✓				✓			
$R_{0.936}/R_{0.87}$ (Bit 22)	O		O		O		O			
$BT_{3.7}$ - $BT_{3.9}$ (Bit 23)	O		O				O		O	
Temporal Consistency (Bit 24)	✓	✓								O
Spatial Variability (Bit 25)	✓	✓								

3.0 Algorithm Description

The theoretical basis of the algorithms and practical considerations are contained in this section. For nomenclature, we shall denote the satellite measured solar reflectance as R, and refer to the infrared radiance as brightness temperature (equivalent blackbody temperature determined using the Planck function) denoted as BT. Subscripts refer to the wavelength at which the measurement is made. The strategy for this cloud mask algorithm is to start with single pixel (1000 m field of view) tests. Cloud detection using automated textural classification techniques were considered for difficult scenes (e.g., polar conditions); however, it is anticipated that the many spectral channels of MODIS may negate the use of textural applications. The disadvantage of textural methods is the required CPU, an extreme disadvantage when operating a real-time cloud mask. When confidence levels are below 95%, spatial uniformity tests are then applied. Over water the clear pixel results are measured for spatial and temporal consistency.

Many of the single pixel tests rely on radiance (temperature) thresholds in the infrared and reflectance thresholds in the solar. These thresholds vary with surface emissivity, with atmospheric moisture and aerosol content, and with MODIS viewing scan angle. A large part of the algorithm preparation will be to characterize the different situations and the different thresholds. This section describes these spectral tests.

3.1 Confidence Flags

Most of the single pixel tests that are discussed in Section 3.2 rely on thresholds. Thresholds are never global. There are always exceptions. For example, the ratio of reflectance at 0.86 to 0.66 μm identifies cloud for values in the range $0.9 < R_{0.87}/R_{0.66} < 1.1$. It seems unrealistic to label a pixel with $R_{0.87}/R_{0.66} = 1.09$ as cloudy, and a neighboring pixel with the ratio of 1.11 as non-cloudy. Rather, as one approaches the threshold limits, the certainty or confidence in the labeling becomes more and more uncertain. An individual confidence flag is assigned to each single pixel test and is a function of how close the observation is to the thresholds. The individual conf-

dence flags are combined to produce the final cloud mask flag for the output file (bits 1 and 2).

The uncertainty is a function of instrument noise in that channel and the magnitude of the correction that was necessary due to surface spectral radiative properties, as well as atmospheric moisture and/or aerosol reflection contributions. The individual confidence flag will indicate a confidence level for each single pixel test result. The initial FOV obstruction determination is an amalgamation of all confidence flags and single pixel test results (Section 3.2.11). This determination will dictate whether additional testing (e.g., spatial uniformity tests) is warranted to improve the confidence. The final cloud mask determination (bits 1 and 2) is a clear-sky confidence with one of four levels associated with it: definitely clear, probably clear, possibly clear and definitely obstructed. This approach quantifies our confidence in the derived cloud mask for a given pixel. This section describes the method of assigning a confidence to a given spectral test.

Many cloud detection schemes have a single threshold for a given test. For example, if the visible reflectance over the ocean is greater than 6% then the pixel is set to cloudy. The cloud masking is designed to provide information on how much confidence a user can place on the result. Each test is assigned a value between 0 and 1 representing increasing confidence in clear-sky conditions. Figure 2 is a graphical representation of how a confidence level is assigned for a spectral test. The abscissa represents the observation and the ordinate the clear-sky confidence level. In this test, an observation greater than a value of γ is determined to be a high confidence clear scene and assigned a value of 1. An observation with a value less than α is cloudy and assigned a confidence level of 0. These high confidence clear and cloud thresholds, γ and α respectively, are determined from observations and/or theoretical simulations.

Values between α and γ are assigned a value between 0 and 1 (or 1 and 0). Assignment is based on a linear function. We have experimented with assigning confidence values based on S-functions:

$$S(x;\alpha,\beta,\gamma)=\begin{cases}0 & \text{for } x\le\alpha\\ 2\left(\dfrac{x-\alpha}{\gamma-\alpha}\right)^2 & \text{for } \alpha\le x\le\beta\\ 1-2\left(\dfrac{x-\alpha}{\gamma-\alpha}\right)^2 & \text{for } \beta\le x\le\gamma\\ 1 & \text{for } x\ge\gamma\end{cases} \tag{2}$$

The S-function is quadratic between the points α and γ. If the '2' exponent in the above equation is replaced with a 1, then the S-function becomes linear Experiments indicate that changing between a quadratic and linear function primarily affects cloud masking at the edge of cloud systems. For simplicity we have stayed with the linear function.

In the final cloud mask only four levels of confidence are provided Numerical values are assigned to each of these four confidence levels, 0.99 confidence of clear, 0.95, 0.66 and less than 0.66. These numerical values are set based on how close the observed value is to a set of thresholds. A description of how the final confidence level is determined is given in section 3.2.11.

Bits 13 through 23 represent the results from independent cloud tests, with no confidence associated with the output. The β value in Figure 2 is the pass/fail threshold for agiven test. Each test therefore has a minimum of three threshold values for pass/fail, high confidence pass and high confidence fail Some tests, such as the visible ratio test, identify cloud if the observations fall

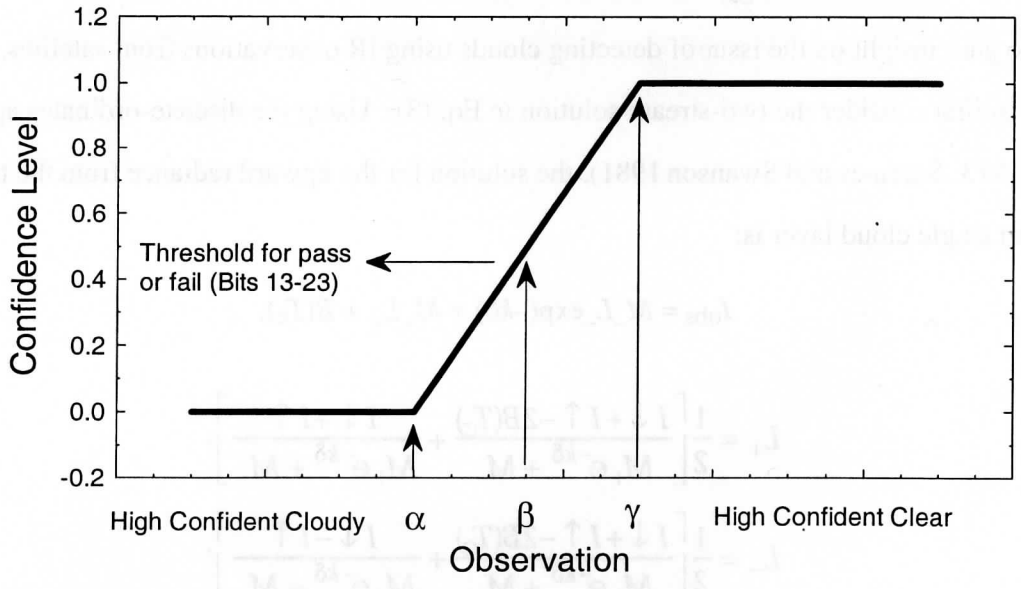

Figure 2. A graphical depiction of three thresholds used in cloud screening.

within a given range (e.g., $0.9 < R_{0.87}/R_{0.66} < 1.1$). For these range tests there are six thresholds, three for each end.

3.2 Theoretical Description of Cloud Detection

This section discusses the physics of detecting clouds using multispectral radiances from a given field of view (FOV) or an array of FOVs, presents the application with MODIS data, and indicates various problem areas.

3.2.1 Infrared Brightness Temperature Thresholds and Difference (BTD) Tests

The azimuthally-averaged form of the infrared radiative transfer equation is given by

$$\mu \frac{\mathrm{d}\, I(\delta,\mu)}{\mathrm{d}\,\delta} = I(\delta, \mu) - (1- \omega_0)B(T) - \frac{\omega_0}{2} \int_{-1}^{1} P(\delta, \mu, \mu')\, I(\delta, \mu')\, \mathrm{d}\mu'. \tag{3}$$

In addition to atmospheric structure, which determines $B(T)$, the parameters describing the transfer of radiation through the atmosphere are the single scattering albedo, $\omega_0 = \sigma_{sca}/\sigma_{ext}$, which ranges between 1 for a non-absorbing medium and 0 for a medium that absorbs and does not scatter energy, the optical depth, δ, and the Phase function, $P(\mu, \mu')$, which describes the direction of the scattered energy.

To gain insight on the issue of detecting clouds using IR observations from satellites, it is useful to first consider the two-stream solution to Eq. (3). Using the discrete-ordinates approach (Liou 1973; Stamnes and Swanson 1981), the solution for the upward radiance from the top of a uniform single cloud layer is:

$$I_{obs} = M\_L\_\exp(-k\delta) + M_+L_+ + B(T_c), \tag{4}$$

where

$$L_+ = \frac{1}{2}\left[\frac{I\downarrow + I\uparrow - 2B(T_c)}{M_+ e^{-k\delta} + M_-} + \frac{I\downarrow + I\uparrow}{M_+ e^{-k\delta} + M_-}\right], \tag{5}$$

$$L_- = \frac{1}{2}\left[\frac{I\downarrow + I\uparrow - 2B(T_c)}{M_+ e^{-k\delta} + M_-} + \frac{I\downarrow - I\uparrow}{M_+ e^{-k\delta} - M_-}\right], \tag{6}$$

$$M_{\pm} = \frac{1}{1 \pm k}\left(\omega_{\circ} \mp \omega_{\circ} g(1-\omega_{\circ})\frac{1}{k}\right), \tag{7}$$

$$k = \left[(1-\omega_{\circ})(1-\omega_{\circ} g)\right]^{\frac{1}{2}}. \tag{8}$$

$I\downarrow$ is the downward radiance (assumed isotropic) incident on the top of the cloud layer, $I\uparrow$ the upward radiance at the base of the layer, and g the asymmetry parameter. T_c is a representative temperature of the cloud layer.

The challenge in cloud masking is detecting thin clouds Assuming a thin cloud layer, the effective transmittance (ratio of the radiance exiting the layer to that incident on the base) is derived from equation (4) by expanding the exponential The effective transmittance is a function of the ratio of $I\downarrow/I\uparrow$ and $B(T_c)/I\uparrow$. Using atmospheric window regions for cloud detection minimizes the $I\downarrow/I\uparrow$ term and maximizes the $B(T_c)/I\uparrow$ term. Figure 3 is a simulation of differences in brightness temperature between clear and cloudy sky conditions using the simplified set of equations (4)-(8). In these simulations, there is no atmosphere, the surface is emitting at a blackbody tem-

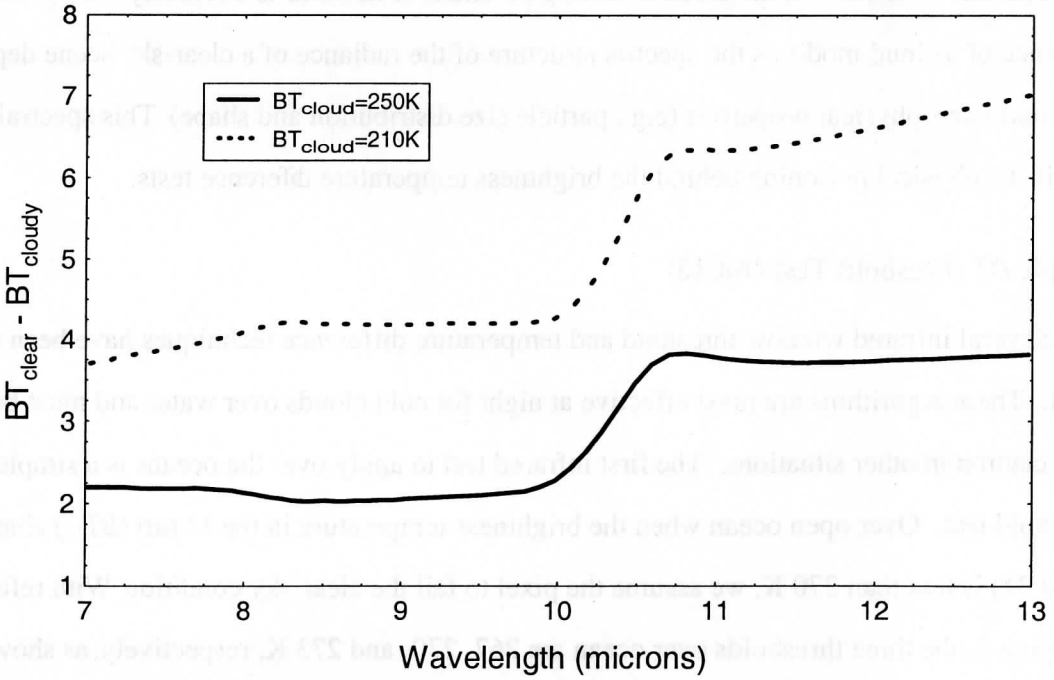

Figure 3. A simple simulation of the brightness temperature differences between a "clear" and cloudy sky as a function of wavelength. The underlying temperature is 290 K and the cloud optical depth is 0.1. All computations assume ice spheres with r_e = 10 μm.

perature of 290 K, the cloud particles are ice spheres with a gamma size distribution assuming an effective radius of 10 μm, and the cloud optical depth $\delta = 0.1$. Two cloud temperatures are simulated (210 K and 250 K). Brightness temperature differences between the clear and cloudy sky result because of non-linearity of the Planck function and because of spectral variation in the single scattering properties of the cloud. The magnitude of the difference is also a function of the temperature difference between the cloud and underlying atmosphere. This figure does not include the absorption and emission of atmospheric gases which also generates brightness temperature differences. Observations of brightness temperature differences at two or more wavelengths can help separate the atmospheric signal from the cloud effect.

The anticipation is that the infrared threshold techniques will be very sensitive to thin clouds, given the appropriate characterization of surface emissivity and temperature. For example, with a surface at 300 K and a cloud at 220 K, a cloud with an emissivity of 0.01 affects the brightness temperature by 0.5 K. Since the expected noise equivalent temperature of MODIS infrared window channel 31 is 0.05 K, the cloud detecting potential of MODIS is obviously very good. The presence of a cloud modifies the spectral structure of the radiance of a clear-sky scene depending on cloud microphysical properties (e.g., particle size distribution and shape). This spectral signature is the physical reasoning behind the brightness temperature difference tests.

Simple *BT* threshold Test (Bit 13)

Several infrared window threshold and temperature difference techniques have been developed. These algorithms are most effective at night for cold clouds over water and must be used with caution in other situations. The first infrared test to apply over the oceans is a simple threshold test. Over open ocean when the brightness temperature in the 11 μm (BT_{11}) channel (band 31) is less than 270 K, we assume the pixel to fail the clear-sky condition. With reference to Figure 2, the three thresholds over ocean are 267, 270, and 273 K, respectively, as shown in Figure 4.

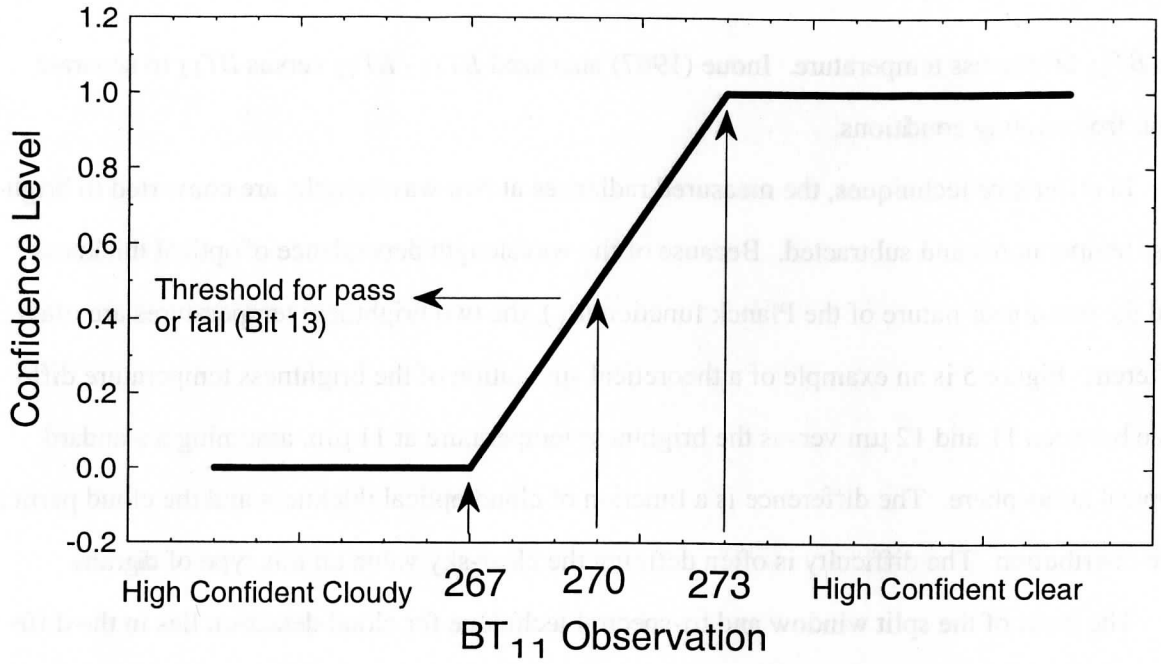

Figure 4. Thresholds for the simple IR window cold cloud test.

Cloud masking over land surface from thermal infrared bands is more difficult than over ocean due to potentially larger variations in surface emittance Nonetheless, simple thresholds can be established over certain land features For example, over desert regions we can expect that $BT_{11} < 273$ K denotes cloud. Such simple thresholds will vary with ecosystem, season, and time of day, and are under investigation. Therefore, at launch, the simpleBT_{11} threshold test will be applied only over ocean during both day and night (cf. Table 4).

BT_{11} - BT_{12} and $BT_{8.6}$ - BT_{11} Test (Bit 18)

As a result of the relative spectral uniformity of surface emittance in the IR, spectral tests within various atmospheric windows (such as bands 29, 31, 32 at 8.6, 11, and 12μm, respectively) can be used to detect the presence of cloud. Differences betweenBT_{11} and BT_{12} are widely used for cloud screening with AVHRR measurements, and this technique is often referred to as the split window technique. Saunders and Kriebel (1988) usedBT_{11} - BT_{12} differences to detect cirrus clouds—brightness temperature differences are greater over thin clouds than over-clear or overcast conditions. Cloud thresholds were set as a function of satellite zenith angle and

the BT_{11} brightness temperature. Inoue (1987) also used BT_{11} - BT_{12} versus BT_{11} to separate clear from cloudy conditions.

In difference techniques, the measured radiances at two wavelengths are converted to brightness temperatures and subtracted. Because of the wavelength dependence of optical thickness and the non-linear nature of the Planck function (B_λ), the two brightness temperatures are often different. Figure 5 is an example of a theoretical simulation of the brightness temperature difference between 11 and 12 μm versus the brightness temperature at 11 μm, assuming a standard tropical atmosphere. The difference is a function of cloud optical thickness and the cloud particle size distribution. The difficulty is often defining the clear-sky value on this type of diagram.

The basis of the split window and tri-spectral technique for cloud detection lies in the differential water vapor absorption that exists between different window channel (8.6 and 11μm and 11 and 12 μm) bands. These spectral regions are considered to be part of the atmospheric window, where absorption is relatively weak. Most of the absorption lines are a result of water vapor molecules, with a minimum occurring around 11μm. Since the absorption is weak, BT_{11} can be corrected for moisture absorption by adding the scaled brightness temperature difference of two

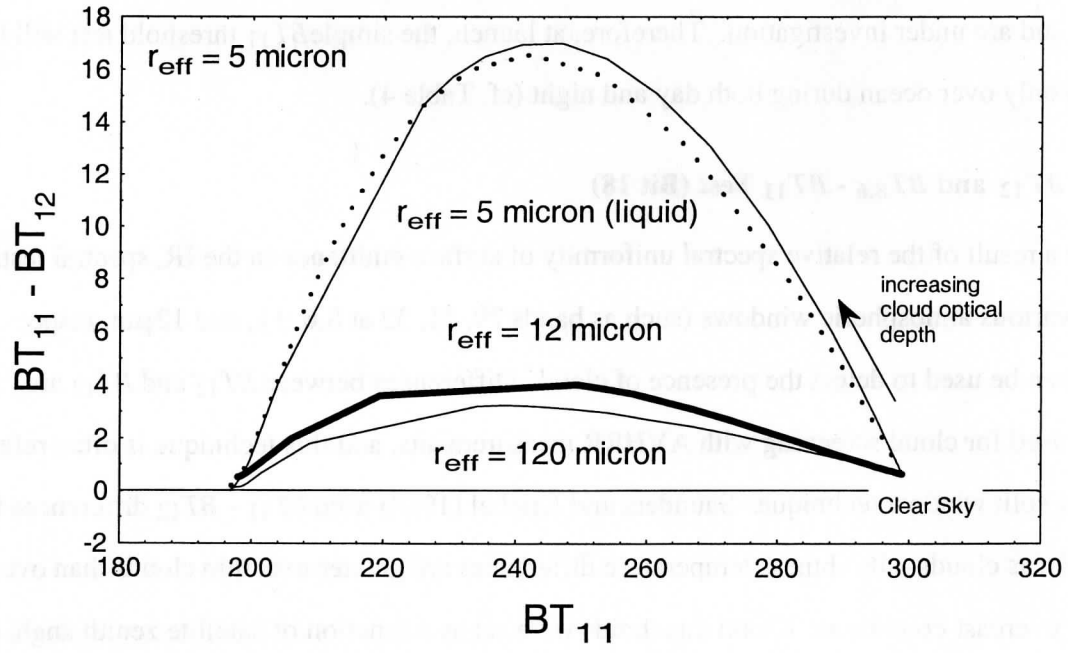

Figure 5. Theoretical simulations of the brightness temperature difference as a function of BT_{11} for a cirrus cloud of varying cloud microphysical properties.

spectrally close channels with different water vapor absorption coefficients; the scaling coefficient is a function of the differential water vapor absorption between the two channels This is the basis for sea surface temperature (SST) retrieval.

The surface temperature, T_s, can be determined using remote sensing instruments if observations are corrected for water vapor absorption effects,

$$T_s = BT_{11} + \Delta BT, \tag{9}$$

where BT_{11} is a window channel brightness temperature To begin, the radiative transfer equation for a clear atmosphere can be written

$$I_{\lambda,\mathrm{clr}} = B\lambda(T(p_s))\tau\lambda(p_s) + \int_{p_s}^{p_0} B_\lambda(T(p))\frac{\mathrm{d}\tau_\lambda(p)}{\mathrm{d}p}\mathrm{d}p. \tag{10}$$

As noted above, absorption is relatively weak across the window region so that a linear approximation is made to the transmittance

$$\tau = 1 - k_\lambda u, \tag{11}$$

Here k_λ is the absorption coefficient of water vapor and u is the path length. The differential transmittance then becomes

$$\mathrm{d}\tau_\lambda = -k_\lambda \mathrm{d}u. \tag{12}$$

Inserting this approximation into the window region radiative transfer equation will lead to

$$I_{\lambda,\mathrm{clr}} = B_{\lambda,s}(1 - k_\lambda u) + k_\lambda \int_0^{u_s} \bar{B}_\lambda \,\mathrm{d}\,u. \tag{13}$$

Here, $\overline{B_\lambda}$ is the atmospheric mean Planck radiance Since $B_{\lambda,s}$ will be close to both $I_{\lambda,\mathrm{clr}}$ and $\overline{B_\lambda}$, we can linearize the radiative transfer equation with respect to T_s

$$BT_{b\lambda} = T_s(1 - k_\lambda u_s) + k_\lambda u_s \overline{BT_\lambda}, \tag{14}$$

where $\overline{BT_\lambda}$ is the mean atmospheric temperature corresponding to $\overline{B_\lambda}$. Using observations from two window channels, one may ratio this equation, cancel out common factors and rearrange to end up with the following approximation

$$\frac{T_S - BT_{\lambda,1}}{T_S - BT_{\lambda,2}} = \frac{k_{\lambda,1}}{k_{\lambda,2}} \quad . \tag{15}$$

Solving the equation for T_S yields

$$T_S = BT_{\lambda,1} + \frac{k_{\lambda,1}}{k_{\lambda,2} - k_{\lambda,1}} (BT_{\lambda,1} - BT_{\lambda,2}). \tag{16}$$

Thus, with a reasonable estimate of the sea surface temperature and total precipitable water (on which k_λ is dependent), one can develop appropriate thresholds for cloudy sky detection For example,

$$BT_{11} + a_{PW}(BT_{11} - BT_{12}) < \text{SST}, \tag{17}$$

or

$$BT_{11} + b_{PW}(BT_{11} - BT_{8.6}) < \text{SST}, \tag{18}$$

where a_{PW} and b_{PW} are determined from a lookup table as a function of total precipitable water vapor (PW). This approach has been used operationally for 4 years using 8.6 and 11μm band-widths from the NOAA-10 and NOAA-12 and the 11 and 12 μm bandwidths from the NOAA-11, with a coefficient independent of PW (Menzel *et al.* 1993, Wylie *et al.* 1994).

To demonstrate this technique with observations, a global data set of collocated AVHRR GAC 11 and 12 μm and HIRS 8.6 and 11 μm scenes were collected and the total column PW was estimated from integrated model mixing ratios to determine a direct regression between PW and the split window thresholds. The regressions were then modified for use withMAS bandwidths in TOGA/COARE data sets. Simulations and observations have shown the regression slopes to be consistent with those found for the AHVRR/HIRS clear scenes; however, the intercept values needed adjustment.

A disadvantage of the split window brightness temperature difference (BTD) approach is that water vapor absorption across the window is not linearly dependent on PW, thus second order relationships are sometimesrequired. MODIS has a unique capabilitysince it has measurements at three wavelengths in the window, 8.6, 11, and 12 μm. The three spectral regions mentioned are very useful in determination of cloud free atmospheres Because the index of refraction varies

quite markedly over this spectral region for water, ice, and minerals common to many naturally occurring aerosols, the effect on the brightness temperature of each of the spectral regions is different, depending on the absorbing constituent.

A tri-spectral combination of observations at 8.6, 11 and 12 μm was suggested for detecting cloud properties by Ackerman *et al.* (1990). Strabala *et al.* (1994) further explored this technique by utilizing very high spatial-resolution data from MAS. The physical premise of the technique is that ice and water vapor absorption peak in opposite halves of the window region; so that positive 8.6 minus 11 μm brightness temperature differences indicate cloud while negative differences, over oceans, indicate clear regions. The relationship between the two brightness temperature differences and clear-sky have also been examined using collocated HIRS and AVHRR GAC global ocean data sets. As the atmospheric moisture increases, $BT_{8.6} - BT_{11}$ decreases while $BT_{11} - BT_{12}$ increases.

Based on these observations, a threshold is set for clear-sky conditions. The clear-sky threshold is set for both differences:

$$\text{T8M11} = -3.19767 - 1.64805 \ln (\text{PW}), \tag{18}$$

$$\text{T11M12} = -0.456924 + 0.488198\ \text{PW}. \tag{19}$$

If $BT_{8.6} - BT_{11} > \text{T8M11}$ and $BT_{11} - BT_{12} > \text{T11M12}$, then a cloud is assumed.

High confidence clear conditions are

$$BT_{8.6} - BT_{11} < \text{T8M11} - 0.5 \text{ and } BT_{11} - BT_{12} > \text{T11M12} - 0.5, \tag{20}$$

and low confidence clear conditions are

$$BT_{8.6} - BT_{11} < \text{T8M11} + 0.5 \text{ and } BT_{11} - BT_{12} > \text{T11M12} + 0.5. \tag{21}$$

The above conditions assume an estimate of the precipitable water is available. These equations demonstrate that a relationship between T8M11 and T11M12 exists and thus a PW value is not needed, but rather given a value of T8M11, to be a clear pixel requires T11M12 to fall within a certain range of values. This is demonstrated in Figure 6 using collocated AVHRR and HIRS/2 observations.

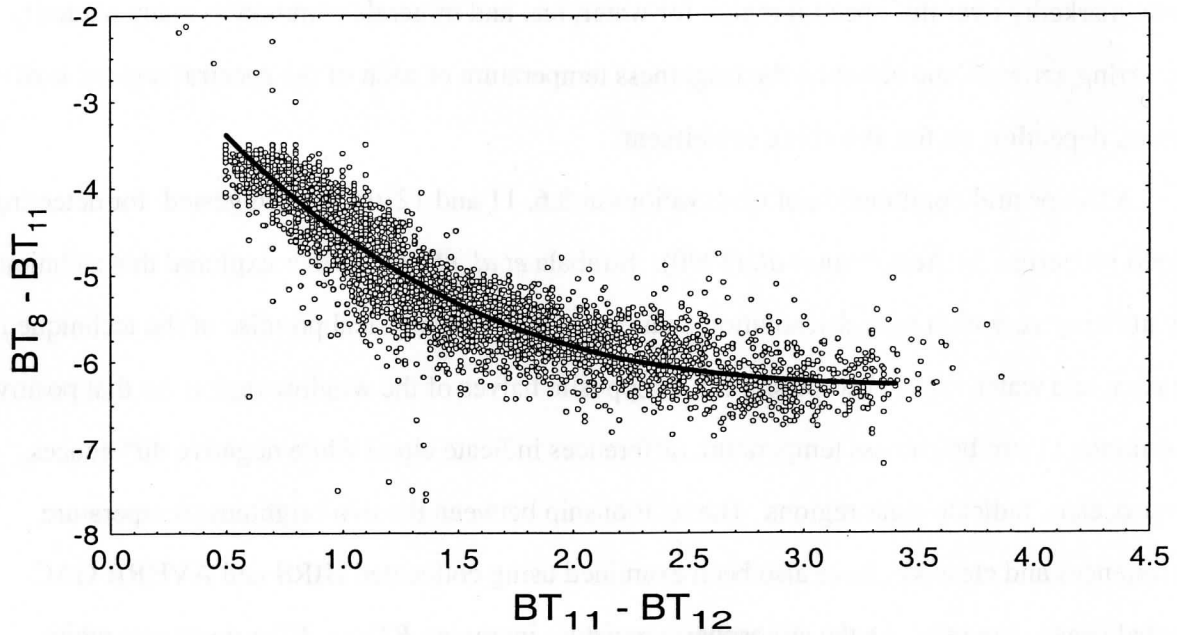

Figure 6. The tri-spectral diagram for clear-sky ocean scenes.

Brightness temperature difference testing can also be applied over land with careful consideration of variation in spectral emittance. For example, $BT_{11} - BT_{8.6}$ has large negative values over daytime desert and is driven to positive differences in the presence of cirrus. Some land regions have an advantage over ocean regions because of the larger number of surface observations, including air temperature and vertical profiles of moisture and temperature. Work on developing brightness temperature difference tests for application over land scenes continues with MAS observations.

BT_{11} - $BT_{3.7}$ Test (Bit 19)

MODIS band 22 (3.9 μm) measures radiances in another window region near 3.5-4μm so that the difference between BT_{11} and $BT_{3.7}$ can also be used to detect the presence of clouds. At night the difference between the brightness temperatures measured in the shortwave (3.7μm) and in the longwave (11 μm) window regions ($BT_{11} - BT_{3.7}$) can be used to detect partial cloud or thin cloud within the MODIS field of view. Small or negative differences are observed only for the case where an opaque scene (such as thick cloud or the surface) fills the field of view of the sensor. Negative differences occur at night over extended clouds due to the lower cloud emissiv-

ity at 3.7 μm.

During the daylight hours the difference between BT_{11} and $BT_{3.7}$ large negative because of reflection of solar energy at 3.7 μm. This technique is very successful at detecting low level water clouds. $BT_{11} - BT_{3.7}$ is not applied over deserts during daytime, as bright desert regions with highly variable emissivities tend to be classified incorrectly as cloudy with this testExperience indicates that the actual thresholds will need to be adjusted for ecosystem type.

Moderate to large differences between BT_{11} and $BT_{3.7}$ result when a non-uniform scene (e.g., broken cloud) is observed. The different spectral responses to a scene of non-uniform temperature is a result of Planck's law. The brightness temperature dependence on the warmer portion of the scene increasing with decreasing wavelength (the shortwave window Planck radiance is proportional to temperature to the thirteenth power, while the longwave dependence is to the fourth power). Differences in the brightness temperatures of the longwave and shortwave channels are small when viewing mostly clear or mostly cloudy scenes; however, for intermediate situations the differences become large (greater than 3°C). Table 5 lists the thresholds used, which are based on previous studies and our own investigations.

Infrared window tests at high latitudes are difficult Distinguishing clear and cloud regions from satellite IR radiances is a challenging problem due to the cold surface temperatures Yamanouchi *et al.* (1987) describe a nighttime polar (Antarctic) cloud/surface discrimination algorithm based upon brightness temperature differences between the AVHRR 3.7 and 11μm channels and between the 11 and 12 μm channels Their cloud/surface discrimination algorithm was more ef-

Table 5. Thresholds used for $BT_{11} - BT_{3.7}$ test for low cloud in the MODIS cloud mask algorithm.

Scene Type	Threshold	High confidence clear	Low confidence clear
Day ocean	-8.0 K	-6.0 K	-10.0 K
Night ocean	0.60 K	0.50 K	0.70 K
Day land	-12.0 K	-10.0 K	-14.0 K
Night land	0.60 K	0.50 K	0.70 K
Day snow/ice	-9.0 K	-7.0 K	-11.0 K
Night snow/ice	0.60 K	0.50 K	0.70 K
Night desert	-18.0, -3 K	>-16, <-5 K	<-20, >-1 K

fective over water surfaces than over inland snow-covered surfaces. A number of problems arose over inland snow-covered surfaces. First, the temperature contrast between the cloud and snow surface became especially small, leading to a small brightness temperature difference between the two infrared channels. Second, the AVHRR channels are not well-calibrated at extremely cold temperatures (< 200 K). This latter condition will be much less of a problem with MODIS.

$BT_{3.7}$ - BT_{12} Test (Bit 17)

This window brightness temperature difference test is applied during the nighttime over some, but not all, surfaces (cf. Table 4). This difference is useful for seperating thin cirrus and cloud free condition over land (Hutchison and Hardy 1995).

$BT_{6.7}$ and BT_{11} - $BT_{6.7}$ Test (Bit 15)

Detection of clouds over polar regions during winter is difficult. Under clear-sky conditions, strong surface radiative temperature inversions often exist over polar regions during winter. Thus, IR channels whose weighting function peaks low in the atmosphere will often have a larger BT than a window channel. For example, $BT_{8.6} > BT_{11}$ in the presence of an inversion. The surface inversion can also be confused with thick cirrus cloud; this can be mitigated by other tests (e.g., the magnitude of BT_{11} or the BT_{11} - BT_{12}). Analysis of BT_{11} - $BT_{6.7}$ has shown large negative difference in winter time over the Antarctic Plateau and Greenland, which may be indicative of a strong surface inversion and thus clear skies (Ackerman 1996a). In clear-sky situations, the 6.7 μm radiation measured by satellite instruments is emitted by water vapor in the atmospheric layer between approximately 200 and 500 hPa (Soden and Bretherton 1993; Wu *et al.* 1993) and has a brightness temperature ($BT_{6.7}$) related to the temperature and moisture in that layer. The 6.7 μm radiation emitted by the surface or low clouds is absorbed in the atmosphere and is not sensed by the satellite instruments. On the other hand, absorption by atmospheric gases is weak at 11 μm. Under clear-sky conditions, the measured 11 μm radiation originates primarily at the surface, with a small contribution by the near-surface atmosphere. Because the surface is

normally warmer than the upper troposphere, BT_{11} is normally warmer than the 6.7 μm brightness temperature; thus the difference, BT_{11} - $BT_{6.7}$, is normally greater than zero. Large negative differences in BT_{11} - $BT_{6.7}$ (less than -10 K) exist over the Antarctic Plateau and Greenland during their respective winters and are indicative of clear-sky conditions and the existence of strong low-level temperature inversions.

In polar regions, strong surface temperature inversions can develop as a result of longwave energy loss at the surface due to clear-skies and a dry atmosphere. Figure 7 is a temperature (solid-line) and dew point temperature (dashed-line) profile measured over the South Pole at 0000 UTC on 13 September 1995 and illustrates this surface inversion. On this day the temperature inversion was approximately 20 K over the lowest 100 m of the atmosphere. The surface temperature was more than 25 K colder than the temperature at 600 hPa. Temperatures over Antarctica near the surface can reach 200 K (Stearns *et al.* 1993), while the middle troposphere is ~235 K. Under such conditions, satellite channels located in strong water vapor absorption bands, such as the 6.7 μm channel, will have a warmer equivalent brightness temperature than the 11 μm window channel. A simulation of the HIRS/2 BT_{11} - $BT_{6.7}$ difference using Figure 7 temperature and moisture profile was -14 K. This brightness temperature difference between 11 and 6.7 μm is an asset for detecting cloud-free conditions over elevated surfaces in the polar night (Ackerman 1996a). Clouds inhibit the formation of the inversion and obscure the inversion from satellite detection if the IWP is greater than approximately 20 g m^2. A positive difference of BT_{11} - $BT_{6.7}$ is a cloud; differences smaller than -10°C are representative of cloud.

3.2.2 CO_2 Channel Test for High Clouds (Bit 14)

CO_2 slicing (Smith and Platt 1978; Wylie and Menzel 1989) is a useful method for sensing cloud amount and the height of clouds. CO_2 slicing is not a simple test and therefore is not incorporated into the cloud mask algorithm. A separate product, MOD06, includes results from CO_2 slicing. Simple tests using the CO_2 channels are useful for cloud detection, particularly high

clouds. Whether a cloud is sensed by these bands (MODIS bands 33-36) is a function of the weighting function of the particular channel and the altitude of the cloud.

MODIS band 35 (13.9 μm) provides good sensitivity to the relatively cold regions of the at-

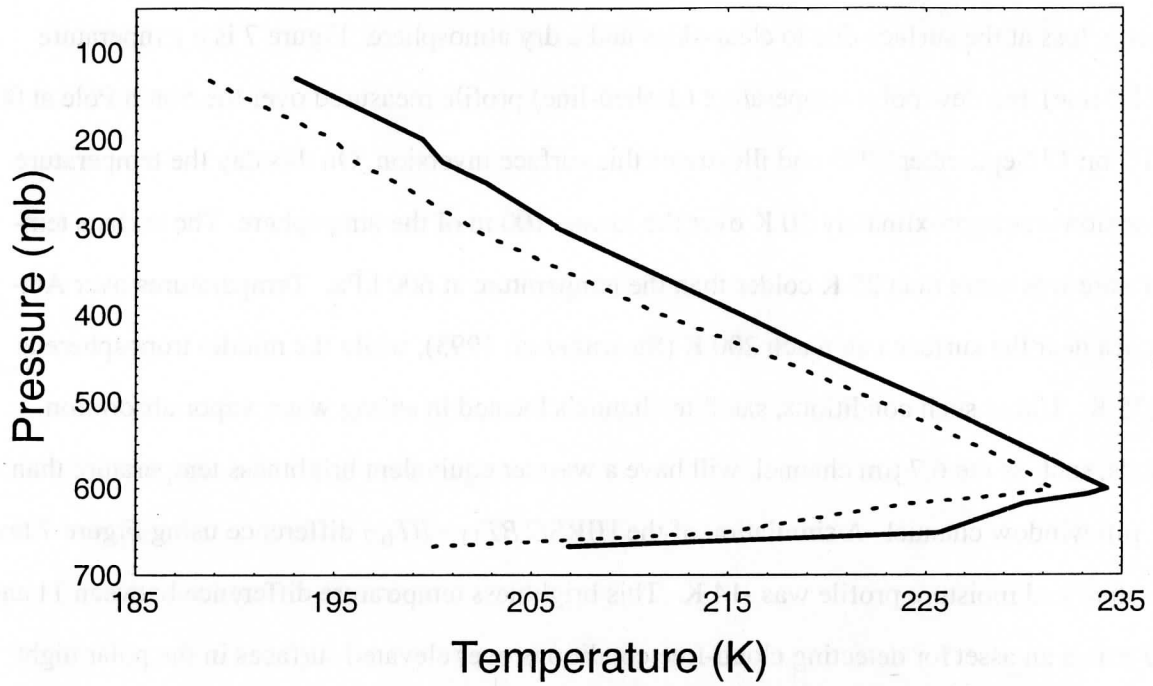

Figure 7. Vertical profile of atmospheric temperature and dew point temperature over the South Pole on 13 September 1995. The deep surface radiation inversion is useful for clear-sky detection.

mosphere. Only clouds above 500 hPa will have strong contributions to the radiance to space observed at 13.9 μm; negligible contributions come from the earth's surface. Thus a threshold test for cloud versus ambient atmosphere and a histogram test should reveal clouds above 500 hPa This test will be used in conjunction with the near infrared thin cirrus test discussed in Section 3.2.5.

Figure 8 depicts a histogram of brightness temperature at 14.0 and 13.6 μm derived from the HIRS/2 instrument (channels 5 and 6 respectively) using the CHAPS data set The narrow peaks at the warm end are associated with clear-sky conditions, or with clouds that reside low in the at-

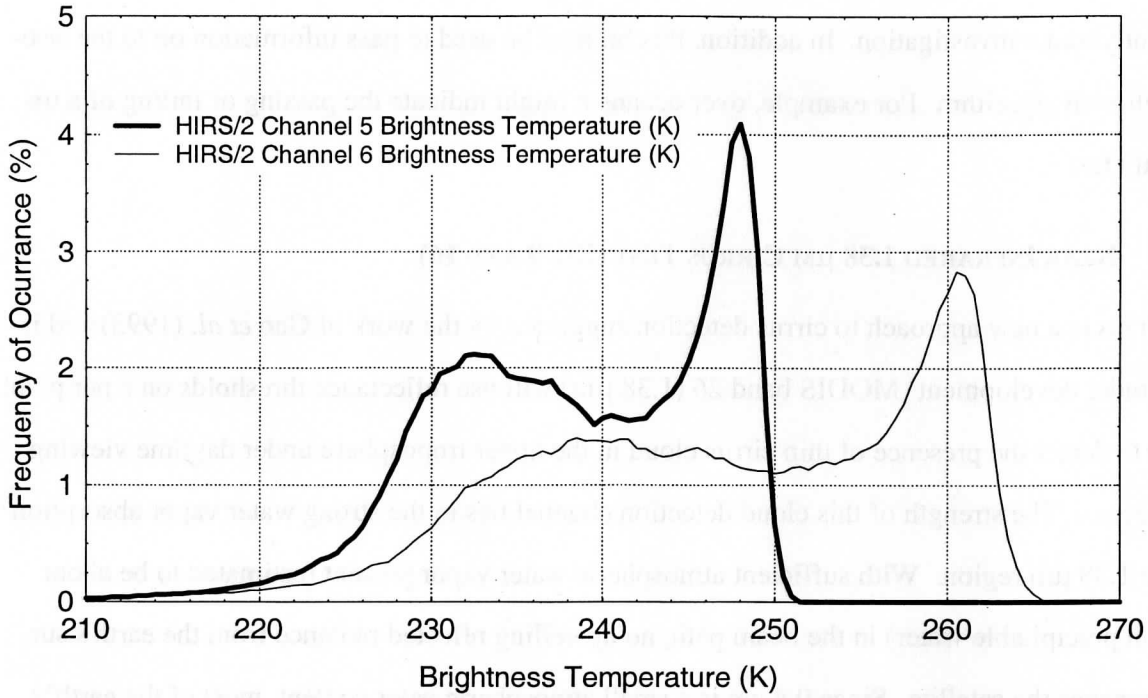

Figure 8. Histogram of BT_{14} and $BT_{13.6}$ HIRS/2 global observations for January 1994, where channel 5 (6) is centered at 14.0 (13.6) μm.

mosphere. Based on these observations the initial clear-sky threshold is 241 K with low and high confidence thresholds of 239 K and 244 K respectively. These thresholds will have to be modified for MODIS due to different spectral characteristics of the two instruments.

Under investigation is a brightness temperature difference test between 13.9 and 13.6μm. This difference test would be incorporated into the simple threshold listed above.

3.2.3 NON-CLOUD OBSTRUCTION FLAG (BIT 8)

A heavy aerosol laden atmosphere may result in a low confidence clear scene. Certain simple tests may be constructed that can indicate that the FOV is contaminated with an aerosol and not a cloud. For example, negative values of $BT_{11} - BT_{12}$ are often observed over deserts and can be attributed to the presence of dust storms (Ackerman 1996b). Under such conditions, provided BT_{11} is warm, the non-cloud obstruction bit (Bit 8) would be set. The tri-spectral technique may also be used to flag a region as potentially contaminated with volcanic aerosol. These tests are

currently under investigation. In addition, this bit may be used to pass information on to the aerosol retrieval algorithm. For example, over oceans it might indicate the passing or failing of a uniformity test.

3.2.4 NEAR INFRARED 1.38 μM CIRRUS TEST (BIT 9 AND 16)

This is a new approach to cirrus detection suggested by the work of Gao *et al.* (1993) and is still under development. MODIS band 26 (1.38 μm) will use reflectance thresholds on a per pixel basis to detect the presence of thin cirrus cloud in the upper troposphere under daytime viewing conditions. The strength of this cloud detection channel lies in the strong water vapor absorption in the 1.38 μm region. With sufficient atmospheric water vapor present (estimated to be about 0.4 cm precipitable water) in the beam path, no upwelling reflected radiance from the earth's surface reaches the satellite. Since 0.4 cm is a small atmospheric water content, most of the earth's surface will indeed be obscured in this channel. With relatively little of the atmosphere's moisture located high in the troposphere, high clouds appear bright; reflectance from low and mid level clouds is partially attenuated by water vapor absorption.

Simple low and high reflectance (normalized by incoming solar at the top of the atmosphere) thresholds will be used to separate thin cirrus from clear and thick (near infrared cloud optical depth > ~ 0.2) cloud scenes. These thresholds will be set initially using a multiple-scattering model with the assumption of no surface reflectance contribution to the satellite observed radiance, i.e., a dark background. Ben-Dor (1994) analyzed a scene from the AVIRIS to demonstrate that thin cirrus detection using 1.38 μm observations may be more difficult for elevated surfaces, dry atmospheric conditions, and high albedo surfaces. New injections of volcanic aerosols into the stratosphere may also impact this test. Any ambiguity of high thin versus low or mid level thick cloud will be resolved by a test on the cloud height using a CO_2 sensitive MODIS channel 35 (see section 3.2.2).

The MAS 1.88 μm channel is being used as a surrogate to MODIS channel 26 to gain experience with defining the thin cirrus bit. If the reflectance lies above the clear-sky threshold and

less than a thick cloud, then the thin cirrus bit will be set to 0 (thin cirrus detected). We subjectively define a thin cirrus as a cloud that has a small impact on the visible reflectance, enabling atmospheric correction to be applied to retrieve land surface properties (i.e., NDVI). A definition of thin cirrus in terms of optical depth is currently under investigation by the land and atmosphere MODIS science groups. Figure 1 demonstrates the potential utility of the 1.38 μm channel. The three panels are observations from the MAS during the SUCCESS field campaign. The MAS has a 1.88 μm channel which, like the 1.38μm channel, is near a strong water vapor absorption band. The panel to the left is a visible image that has been histogram normalized. The right panel is an 11 μm image where dark regions represent cold scenes. The center scene is the 1.88 μm image which clearly shows the presence of contrails that are difficult to see in the 11μm image and indiscernible in the 0.66μm image. Given the sensitivity to thin high clouds, the new MODIS 1.38 μm channel may detect a much larger cloud coverage than previous satellite algorithms have indicated. For this reason we are planning a level three product that keeps track of thin cirrus cloud.

The initial 1.38 μm reflectance thresholds will be based on theoretical simulations and adjusted using inflight data (clear air radiance map) after MODIS is launched.

3.2.5 Infrared Thin Cirrus Test (Bit 11)

This second thin cirrus bit indicates that IR tests detect a thin cirrus cloud. This test is independent of the thin cirrus flagged by the MODIS 1.38 μm channel. This test will apply brightness temperature differences tests to detect the presence of thin cirrus. The APOLLO scheme tests for the presence of thin cirrus using the split window analysis. Analysis of BT_{11}-BT_{12} and BT_8-BT_{11} is also effective in detecting the presence of thin cirrus clouds. During night over land the $BT_{3.7}$-BT_{12} is also used.

3.2.6 Detection of Cloud Shadows (Bit 10)

The detection of cloud shadows is a problem that has not been addressed adequately in the literature. Clear-sky scenes that are potentially affected by shadows can be theoretically com-

puted given the viewing geometry, solar azimuth and zenith angles, cloud edges distribution and cloud altitude. This approach requires too much CPU to run operationally, and all the information (e.g., cloud altitude) is not available to the cloud mask algorithm Therefore, as with clouds, solar reflectance tests will be explored for a cloud shadow detection algorithm Further work in this area has been initiated.

Currently, the cloud masking algorithm checks for shadows whenever a high confident clear scene is identified Shadow detection is based on reflectance at 0.94, 0.87 and 0.66 μm. A shadow is determined present if $R_{0.936} < 0.12$ and $R_{0.87}/R_{0.66} > 0.9$.

An example of the results of the shadow algorithm are shown in Figure 9 The left hand panel is a 0.66 μm image, and the right hand panel represents the masking shadow algorithm Dark regions are shadowed regions; gray, non-shadowed; and white, cloudy scenes.

We are also exploring using differences between $BT_{3.9}$ and $BT_{4.0}$ for shadow detection. Over land during the day, $BT_{3.9} > BT_{4.0}$ because there is more reflected solar energy at 3.9 μm. In shadowed regions the incident solar radiation at 3.9 μm is reduced, and the brightness temperature differences are smaller.

The issue of shadows caused by mountainous terrain has also been raised by the MODIS community. These shadows would be directly calculable from digital elevation maps, solar geometry considerations, and the cloud mask The first two considerations would indicate the FOVs where terrain shadow could occur; the last would determine whether sunlight is available to cause the shadow. The cloud mask will not separate shadows caused by terrain from those caused by clouds.

3.2.7 VISIBLE REFLECTANCE TEST (BIT 20)

This is a single channel test whose strength is discriminating bright clouds over dark surfaces (e.g., stratus over ocean) and weakness is clouds over bright surfaces (e.g., snow). Two different channels are used in this test dependent on the ecosystem The 0.66 μm (band 1) is used over oceans, land and snow/ice regions. The 0.88 μm reflectance test is also applied oversnow/ice and

desert scenes. The nominal thresholds are given below.

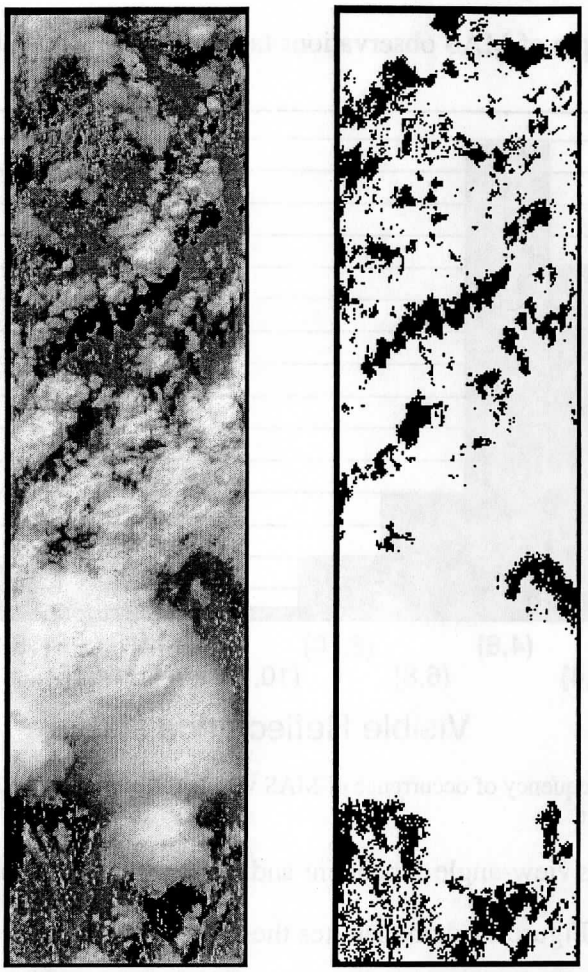

Figure 9. An example of the shadow testing using MAS data over the north slope of Alaska (13 June 1995). The panel to the right demonstrates the results from shadow testing, black regions are shadowed, white ar eas are cloudy or non-shadowed.

Table 6. Thresholds used for $R_{0.66} - R_{0.87}$ test for the MODIS cloud mask algorithm.

Scene Type	Threshold	High confidenc clear	Low confidenceclear
$R_{0.66}$			
Day ocean	0.07	0.065	0.08
Day land	0.16	0.14	0.18
Day polar	0.20	0.22	0.18
$R_{0.87}$			
Day polar	0.10	0.12	0.08
Desert	0.30	0.26	0.34

These thresholds are being set based on observations from AVHRR and MAS.

Figure 10 is an example of MAS observations taken over the tropical ocean.

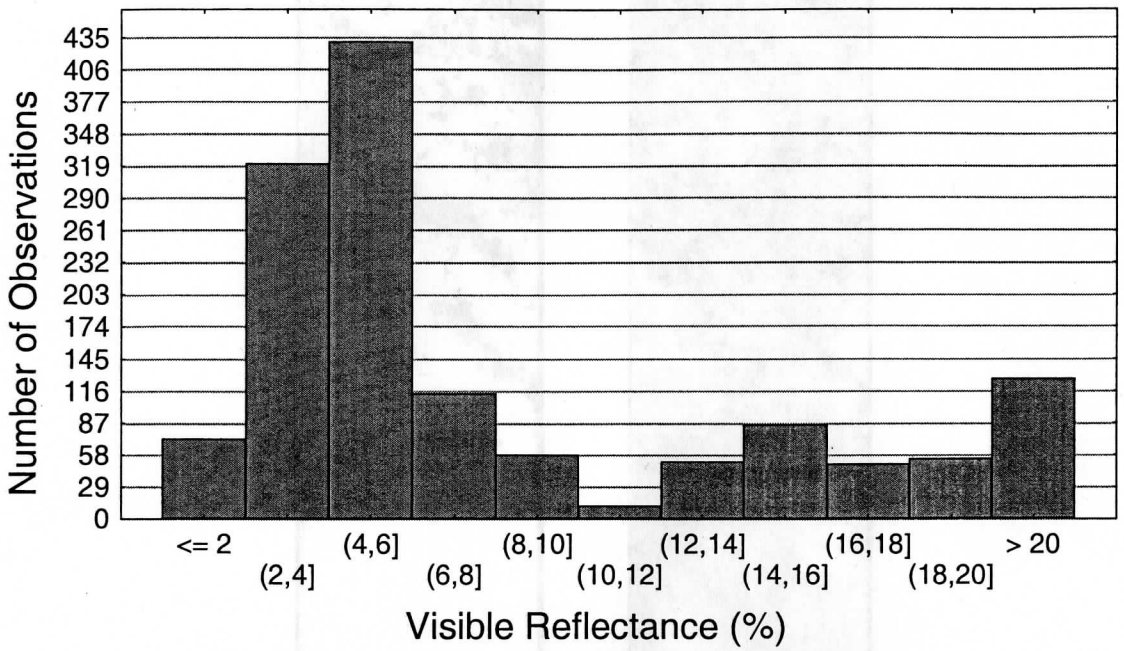

Figure 10. Histogram of the frequency of occurrence of MAS visible reflectance $R_{0.66}$ during part of the TOGA COARE experiment.

The reflectance test is view-angle dependent and is also applied in sun glint regions as identified by the sun glint test. Figure 11 demonstrates the angular dependence of the 0.66 μm reflectance test. A histogram analysis of the reflectances from AVHRR data was performed for 1° increments of reflected sun angle, θ_r. The histogram peak, the histogram mean, and the mean value plus 3 standard deviations about the mean reflectance were determined as a function of θ_r. The reflectance thresholds over water are therefore a function of θ_r.

3.2.8 Reflectance Ratio Test (Bit 21)

The reflectance ratio test uses channel 2 divided by channel 1 ($R_{0.87}/R_{0.66}$). This test makes use of the fact that the spectral reflectance at these two wavelengths is similar over clouds (ratio is near 1) and different over water and vegetation. Using AVHRR data this ratio has been found to be between 0.9 and 1.1 in cloudy regions. If the ratio falls within this range, cloud is indicated New analyses (McClain 1993) suggest that the minimum value may need to be lowered to about

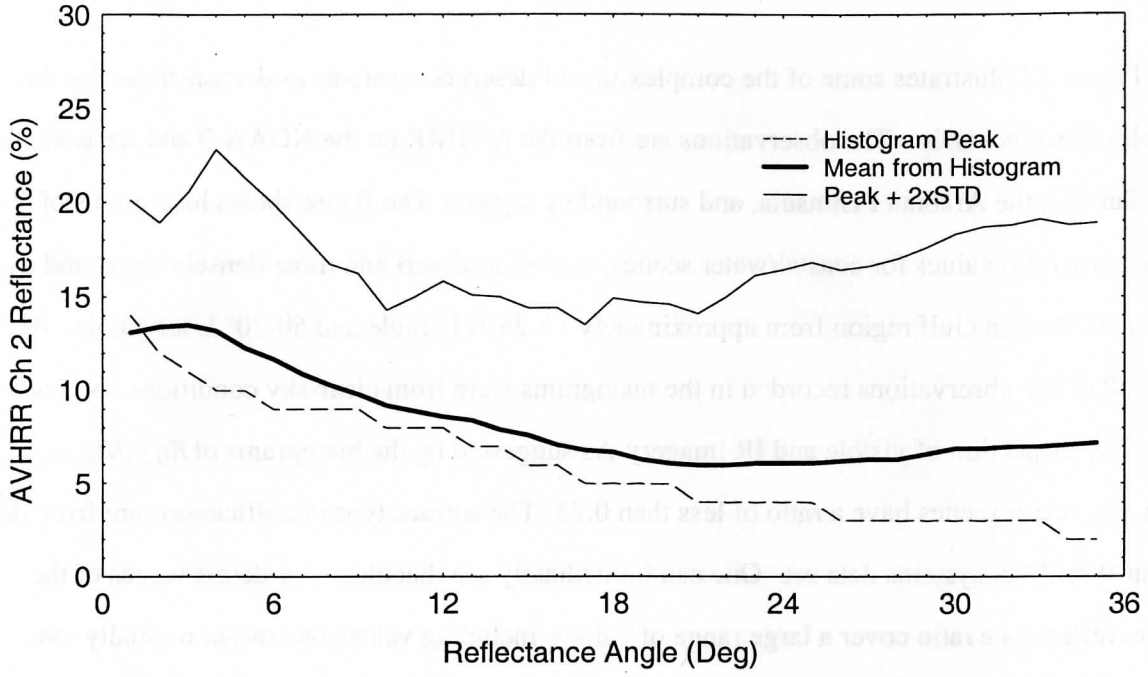

Figure 11. AVHRR channel 2 reflectance as a function of reflectance angle derived from NOAA-14 CHAPS data.

0.8, at least for some cases. For cloud-free ocean the ratio is expected to be less than 0.75 (Saunders and Kriebel 1988). This ratio is generally observed to be greater than 1 over vegetation. Adjustments to the ratio thresholds will be made as necessary for MODIS data and must be a function of the ecosystem as noted below.

Figure 12 illustrates some of the complexities of desert ecosystems as demonstrated by the visible reflectance ratio. The observations are from the AVHRR on the NOAA-9 and are over the Arabian Sea, the Arabian Peninsula, and surrounding regions The figure shows histograms of reflectance ratio values for coastal/water scenes, as well as desert and more densely vegetated areas in the Persian Gulf region from approximately 15-25° N latitude and 50-70° E longitude. Almost all of the observations recorded in the histograms were from clear-sky conditions, as determined by inspection of visible and IR imagery As suggested by the histograms of $R_{0.87}/R_{0.66}$, clear-sky ocean scenes have a ratio of less than 0.75. The surface type classifications are from the Olson World Ecosystems data set. One can immediately see that clear-sky desert values of the visible reflectance ratio cover a large range of values, including values one might normally associate with cloudy skies over vegetated surfaces. Also note the large amount of overlap between the desert and shrub/grassland categories. This figure shows that clear-sky spectral threshold tests need to be applied very carefully in arid regions and also points out the need for high-resolution ecosystem maps. This test will not be performed over desert, semi-desert, snow/ice, or some agricultural ecosystems.

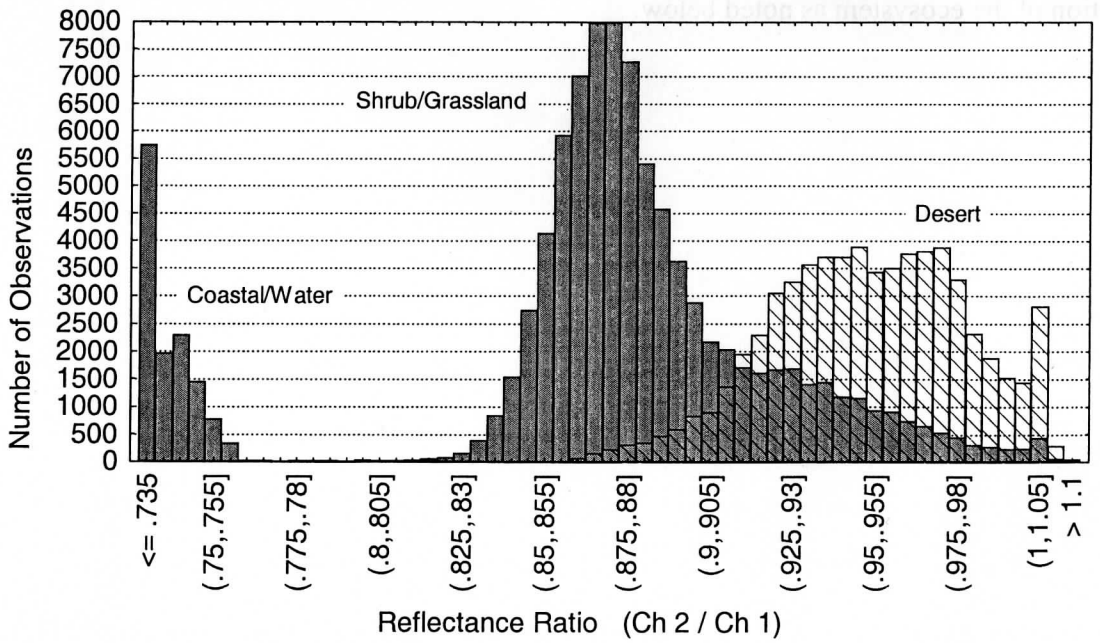

Figure 12. Histogram of the frequency of occurrence of the AVHRR reflectance ratio $R_{0.86}/R_{0.63}$ for a scene over the Arabian peninsula and Arabian Sea.

This reflectance ratio test may also be performed over water during the daytime. When applied in regions of possible sun glint, an angular dependence is included in the thresholds. These thresholds are based on analysis of AVHRR LAC and GAC data and the APOLLO algorithm. A histogram analysis of the visible ratio from AVHRR data was performed for 1° increments of reflected sun angle, θ_r. Figure 13 plots the histogram peak, the histogram mean, and the mean value plus 3 standard deviations as a function of θ_r. This analysis was used to set the dependence of the ratio test in the sun glint region. Mixed land and water fields-of-view produce a ratio that is similar to cloud.

The Global Environment Monitoring Index (GEMI) attempts to correct for atmospheric correction in deriving a vegetation index [*Pinty and Verstraete* 1992; *Leprieur et al.* 1996]. We have found this approach to be a better discriminator of cloud over land. The test,

$$\eta(1-0.25\eta)-\frac{r_{.87}-0.125}{1-r_{.87}}; \qquad \eta=\frac{2(r_{.66}-r_{.87})+1.5r_{.66}+0.5r_{.87}}{r_{.66}+r_{.87}+0.5}$$

is deemed cloudy if the value is less than a given threshold. This test does not work well over desert or coastal scenes, and is therefore not executed in these ecosystems.

3.2.9 NIR Reflectance Test (Bit 22)

Clouds that are low in the atmosphere are often difficult to detect with infrared techniques. The thermal contrast between clear-sky and low cloud is small and sometimes undetectable. Reflectance techniques, including the reflectance ratio test can be applied during daylight hours over certain ecosystems. Use of the MODIS band 18 at 0.936 μm also offers help under daytime viewing conditions. As documented by the work of Gao and Goetz (1991), this channel is strongly affected by low level moisture. When low clouds are present, they obstruct the low level moisture, hence increasing the reflectance in channel 18.

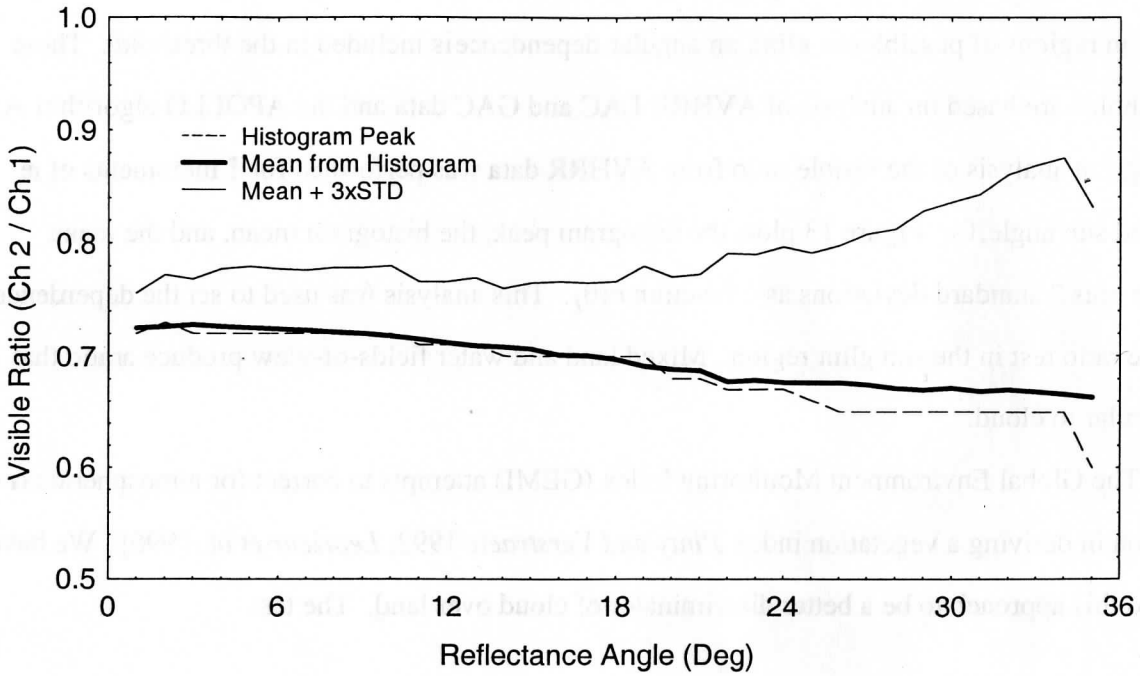

Figure 13. The dependence of NOAA-14 AVHRR reflectance ratio $R_{0.86}/R_{0.63}$ as a function of reflectance angle near the sunglint region over ocean.

Gao and Goetz (1991) proposed a ratio test using spectral channels near 0.94, 1.04, and 1.14 μm. Reflectance of many surfaces is linear between these wavelengths while absorption by water vapor is different across this spectral region, allowing discrimination between cloud and the ground using a band ratio

$$\frac{R_{0.94} + R_{1.14}}{2R_{1.04}}. \tag{21}$$

MODIS does not have channels at these three wavelengths; however, other water vapor channels in the near-infrared may prove useful for cloud detection over land A reflectance ratio of band 18 over band 16 (0.865 μm, an atmospheric window with surface reflectance characteristics similar to channel 18) is under investigation.

3.2.10 $BT_{3.7}$ - $BT_{3.9}$ TEST (BIT 23)

Brightness temperature difference techniques have been developed using difference between $BT_{3.7}$ and window channels at 11 and 12 μm. Over land the spectral variation in surface emissiv-

ity can present difficulties in applying the brightness temperature difference test To avoid this problem of surface emissivity, we are investigating using a brightness temperature difference between $BT_{3.7}$ and $BT_{3.9}$. During the daylight hours the difference increases because of the increased solar energy at 3.7 μm.

This difference technique is also being explored for shadow detection over surfaces that have a high reflectivity in this wavelength region.

3.2.11 CONFIDENCE FLAGS

Each of the tests above returns a confidence level ranging from 1 (high confidence that the pixel is clear) to 0 (high confidence that the pixel is cloudy) The individual confidence levels must be combined to determine a final decision on clear or cloudy We shall denote the confidence level of an individual test as F_i and the final quality flag as Q. There are different methods of combining these individual tests to yield the final quality flag (bits 1 and 2) We have experimented with a variety of methods of combining the confidence of individual tests The primary effect occurs on the boundaries of the cloud system.

The final cloud mask confidence could be derived as a product of all the individual tests:

$$Q = \prod_{i=1}^{N} F_i \tag{22}$$

Using this product assures that any test that is high confident cloudy (confidence of 0) will set the final cloud mask as cloudy. This is the proper formulation if all the tests are conditionally independent; however, this is not the case. Different spectral tests are sensitive to the same type of cloud conditions as discussed below. A disadvantage of this product approach is that one cannot improve on the confidence level by increasing the number of tests (N) since $F_i \leq 1$. Thus, if 5 tests have a confidence of 0.95, the final result is $0.95^5 = 0.63$.

The final quality flag could also be set to the minimum confidence level of all applied tests:

$$Q = \min[F_i]. \tag{23}$$

This approach would be a clear-sky conservative approach It makes it insensitive to any test

other than the test that produces the minimum. That is, no matter what the other tests are indicating, a single low confidence test will set the quality flag to obstructed On the other hand, a cloud conservative approach would be to select the maximum confidence level.

$$Q = \max[F_i]. \tag{24}$$

This can be improved upon by the following

$$Q = 1 - \prod_{i=1}^{N}[1 - F_i], \tag{25}$$

a clear-sky conservative case. A test with a high confident clear result sets the bit to clear.

Several tests are not independent of one another. For example, consider daytime over oceans in regions without sun glint. If stratocumulus clouds are present, they will likely be detected by the visible reflectance test, the reflectance ratio test and the $BT_{11} - BT_{3.7}$. These same tests will likely miss the presence of thin uniform cirrus clouds, which would probably be detected by the tri-spectral tests (combinations of $BT_{8.7}$, BT_{11}, and BT_{12}). Very thin cirrus clouds would best be detected by the 1.38 and 13.9 μm tests, two tests which have difficulty detecting low level clouds Because of this overlap in the type of clouds different tests detect, each test is considered in one of five groups. The five groups are:

Group I (Simple IR threshold test)

BT_{11}

$BT_{13.9}$

$BT_{6.7}$

Group II (Brightness temperature difference)

Tri-spectral test ($BT_{8.6}$ - BT_{11} and BT_{11} - BT_{12})

BT_{11} - $BT_{3.9}$

BT_{11} - $BT_{6.7}$

Group III (Solar reflectance tests)

$R_{0.66}$ or $R_{0.87}$

$R_{0.87}/R_{0.66}$

$BT_{3.7} - BT_{3.9}$

Group IV (NIR thin cirrus)

$R_{1.38}$

Group V (IR thin cirrus)

$BT_{3.7} - BT_{12}$

$BT_{11} - BT_{12}$

It is likely that the number of these groups will expand in version 2 of the cloud mask A minimum confidence is determined for each group,

$$G_{i=1,5} = \min[F_i]. \tag{26}$$

The final cloud mask is then determined from the product of the results from each group;

$$Q = \sqrt[N]{\prod_{i=1}^{N} G_i}\ . \tag{27}$$

This approach is still clear-sky conservative If any test is highly confident that the scene is cloudy ($F_i = 0$), the final cloud mask is $Q = 00$.

The algorithm is divided into ten conceptual domains according to surface type and solar illumination:

1. daytime land,
2. daytime water,
3. nighttime land,
4. nighttime water,
5. daytime desert,
6. nighttime desert,
7. daytime snow/ice covered regions, and
8. nighttime snow/ice covered regions.
9. daytime coastal (mixed land and water)

10. nightime coastal (mixed land and water)

"Daytime" is defined as a solar zenith angle$\theta_0 < 85°$ (and the instrument is in daytime mode) The "desert" classification is based on the 10-minute Olson World Ecosystems data set A USGS 1 km land/sea tag file is used for land/water discrimination For all observations within a given domain, it is generally expected that: (i) the same tests may be performed, and (ii) threshold values for each of these tests will not change. It is expected that more domains may be established in the future.

3.2.12 Infrared Window Radiance Spatial Uniformity (Bit 25)

The infrared window spatial uniformity test (applied on 3 by 3 pixel segments) is effective over water and is to be used with caution in other situations. Most ocean regions are well suited for spatial uniformity tests; such tests may be applied with less confidence in coastal regions or regions with large temperature gradients (e.g., the Gulf Stream). Various spatial tests exist such as the spatial coherence and the ISCCP space contrast test.

The spatial coherence test (Coakley and Bretherton 1982) is based on the assumption of a uniform background and single-layered, optically thick cloud systems The method is based upon the computation of the mean and standard deviation for a group of pixels using 11μm radiances. When the standard deviation is plotted versus the mean, an arch shaped structure is often observed. The warm pixels with low values of standard deviation are assumed to be clear regions The clear-sky FOVs can be selected as those within a standard deviation threshold (which is fixed at a small value) of the warm foot of the arch. Note that the derived clear-sky foot of the arch should have a temperature consistent with the thresholds derived using the individual FOV tests.

The ISSCP space contrast (sc) test, described in Rossow and Garder (1993), is similar to that of spatial coherence and is physically based upon the fact that clear pixels tend to be warmer than cloudy pixels and exhibit less spatial variability First, for a small local region the pixel with the largest brightness temperature (BT_{11}^{max}) is found. All pixels colder than the spatial contrast (BT_{11}^{max} - Δ_{sc}) value are labeled as cloudy; all others, including the warmest pixel are labeled as

undecided. The size of the contrast threshold must be larger than the magnitude of natural variation at the surface and smaller than that caused by clouds. Values of Δ_{sc} near 3.5°C are common over ocean regions. It is important that the class of pixels be identical and that the size of the region be chosen carefully. When extending into coastal regions and land regions containing mixed land and water, pixels are excluded from this test since the inherent contrast between land and water surface radiances would dominate the results. For regions that are too large, there is increased likelihood of spatial variations in surface parameters. The shape of the test regions can also be important since meridional gradients in surface temperature generally are larger than zonal gradients.

Similar spatial tests will be incorporated into the MODIS cloud mask for uncertain obstructed FOVs. The specific test will likely depend on how the data stream is structured regarding the ease of compositing pixels over geographic regions. Uniform stratus can also give the appearance of a uniform ocean, thus the spatial tests must often complement the threshold tests (e.g., the tri-spectral test).

The MODIS cloud mask currently uses a spatial variability test over oceans and large lakes. The tests are used to modify the confidence of a pixel being clear. If the confidence flag of a pixel is < 0.95, the variability test is implemented. If the difference between the pixel of interest and any of the surrounding pixel brightness temperatures is >0.5°C, the scene is considered variable and the confidence lowered.

Surface temperature variability, both spatial and temporal, is larger over land than ocean, making land scene spatial uniformity tests difficult. MODIS spatial uniformity tests over land will be constrained to similar ecosystems in a given geographic regime. These tests have yet to be developed.

3.2.13 Visible Reflectance Uniformity Test (Bit 25)

The reflectance uniformity test (similar to CLAVR) is applied by computing the maximum and minimum values of MODIS band 1 (0.66μm) or band 2 (0.87 μm) reflectances within a 3×3

pixel array. Pixel arrays with band 1 reflectance differences greater than threshold 1 (around 9%) over land or band 2 reflectance differences greater than threshold 2 (possibly 0.3%) over ocean are labeled in CLAVR as mixed (Stowe*et al.* 1995). The value over ocean is low because a cloud-free ocean is almost uniformly reflective, while non-uniformity is assumed to be caused by cloudiness. This test will be refined for MODIS applications: first, by requiring that the ecosystem be the same for the pixel array; second, the mean and standard deviation of reflectance values for each ecosystem will be computed as a function of season; and third, the reflectance threshold will be a function of satellite zenith and view angle This test will only be applied to uncertain obstructed FOVs.

3.2.14 250 M VISIBLE TESTS (BIT 32-47)

The reflectance test (Section 3.2.7) and the reflectance ratio test (Section 3.2.8) are used for clear-sky determination of the 250 m resolution channels These tests will be a function of ecosystem and will be angularly dependent. The results are a simple yes/no decision and do not incorporate the results from the 1 km resolution tests.

3.2.15 CLEAR-SKY RADIANCE COMPOSITE MAPS

Composite maps have been found to be very useful by ISSCP. The MODIS cloud mask will also rely on composite maps, but probably to a lesser extent since the advantages of higher spatial resolution and more spectral bands will change the application and the need The ISCCP developed clear-sky reflectance and temperature composites detect clouds over a given 32-km square area by comparing the pixel radiances to the clear-sky composite values with some added thresholds (Rossow and Garder 1993). These composites are based on the observation that variations in visible clear reflectances usually are smaller in time than in space, especially over land. Variations of surface solar reflectances generally are smaller than variations of cloud reflectances Therefore, it is assumed that the characteristic shape of the darker part of the visible radiance distribution is at most weakly dependent upon surface type (Sèze and Rossow 1991a, b). The mini-

mum reflectance value for band 1 is used to estimate clear values Corrections to the minimum values are inferred from the shapes of the visible reflectance distribution associated with different surface types.

ISCCP (Rossow and Garder 1993) classifies scenes into nine types depending on the time scale and magnitude of the clear-sky radiance variations ISCCP employs clear-sky radiance maps composited over different time periods For example, the clear-sky reflectance values for land and ocean regions whose surface characteristics vary the most rapidly are estimated using short-term composite maps. Sparsely vegetated surfaces generally exhibit more spatial variability than heavily vegetated surfaces (Matthews and Rossow 1987) but are also generally less cloudy For sparsely vegetated arid regions a long-term composite map is usedto refine the clear-sky reflectance thresholds. They also tend to be more uniform from one geographic location to another. For vegetated regions the clear-sky reflectance maps are composited over a short time interval . The IR clear-sky maps are also composited at different time scales, depending on surface type.

One of the primary difficulties in using the ISCCP approach as currently formulated is the angular dependence of clear-sky reflectance Although cross-track scanning sun-synchronous satellites such as the NOAA AVHRR repeat the angular viewing conditions on a regular 11-day cycle, the solar zenith angle slowly varies and the cloudiness conditions may prevent the determination of clear-sky reflectance at some points in the 11-day cycle ISCCP relies on an empirical bidirectional reflectance model for clear-sky ocean (Minnis and Harrison 1984a) reflectance Thus, over ocean, the angular problems are minimized Over land, ISCCP assumes isotropic clear-sky reflectance although it has been established that the anisotropy of land scenes is significant (e.g., Kriebel 1978; Tarpley 1979; Minnis and Harrison 1984b; Suttles *et al.* 1988). For $\theta_0 < 85°$ the vegetated land clear-sky anisotropic reflectance factor $R(\kappa, \theta_0, \theta, \phi)$, where κ is a surface type, can vary from 0.6 to 1.6 (e.g., Suttles *et al.* 1988) for $\theta < 70°$. Thus, there is the potential for clear-sky reflectance errors as great as 300% if one assumes that the measurement taken at a particular set of viewing conditions represents the reflectance at all viewing angles for a given value of θ_0. Systematic changes of albedo with θ_0 are also not considered for land surfaces. The

reflectance anisotropy over snow and desert scenes is generally not as great as that over vegetated surfaces, but the absolute changes in reflectance are as great because of the higher albedos over these surfaces. An advantage of ISCCP is that a time series of images is used in cloud screening.

Some features of the ISCCP methodology cannot be applied to MODIS due to the fact that processing will be accomplished in near-real time; however, composite clear-sky infrared observations over ocean surfaces will be used to increase confidence of clear/cloudy scene identifications. The lack of reflected solar energy during nighttime processing has the overall effect of decreasing confidence in the cloud mask output. We can restore a certain amount of confidence by use of clear-sky data maps. A prototype algorithm has been formulated and tested for use with nighttime ocean observations using AVHRR data. The method and test results are presented below.

We propose to use cloud-cleared 11 μm brightness temperatures from daytime processing as input to the nighttime cloud masking algorithm. Single-pixel, high quality (confidence of unobstructed surface > 0.95) clear-sky values of brightness temperature will be obtainable by the MODIS cloud masking algorithm during daylight hours when solar reflectance is available. These values will be incorporated into an eight-day composite equal-area grid at 25 km resolution. The file containing the composite data will be updated after each day is processed; that is, the clear-sky observations from day one of the previous eight days will be eliminated and those from the current day will be added. Eight days was chosen as the integration time because this corresponds to the precession period of high-inclination polar orbiting satellites. Seasonal changes in ocean temperature will also be adequately represented. Mean, maximum and minimum values of 11 μm brightness temperatures will be made available to the nighttime algorithm.

Even though the final output of the cloud mask is given by only four confidences of non-obstructed surface (> 0.99, > 0.95, > 0.66, and obstructed), internally the algorithm has four additional confidence levels (> 0.34, > 0.05, > 0.01, and < 0.01). One of these seven numeric confidence values is assigned to each single pixel processed. After this initial assessment, each pixel's 11 μm brightness temperature will be compared to the daytime composite values for the appo-

priate gridbox. This comparison is designed to detect inconsistencies between the instantaneous pixel IR measurement and an expected confidence value (for that measurement) based on the previous eight days of data. If the observed value is less than the minimum composite value then the pixel confidence is lowered by two levels. If the observation is greater than or equal to the minimum but less than the mean then the confidence is downgraded by only one level. In the same way, confidences are raised when instantaneous brightness temperatures are greater than the mean and/or maximum composite values. This method allows for lessened confidence in the basic algorithm when applied in the absence of solar reflection but also recognizes the validity of the IR threshold tests. It also has the effect of eliminating many mid-range confidences (>0.34, > 0.66) and adding them to either higher or lower percentage categories.

It should be noted that, in this simple and straightforward implementation of clear-sky composite maps, there are several common problems that are not explicitly addressed. One problem is change in air mass characteristics that occurs regularly in mid-latitudes and often at higher frequency than eight days. Changes in lapse rate and total column precipitable water amounts could lead to invalid composite values for any given day. However, since the entire algorithm is tuned as much as possible (via threshold test confidence intervals) to detection of *clear* sky, as opposed to *cloudy* sky, it is anticipated that errors of this kind will not result in large numbers of false clear-sky identifications. Another possible source of error is the limb-darkening effect. Problems could occur when comparing instantaneous brightness temperatures from large viewing zenith angles with composites taken primarily from near-nadir views and vice versa. In the former case, lessened confidences near the limb are possible but this is a general problem in remote sensing with scanning instruments and is not necessarily an error. Discriminating clear-sky from clouds is more difficult at limb view angles even for expert image analysts. In the latter case, the same argument is made as before, that the cloud mask algorithm is (properly) tuned towards maximum cloud detection so that it is more likely to falsely identify a cloud than clear sky.

The algorithm was tested using GAC data collected during July 1985 by AVHRR on board the NOAA-9 polar orbiting satellite. The region encompassing 60° north to 40° south latitude

and 40° west to 20° east longitude was selected for the test domain. This area was chosen because of the large range of ocean temperatures as well as atmospheric and cloud conditions found within it. The AVHRR cloud mask algorithm is necessarily different from that of MODIS because of a much more limited set of spectral channels as well as much wider bandwidth. However, because the orbital characteristics, areal coverage, and spatial resolution are comparable, AVHRR was chosen as the input for the test.

First, daytime clear-sky ocean brightness temperatures were collected during the first eight days of the month with each day's results stored separately. Next, nighttime ocean clear-sky results were generated for the second eight days of the month with no information supplied to the algorithm from the daytime. Daytime results were also compiled as during the first set of days. Finally, nighttime observations from the second eight days were processed again, but this time with the appropriate daytime brightness temperature information made available to the algorithm, as detailed above.

Some results of the test are illustrated in Figure 14, which shows brightness temperature histograms of the gridbox means, minima, and maxima for the second eight day period from the region within 0° to 30°S and 10°W to 30°W. Means were calculated from one sum over the period, and minima and maxima were the two extreme values. The bottom graph shows results with no input from daytime processing. Low level clouds are the predominant type in this part of the world in July and are often difficult to detect at night. Note the skew of the mean and minimum histograms toward colder temperatures. This generally indicates cloud contamination. The secondary maximum that peaks between 275 and 280 K in the minimum histogram indicates some persistent low cloud feature that went consistently undetected by IR threshold and 11 μm variability tests. The top graph shows the improvement after adding temperature information from daytime processing. All three of these histograms show a more or less normal distribution as one would expect from clear sky measurements. Also note that the maximum temperature histograms are very nearly identical in both graphs, again as expected.

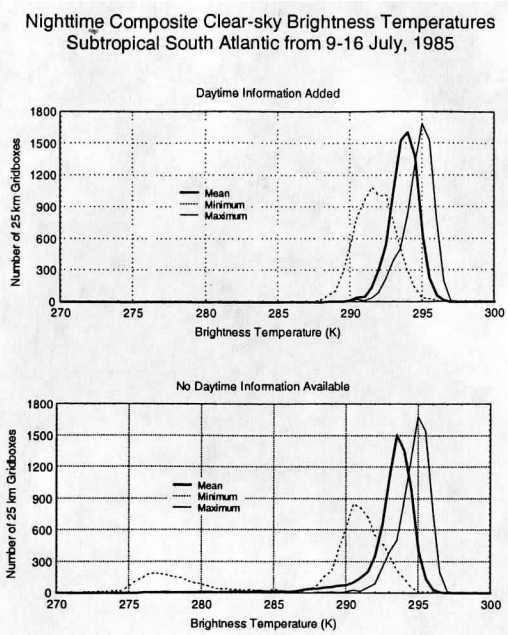

Figure 14 . Frequency of occurrence of clear-sky BT_{11} including daytime observations (top) and excluding daytime observations (bottom). These results were obtained over the subtropical south Atlantic from 9-16 July 1985.

Figure 15 shows representations of both day and night composite clear-sky (confidence of non-obstructed surface > 0.95) maps at 0.5° resolution. Each color represents a 4 K range with warmest temperatures being red (296-299 K) and decreasing in 4 K increments through green, blue, and navy. A few very cold surface values are indicated by tan (272-275K) and beige (268-271 K). Gray areas are land surfaces or indicate regions for which no clear sky was identified by the algorithm. Both maps show the same large-scale features in ocean surface temperature. It is obvious, however, that the extra information provided by reflected solar energy during the daytime results in a smoother, more continuous field. This figure shows that the nighttime algorithm has more problems finding clear sky in regions dominated by low level clouds, however, it can be seen that this results mainly in low confidences of clear sky rather than in biased clear-sky mean brightness temperatures. It should also be pointed out that the number of orbits processed differed between day and night so that even under perfect conditions, the two maps would not be

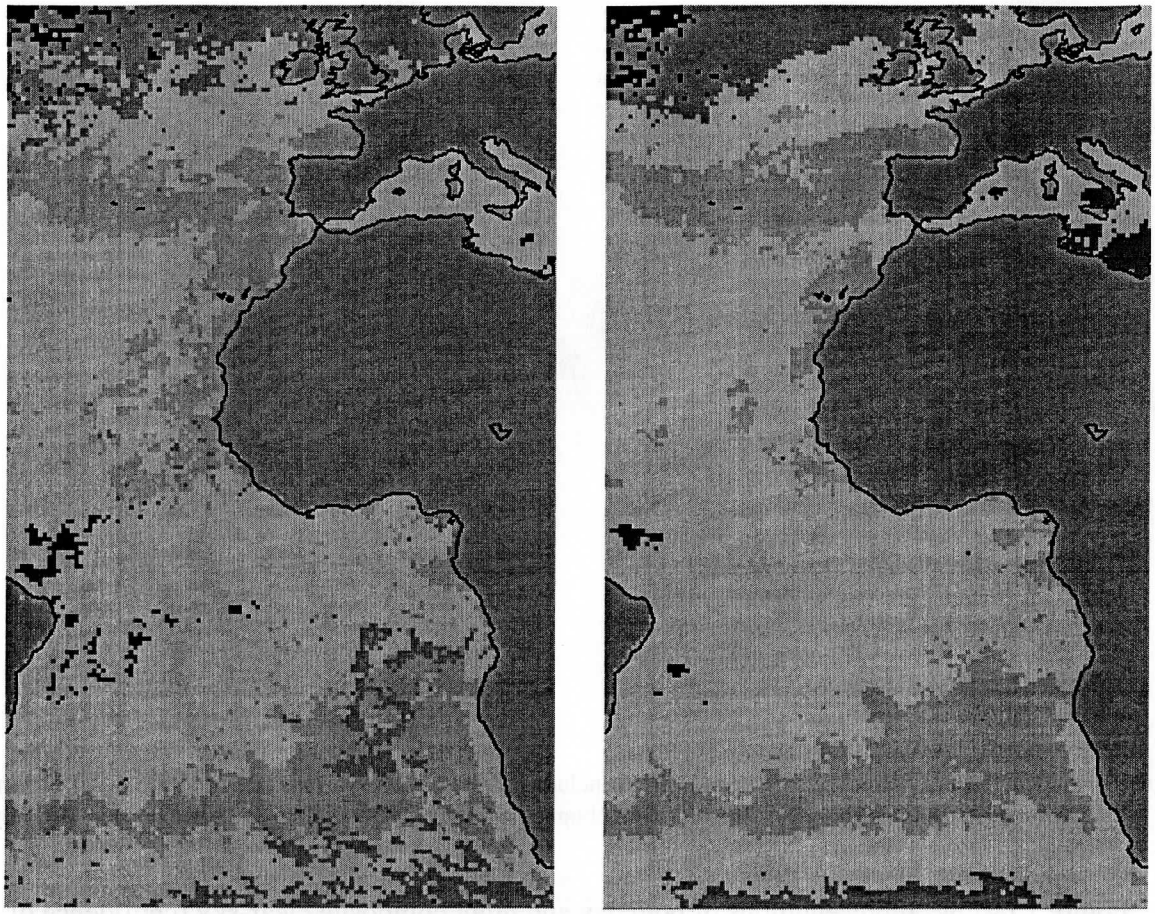

Figure 15. Clear-sky composite maps of brightness temperature (11 μm) from the AVHRR cloud mask for night (left) and day (right). The composite only includes those pixels with confidence > 0.95. Each color represents a range of 4 K, and ranges from red (296-299 K) through dark green, green, blue, and navy (273-276 K).

identical.

Based on this preliminary test, the incorporation of clear-sky brightness temperature maps into the MODIS cloud masking algorithm seems a feasible and straightforward. In addition to having many more spectral channels available, the MODIS processing will also use surface temperatures from forecast model output. With proper treatment, the model information could be a valuable addition in regions which are very cloudy. Indeed, one aspect of the algorithm that deserves further study is the compositing time of daytime clear-sky observations. In regions that are normally very cloudy, such as the North Atlantic, more time may be necessary to acquire a reasonable numbers of samples of clear sky temperatures.

4.0 Practical Application of Cloud Detection Algorithms

In summary, the cloud mask algorithm is divided into eight conceptual domains according to surface type and solar illumination: daytime land, daytime water, nighttime land, nighttime water, daytime desert, nighttime desert, and daytime and nighttime snow or ice surfaces. "Daytime" is defined as a solar zenith angle $\theta_0 < 85°$. The "desert" classification is based on the 10-minute Olson World Ecosystems data set. A USGS 1 km land/sea tag file is used for land/water discrimination. For all observations within a given domain, it is generally expected that (i) the same tests may be performed, and (ii) threshold values for each of these tests will not change. As yet, there are no tests defined for nighttime snow/ice or desert observations. The default nighttime land algorithm is substituted in both cases (cf. Table 4). It is expected that more domains will be established in the future.

Once a pixel has been assigned to a particular domain, the spectral data corresponding to that location are subjected to a series of threshold tests designed to detect the presence of clouds in the instrument FOV. These tests are the heart of the cloud mask algorithm. There are several types of tests, none of which are equally good at detecting all cloud conditions. For example, some are more reliable for low cloud or thin cirrus cloud detection, while others are better at finding any kind of optically thick cloud. Accordingly, tests that indicate similar cloud conditions are grouped together to obtain several intermediate results that are then combined to form a final cloud mask value. The tests are grouped so that independence between them is maximized. All tests which detect thin cirrus might make up a group, for example, while those which find high, cold clouds would form another, and low-level cloud detection tests could make a third set. Of course, few if any spectral tests are completely independent of all other tests.

The result of each spectral threshold test is expressed as a "confidence" that indicates the strength of the observed radiance signature compared to that which is expected for the cloud condition in question. For example, one very fundamental test performed for water surfaces is the "cold cloud test." Over open water any scene with an observed 11 μm brightness temperature

colder than ~270 K must be at least partially cloudy. Therefore, the threshold value for this test is set at that value. The actual cutoff temperature for any given FOV varies slightly, however, because of differing amounts of atmospheric water vapor attenuation due to changes in actual water vapor content or instrument view angle. Consequently, a "confidence window" is constructed with boundaries at 267 and 273 K. Since the ultimate goal of the algorithm is to specify a confidence of clear-sky, an observed brightness temperature of < 267 K is defined to have 0 confidence while a measurement of > 273 K has a confidence of 1. *Note that this confidence does not yet refer to clear-sky conditions, only to the particular condition tested.* In this case it indicates only the extent of confidence that the FOV did *not* contain significant amounts of opaque, cold clouds Observations between 267 and 273 K result in confidences ranging linearly between 0 and 1 Figure 4 showed an example of the relationship between test thresholds and confidence boundaries Note that the threshold value corresponds to a confidence of 0.5.

When all tests within a group have been performed, the minimum resulting confidence from among them is taken to be representative of that group. Then the other groups of tests are performed with group confidences determined in the same way These confidences indicate absence of particular cloud types. A final step is to combine the group confidences, assumed to be independent, by multiplying them together and taking the Nth root (equation 27) Only at this point does the confidence value reflect the surety of clear-sky conditions.

Using this algorithm, most observations have either high confidences (> 0.95) or very low confidences (< 0.05) of unobstructed views of the surface. There are always those difficult scenes, however, that result in intermediate values of the cloud mask These tend to be found at cloud boundaries, or where low clouds are found over water surfaces at night, or over certain land surfaces such as desert or other sparsely-vegetated regions. In these cases (final confidence > 0.05 and < 0.95), spatial and/or temporal continuity tests are conducted. Currently, only spatial continuity testing has been implemented and this only for water surfaces 11 μm brightness temperature differences between the pixel of interest and the surrounding eight are checked for consistency. If all the differences are less than 0.5 K, the confidence is adjusted upward by one

"level" (e.g., > 0.66 to > 0.95). We also plan to use a "clear-sky data map" for testing temporal continuity in order to better discriminate clear-sky scenes from any surface type This processing is still in development.

4.1 Ancillary Data Set Requirements

A number of preprocessing steps will be made before the cloud masking algorithm is applied First, each pixel in the scene will be tagged as being land or water, and if land, a land/water percentage. Second, each land pixel will be classified as to its ecosystem and its elevation will be designated as relatively flat, valley, isolated mountainous region, low mountains or hills, generally mountainous, or extremely rugged mountains From the MODIS snow mask each pixel will be designated as probably/probably not snow or ice covered (MOD10 and MOD29).

Information on surface temperature and sea state will be sought from surface observations, Reynolds blended analysis, and DAO or NCEP model 3-hour surface analyses of temperature and wind speed. Eventually, the MODIS surface temperature over land (MOD11) and over ocean (MOD28) will be used instead.

4.2 Implementation of the Cloud Mask Algorithms

4.2.1 Outline of Cloud Mask Algorithm

The hierarchical approach used in version 3 of the cloud mask is:

(1) Determine if the pixel is of a land or water scene.

(2) Determine the ecosystem type.

(3) Determine if pixel is in a sun glint region.

(4) Determine if the pixel is in a day or night regime.

(5) Retrieve information from snow cover and ice data base.

(6) Update snow cover by implementing simple Normalized Difference Snow Index (NDSI).

(7) Apply appropriate single FOV masking tests and set initial unobstructed FOV determination for the given domain. Initial confidence flag is assigned for each test result, depending on its

relative position to the threshold (see Section 3).

- For daytime testing, solar zenith angles are constrained to be less than 85°.
- Ocean tests are applied between 60°N and 60°S and for large lakes.
- Sun glint occurs when the reflected sun angle lies between 0° and 36°. Reflectance of open water is strongly influenced by illumination and viewing geometry. Sun glint is also a function of surface wind. Wind speed will be available but is currently not used in estimating the sun glint area.
- The land algorithm is applied to non-desert and non-water areas not covered with snow, including islands.
- The desert algorithm is applied to desert ecosystems.
- The snow/ice algorithm is applied to regions with snow on the ground.
- For the single pixel clear-sky determination, 14 single FOV tests are implemented and an obstructed/not obstructed bit set (0 for obstructed, 1 for clear) for each test (bits 8-23).

(8) The single FOV cloud test results are grouped and the minimum of each group determined.

(9) The group minimums are then multiplied together, and the N^{th} root taken (where N represents the number of groups) producing the initial cloud mask (Section 3.2.11). If any of the individual tests are high confidence cloudy (clear confidence of 0), the product is zero.

(10) If confidence level is still uncertain ($0.05 < Q < 0.95$), use spatial uniformity tests on 3×3 pixel regions (Currently not implemented over land).

- Spatial IR variability test applied with band 31 using $\Delta_{sv} = 0.50$ K over water.
- Adjust quality flag if appropriate by increasing or decreasing confidence levels.

(11) Check for temporal consistency (currently applied over water).

- Compare with clear-sky composite.
- Adjust quality flag if appropriate by increasing or decreasing confidence levels

(12) Update clear-sky radiance (composite) maps

4.2.2 CLOUD MASK EXAMPLES

The cloud mask algorithm has been applied to several data sets selected by the cloud mask group, as well as scenes selected by other science team members This section includes several examples of the output from the current version of the MODIS cloud mask. It is not intended as a validation section, but rather as a visual indication of the success and problems of the current version. Other examples are available on the World Wide Web(http://cimss.ssec.wisc.edu/modis/cldmsk/newmask.html).

AVHRR cloud mask data sets

Figure 16 is a three panel image of NOAA-14 AVHRR GAC observations The left most panel is a channel 1 (0.6 μm) image and the middle panela channel 4 (11 μm) image. The scene is over the tropical Pacific Ocean The resulting cloud mask output file is represented in the right most panel. The legend is as follows

Black: High confident clear (bits 1-2 equal 11)

Dark Gray: Probably clear (bits 1-2 equal 10)

Light Gray: Maybe dear (bits 1-2 equal 01)

White: High confident obstructed (bits 1-2 equal 00)

Notice that the confidence in clear-sky scene tends to drop over the sun glint region, as it is difficult to detect clouds in areas affected by sun glint The additional channels of MODIS should improve our clear-sky detection capabilities in sun glint regions.

Another 3 panel image of NOAA-14 AVHRR GAC observations is shown in Figure 17 This scene includes parts of North Africa and the Atlantic Ocean The *blocky* structure of the

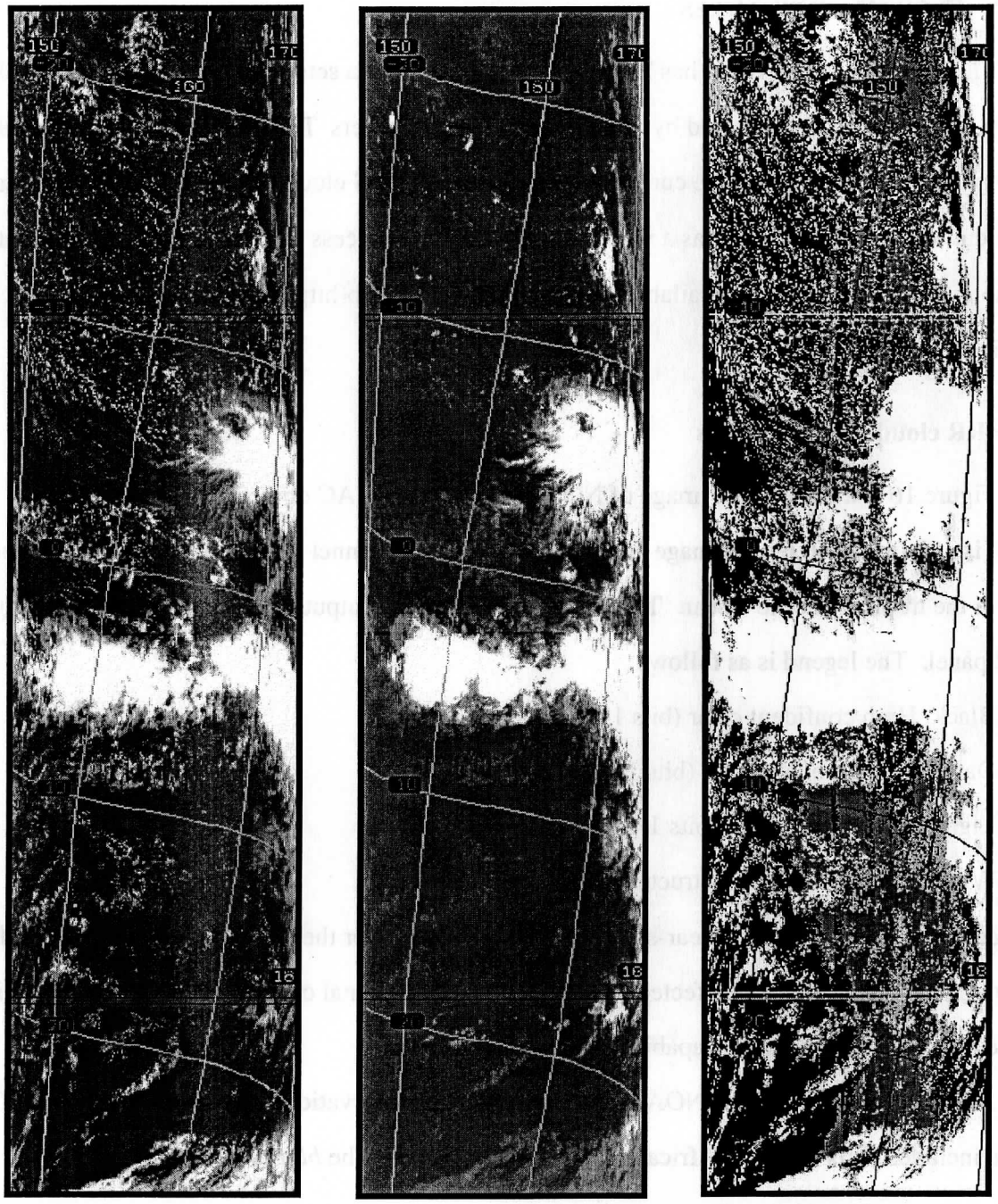

Figure 16. An example of the cloud mask derived from AVHRR data for a scene over the Pacific Ocean (right hand panel), together with images from two of the AVHRR bands used in generating the mask. In the cloud mask results, black denotes high probability clear, white denotes high probability cloudy, and shades of gray lay in between.

cloud mask over land results from the 10-minute ecosystem map; land spectral tests are being applied to desert regions. This points to the need for an accurate global 1 km ecosystem map,

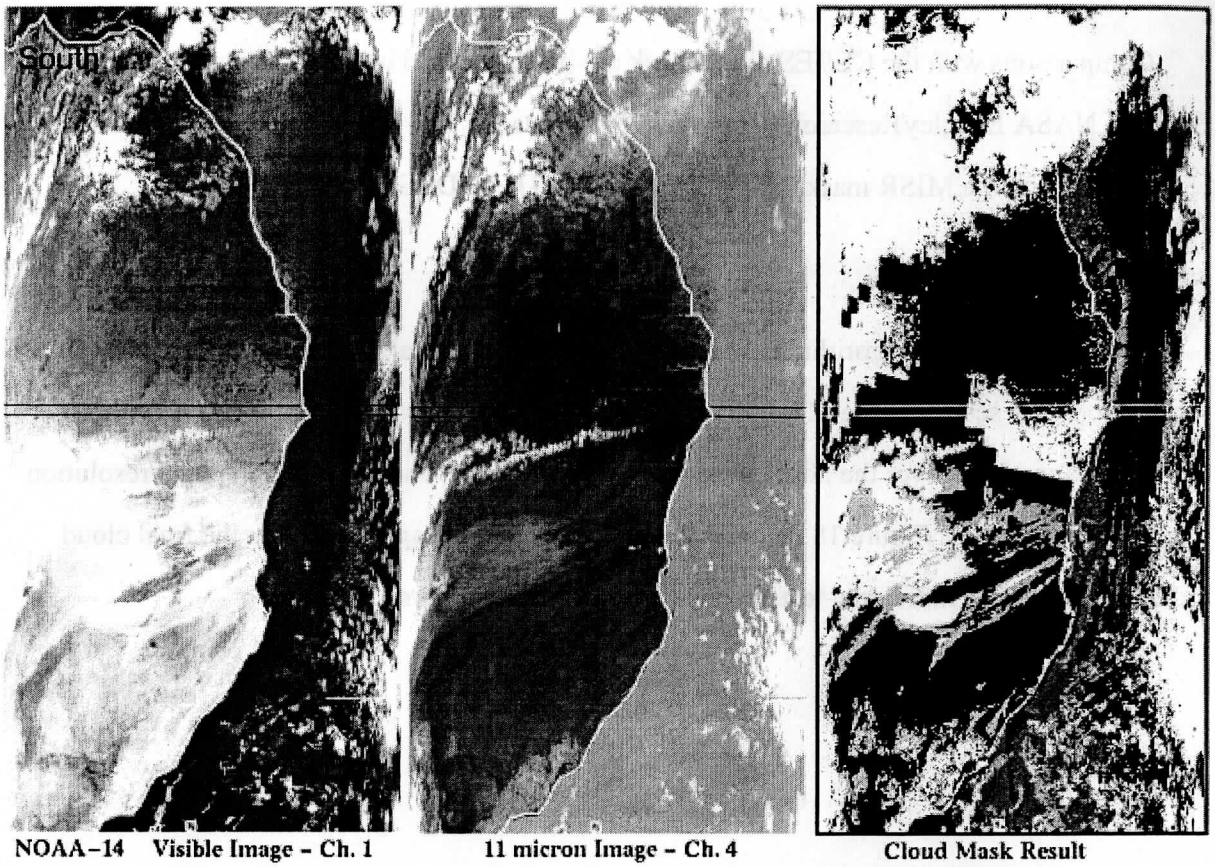

Figure 17. An example cloud mask, together with images at two AVHRR bands, obtained over the eastern Atlantic and west Africa. South is at the top of the figure.

one that is consistent with the land/sea map. The high confidence obstructed scenes over the Saharan region is a dust storm. Most of this dust storm has negative values of BT_{11} - BT_{12}, resulting in the aerosol obstruction bit being set to zero (bit 8 in the mask output file).

Future AVHRR data processing

An entire month of AVHRR GAC data has been obtained from the AVHRR Pathfinder Program. This data set is being processed to gain further experience with implementing clear-sky radiance maps.

Dr. Yoram Kaufman, a MODIS science team member, has provided us with several AVHRR LAC scenes. We are applying the AVHRR cloud mask to this data set. His group will then validate the mask and make recommendations for improvements. Other MODIS science team members are encouraged to submit data for assessing our current capabilities.

Comparisons with the CERES cloud mask are being planned in coordinated with Dr Bryan Baum of NASA Langley Research Center. Comparisons are also planned to compare the MODIS cloud mask with the MISR mask, being developed by Dr. L. Di Girolamo.

MAS cloud mask data sets

The cloud masking algorithm has also been applied to several MAS scenes Here we present results from two scenes of the MAS 50 channel data set. The first scene is from observations made on 7 June 1995 over the north slope of Alaska (tundra). The MAS has a spatial resolution of approximate 50 m. Figure 18 includes visible and infrared images as well as the final cloud mask. Results from individual tests are available from the authors.

The second example of an application of the MAS cloud mask (Figure 19) is of a scenefrom ARMCAS provided by Dr. Si-Chee Tsay. This scene is cloud free, but includes both dark tundra and light sea ice, thus all pixels indicated as high confident cloudy are false detections Many of these falsely detected scenes result from failing the 1.88μm test. Causes and solutions for these failures are under investigation.

Future MAS data processing

The University of Wisconsin-Madison will be applying and validating the MAS cloud mask using data from the recent SUCCESS experiment (see Section 4.6.1).

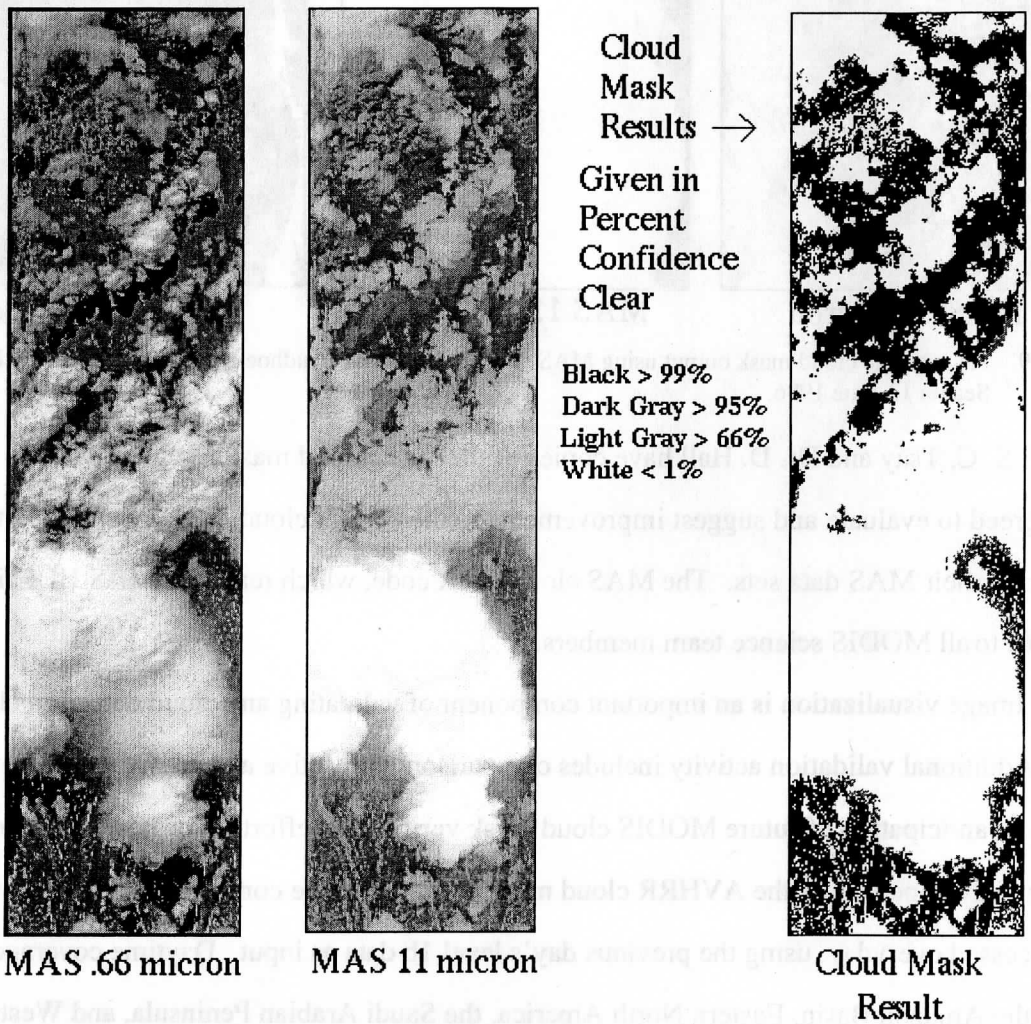

Figure 18. An example cloud mask output using MAS data obtained over the north slope of Alaska on 7 June 1995.

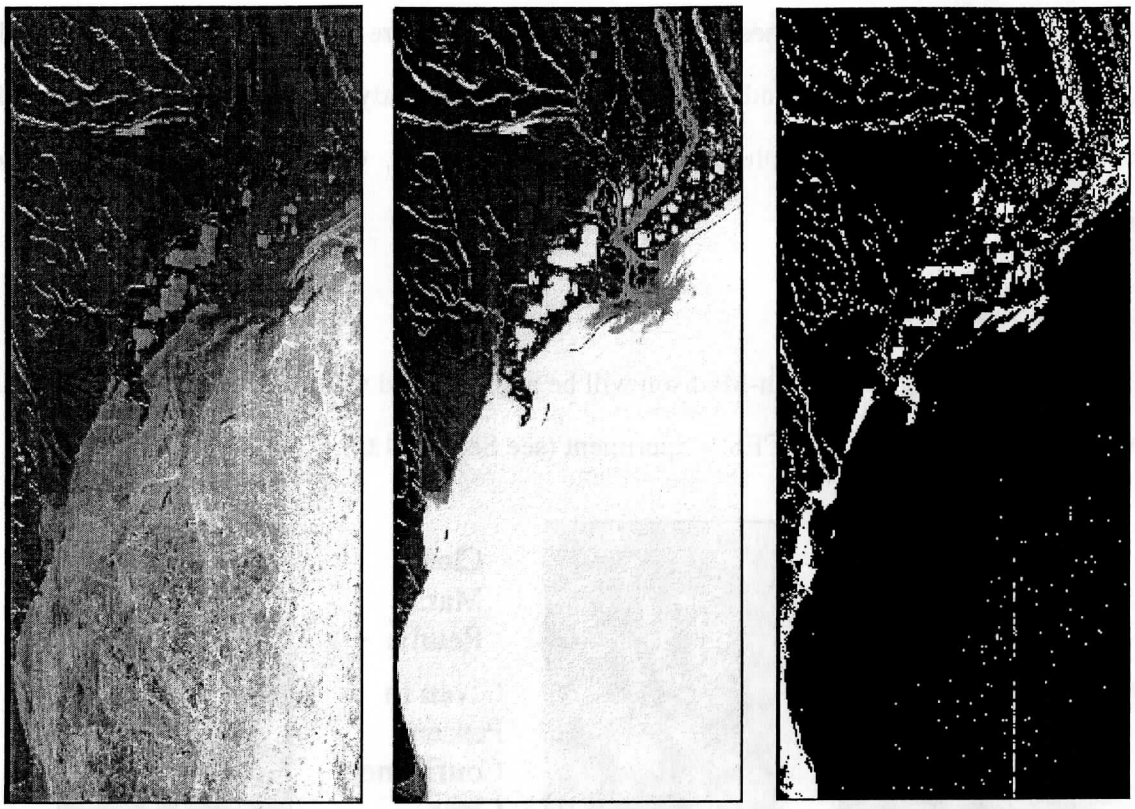

Figure 19. An example cloud mask output using MAS data obtained near Prudhoe Bay and sea ice in the Beaufort Sea on 13 June 1996.

Dr. S. C. Tsay and Dr. D. Hall have copies of the MAS cloud mask FORTRAN code They have agreed to evaluate and suggest improvements to the current cloud mask by applying the algorithm to their MAS data sets. The MAS cloud mask code, which reads the MAS HDF file, is available to all MODIS science team members.

Image visualization is an important component of validating any cloud detection algorithm. Additional validation activity includes comparison with active and passive measurements of clouds. In anticipation of future MODIS cloud mask verification efforts, a prototype methodology has been developed using the AVHRR cloud mask product. Three complete AVHRR GAC orbits are processed everyday, using the previous day's level 1b data as input. Daytime coverage includes the Amazon Basin, Eastern North America, the Saudi Arabian Peninsula, and Western Europe. Hourly surface observations from ten manned weather stations in North America, closest

in time to the satellite measurement, are collected and compared to the cloud mask output. Figure 20 is a 3-D histogram that compares the surface observation with the closest AVHRR pixel, for the months of August and September 1997. Weather station reported cloud coverage is plotted on the x-axis and the satellite derived clear sky confidence level on the y-axis. The z-axis is the frequency of occurrence in each category. Surface observed cloudiness is reported as "few", "scattered", "broken" and "overcast". Sky coverage for these categories is 1/8-2/8, 3/8-4/8, 5/8-7/8 and 8/8, respectively. The cloud mask is generally doing a satisfactory job, particularly under clear skies. This is a result of the conservative nature of the cloud mask, where only very high confidence pixels are designated as clear. Frequencies of confidences associated with the surface observed cloud coverage of few, scattered, broken and overcast categories are as expected—with the likelihood of having clouds directly overhead increases with increasing cloud cover.

To better quantify the MAS algorithm we compare MAS cloud mask with observations of the Cloud Lidar System (CLS) [*Spinhirne et al.* 1996]. During the SUCCESS experiment the MAS flew along with the lidar. The CLS algorithm detects a maximum of five cloud tops and cloud bottom altitude based the backscatter signal. Collocation of the MAS and CLS follows the work of *Spinhirne and Hart* [1990]. Each collocated scene consists of the CLS cloud product along with approximately 250 to 300 MAS pixels. The percentage of pixels labeled high confident clear, probably clear, uncertain, and low confident clear are determined for each collocated scene. A total of 5072 collocated samples are analyzed representing a variety of cloud conditions. We have categorized the CLS observations into three categories:

Clear—no cloud was detected by the lidar;

Thin cloud—cloud boundary was detected, but a surface return signal was also received;

Thick cloud—cloud boundary was detected with no surface return signal.

Histograms of the percentage of pixels in a given confidence interval are plotted for each CLS cloud type category are shown in Figure 21. Nearly all of the CLS labeled clear scenes are identified as high confident clear by the MAS cloud masking algorithm. Essentially all of the CLS labeled thick cloud scenes are labeled as cloudy by the cloud mask. The thin cloud category are

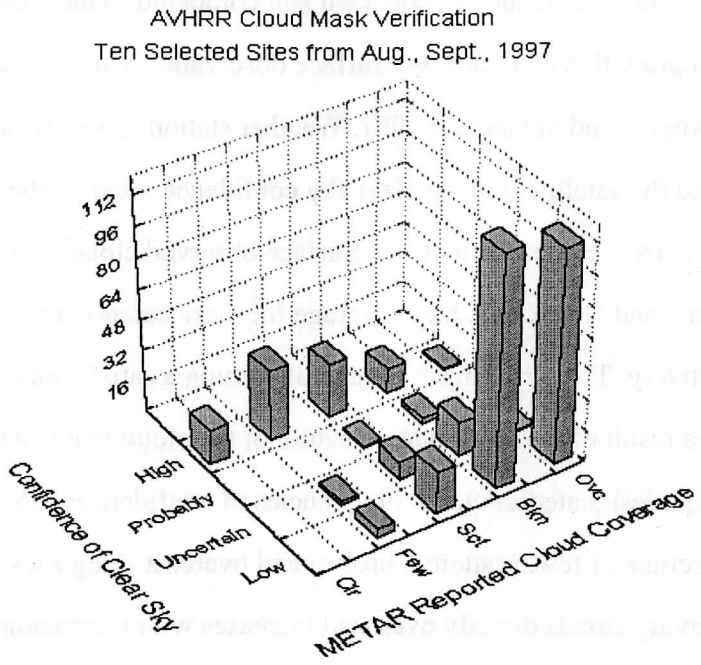
AVHRR Cloud Mask Verification
Ten Selected Sites from Aug., Sept., 1997
112
96
80
64
48
32
16
High
Probably
Uncertain
Low
Confidance of Clear Sky
Clr
Few
Sct
Bkn
Ovc
METAR Reported Cloud Coverage

Figure 20. Comparison of surface cloud reports and AVHRR cloud mask results.

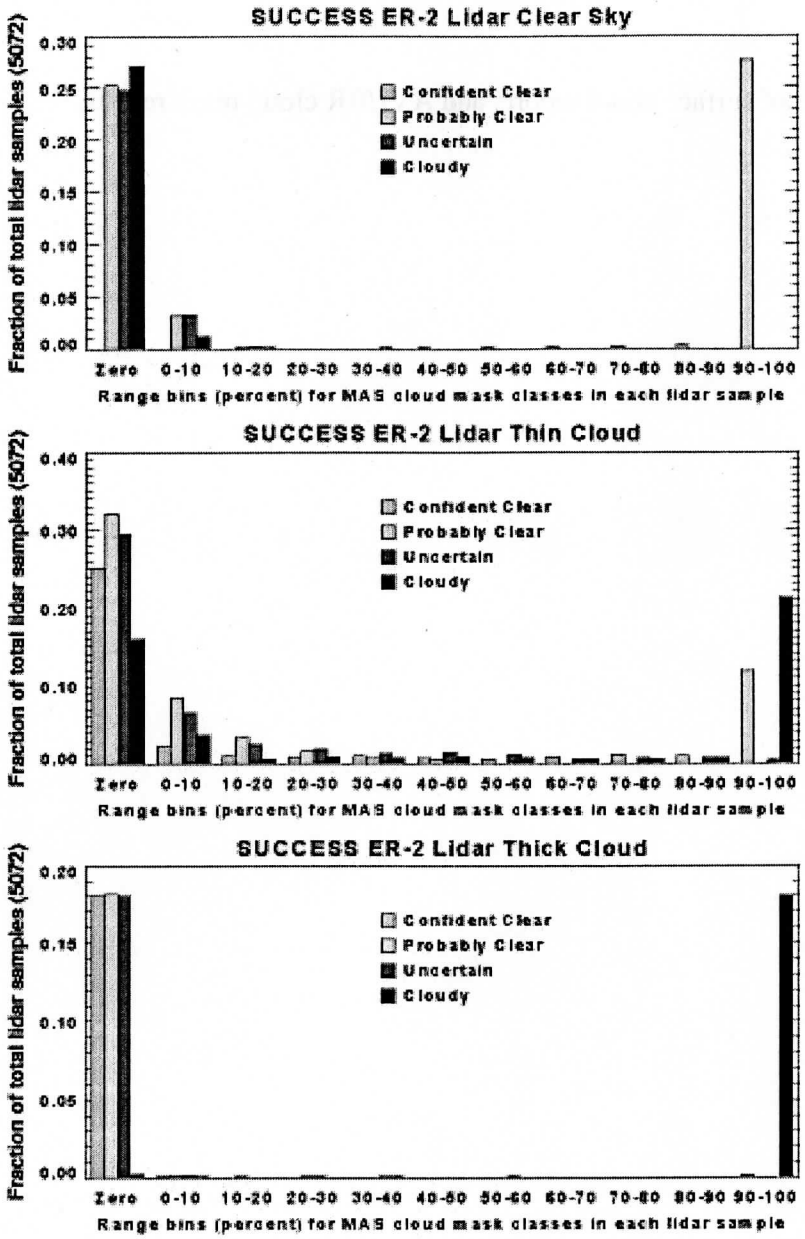

Figure 21. Comparisons between the MAS cloud mask algorithm and CLS [Spinhirne*et al.* 1996] cloud boundary retrieval for five days of the SUCCESS experiment. Cloud mask confidence is compared with three lidar categories: no cloud (top panel), thin cloud (middle panel), and thick cloud (bottom panel).

4.3 Interpreting the cloud mask

This section provides examples of how to interpret output from the cloud mask algorithm They are suggested approaches and not strict rules. We recognize that each MODIS science team member will know how to best use the cloud mask for their applications We are open to working with science team members to develop interpretation procedures similar to those listed blow.

4.3.1 CLEAR SCENES ONLY

Certain applications have little tolerance for cloud or shadow contamination This is an example of how these applications (e.g., bidirectional reflectance models) might interpret the cloud mask output.

1. Read bit 0 to determine if a cloud mask was determined, if this bit is 0 no further processing of the pixel is required.
2. If necessary, read bits 3 through 7 to determine scene domain.
3. Read bits 1 and 2; if both bits are *not* equal to 1, then some tests suggest the presence of cloud, and the pixel is skipped.
4. Read bit 9 to determine if a thin cirrus cloud is present (bit value of 0) An optically thin cirrus cloud may set bit 9 but not be classified as a cloudy scene.
5. Read bit 10 to determine if shadow contamination is present; do not process data if this bit is 0.
6. Daytime algorithms may (depending on application) read bits 32 through 47 to assess potential subpixel contamination or scene variability.

4.3.2 CLEAR SCENES WITH THIN CLOUD CORRECTION ALGORITHMS

Some algorithms may be insensitive to the presence of thin cloud or may apply appropriate correction algorithms. This is a suggested application; after launch minor modifications may be implemented depending on the performance of the cloud masking algorithm Two examples are

given, one that might be appropriate for Normalized Difference Vegetation Index (NDVI) and the second for sea surface temperature (SST) retrievals.

Interpretation procedure that might be useful for NDVI retrievals:

1. Read bit 0 to determine if a cloud mask was determined; if this bit is 0, no further processing of the pixel is required.
2. Read bits 3 through 7 to determine if scene domain is appropriate (e.g., land and day-time)
3. Read the confidence flag—bits 1 and 2. If high confident cloudy (value of 00), do not process pixel. A value of 01 for bits 1 and 2 (possibly cloudy) often occurs around cloud edges and retrieving NDVI may not be appropriate with this confidence level If both bits are equal to 1, then most tests are suggesting clear scenes; proceed with steps 4-7. If confidence bits are 10, then detailed checking of bits 13 through 25 may be required to determine NDVI algorithm processing path.
4. Read bits 9 and 11 to determine if a thin cirrus cloud is present (bit value of 0) An optically thin cirrus cloud may set bits 9 or 11, but not be classified as a cloudy scene Some of the MODIS solar channels are not as sensitive to thin cirrus as the 1.38μm band (see Figure 1 for a corresponding example using the MAS 1.88μm channel). If thin cirrus is detected, apply appropriate correction algorithms.
5. Check that reflectance tests (bits 20 and 21) did not detect cloud. Note that a value of 0 indicates that either a cloud is present or the test was not run. This test is not run if over snow or solar zenith angles greater than 85°.
6. Read bit 10 to determine if shadow contamination is present Shadows might bias the NDVI product.
7. Read bits 32 through 47 to assess cloud contamination. This would not be recommended if snow is indicated.

Interpretation procedure that might be useful for SST retrievals.

1. Read bit 0 to determine if a cloud mask was determined; if this bit is 0, no further

processing of the pixel is required.

2. Read bits 3 through 7 to determine if the scene is water or if sun glint is present.
3. Read the clear confidence flag—bits 1 and 2. If high confident cloudy (value of 00), do not process pixel. A value of 01 for bits 1 and 2 (possibly cloudy) often occurs around cloud edges and retrieving SST may not be appropriate with this confidence level. If both bits are equal to 1, then most tests are suggesting clear scenes; proceed with steps 4-9. If the confidence is 10, then detailed checking of bits 13 through 25 may be required to determine SST algorithm processing path For example, if confidence bits are 10 and pixel is in a sun glint region, determine how many IR tests are detecting cloud. If all IR tests are passing, then continue with steps 4-8. If the IR tests are failing, then pixel contamination is likely In this case the SST should either be retrieved with caution, or appropriate corrections to the IR channels should be made.
4. Read bit 9 to determine if a thin cirrus cloud is present (bit value of 0) An optically thin cirrus cloud may set bit 9 but not be classified as a cloudy scene If thin cirrus is detected, apply appropriate IR correction algorithms. Corrections require other cloud products, such as cloud emissivity and cloud effective temperature (MOD06).
5. Check that IR tests did not detect cloud. The greater the number of IR tests that did not detect cloud, the more confidence one has in the SST product. Note that a value of 0 indicates that either a cloud is present or the test was not run.
6. Check spatial variability test results Uniform scenes increase confidence that pixel is clear and improves SST accuracy.
7. Read bits 32 through 47 to assess subpixel cloud contamination This would not be recommend in sun glint regions.

4.3.3 CLOUDY SCENES

Use of the cloud mask for cloud scene processing may require a more in-depth analysis than

clear-sky applications, as the mask is clear-sky conservative Here we consider a few approaches to interpreted the cloud mask for cloud property retrievals during the day, that are a function of processing path.

Daytime ocean scene, non-sunglint:

1. Read bit 0 to determine if a cloud mask was determined; if this bit is 0, no further processing of the pixel is required.
2. Read bit 3, if this bit is 0 no further processing ofthe pixel is required (night).
3. Read bits 6 and 7, if 00 then water scene so proceed.
4. Read bit 4, if 0 then sunglint region, may want to place less confidence on product retrieval.
5. Read the confidence flag—bits 1 and 2.
   - If high confident clear (value of 11), Read bit 9 to determine if a thin cirrus cloud is present (bit value of 0). An optically thin cirrus cloud may set bit 9 but not be classified as a cloudy scene If thin cirrus is detected, apply appropriate algorithms or place less confidence on product retrieval If bit 9 is 1, it is clear sky, no further processing is required.
   - If both bits are equal to 00, then the scene is cloudy. Check bit 8 for possible heavy aerosol loading If bit 8 is 0 then pixel may be aerosol contaminated, no further processing or place less confidence on product retrieval If bits are 00 then check individual test to determine ice or water phase For example, if bit 21 is 0 and bit 13 is 1, probably water cloud scene If bits 16 and 17 are 0, probably an ice cloud.
   - If confidence is 10 or 01, then detailed checking of bits 13 through 25 may be required to determine if algorithm should be executed For example, if confidence bits are 10 and pixel is in a sun glint region, additional testing is advised.
6. Check how many tests detected cloud. The greater the number of tests that detected cloud, the more confidence one has in the cloud property product. Note that a value

of 0 indicates that either a cloud is present or the test was not run.

7. Check spatial variability test results
8. Read bits 32 through 47 to assess subpixel cloud contamination This would not be recommended for region with sun glint.

Daytime dark vegetated land regions (for example, forests):

1. Read bit 0 to determine if a cloud mask was determined; if this bit is 0, no further processing of the pixel is required.
2. Read bit 3, if this bit is 0 no further processing of the pixel is required (night)
3. Read bits 6 and 7, if 11 then land scene so check ecosystem for correct type.
4. Read bit 4, if 0 then sunglint region, may want to place less confidence on product retrieval.
5. Read the confidence flag—bits 1 and 2.
   - If high confident clear (value of 11), Read bit 9 to determine if a thin cirrus cloud is present (bit value of 0). An optically thin cirrus cloud may set bit 9 but not be classified as a cloudy scene If thin cirrus is detected, apply appropriate algorithms or place less confidence on product retrieval If bit 9 is 1, it is clear sky, nor further processing is required.
   - If both bits are equal to 00, then the scene is cloudy. Check bit 8 for possible heavy aerosol loading If bit 8 is 0 then pixel may be aerosol contaminated, no further processing or place less confidence on product retrieval If bits are 00 then check individual test to determine ice or water phase For example, if bit 21 is 0 and bit 13 is 1, probably water cloud scene If bits 16 and 17 are 0, probably an ice cloud.
   - If confidence is 10 or 01, then detailed checking of bits 13 through 25 may be required to determine if algorithm should be executed For example, if confidence bits are 10 check the number of solar tests passed, if bits 16, 20, 21 and 23 are 1 then IR tests are indicating cloud, probably do not want to process retrieval that

depend on solar techniques or place less confidence on product retrieval.

6. Check how many tests detected cloud. The greater the number of tests that detected cloud, the more confidence one has in the cloud property product.
7. Read bits 32 through 47 to assess subpixel cloud contamination This would not be recommended for region with variable surface reflectance.

Detection of clouds over snow and ice is a difficult problem One procedure for interpretating the cloud mask output for daytime snow/ice retrieval algorithms follows.

1. Read bit 0 to determine if a cloud mask was determined; if this bit is 0, no further processing of the pixel is required.
2. Read bits 3 through 7 to determine if scene domain is appropriate (e.g., daytime and non-desert).
3. Read bit 5 to determine if snow processing path.
4. Read bits 1 and 2 - the final confidence flag.
   - If high confident cloudy (value of 00) do additional testing. Check bit 19, if cloudy probably low level water cloud.
   - If bits are 10 or 01, check bit 19, if cloudy probably low level water cloud.
   - If high confident clear (value of 11), check for the possible presence of thin cirrus (bit 9 and bit 11).
5. Read bit 10 to determine if pixel is shadowy (currently, shadow detection on snow is very limited).

An interpretation procedure for application with aerosol retrieval algorithms is:

1. Read bit 0 to determine if a cloud mask was determined; if this bit is 0, no further processing of the pixel is required.
2. Read bits 3 through 7 to determine scene domain is appropriate for aerosol retrieval(e.g., daytime land, daytime water, non-desert processing path)
3. Read bit 4 for sunglint contamination, proceed as appropriate.
4. Read bit 5 for snow/ice contamination.

5. Read bits 1 and 2 - the final confidence flag.
   - If high confident clear (value of 11), search for aerosol If bit 10 is 0, possible contaminatin by thin cirrus or high aerosol.
   - If bits 1 and 2 are 00, check bit 8 for heavy aerosol condition If bit 8 is 0, run aerosol retrieval alogithm.
   - If high confident clear (value of 11), check for the possible presence of thin cirrus (bit 9 and bit 11).
   - If land bits are 01 or 10, check bit 8 for heavy aerosol, if bit 8 is 0 proceed with retrieval. If bit 8 is 1 (cloud mask aerosol test did not indicate heavy aerosol, check addition bits
     - check bit 11, if cloudy (bit is 0) cirrus is probably present
     - if bit 19 is 0, probably indicates the presence of a low level cloud, dont process
     - if bit 21 (ratio test) is 0 and appropriate ecosytem (vegetation) probably cloud contaminated scene
6. Read bit 10 to determine if pixel is shadow

4.4 Numerical Programming Considerations

The MODIS Level 2 cloud mask algorithm has been run using simulated MODIS radiances on the GSFC TLCF (SGI) for a MODIS granule (2.5 minutes or 100 scans). Several steps were taken to come to a final volume and load estimate Timing runs were made on the TLCF SGI Power Challenge (modispc) using UNIX /bin/time command on an input granule The processing rate on modispc with the R10000 chip was set at 390 Million Floating Point Operations per Second (MFLOPS), but divided by a factor of 4, which is the ECS average fraction of peak used by a process. The number of Million Floating Point Operations (MFPO) was then multiplied by 1.6 to factor in additional processing needed in a production environment The production code was timed at 15 minutes and 1 second Approximately 60% of the Version 1 cloud mask CPU is con-

sumed in the creation and initialization of the clear-sky radiance files In production mode this file will only be created and initialized once In subsequent granules the file will only be updated If we remove this component of the processing, then the at-launch CPU requirement is approximately

- 0.4 × 15 minutes × 60 seconds/minute = 360 seconds.
- MFPO/granule = 1.6 × (390/4 MFLOPS) × 360 seconds = 56160 MFPO/granule
- MFLOPS = (56160 MFPO/granule × 585.5 granules/day)/86400 seconds/day =380.6 MFLOPS.
- The product Level 2 volume per granule is 8.1 MB.
- 6 bytes × 1354 cross track pixels/scan × 10 along track pixels/scan × 100 scans/granule = 8.1 MB/granule

A full day of MODIS processing will then result in a volume load of 8.1MB/granule× 585.5 granules/day = 4.8 GB/day. The product volume is expected to be slightly greater than this with the addition of metadata fields. Refer to the MODIS atmosphere group QA plan.

4.5 Quality Control

Quality Control is (i) *ambiguous* - pixel may be interpreted in more than one way, (ii) *incomplete* - information is missing or (iii) *incorrect* - information is wrong (i.e., pixel values are bad).

Several approaches to routine quality control are anticipated. Some are:

- Monitor percentage of cloud detection with various tests
  - look for consistency
- Monitor angular dependence of cloud cover
  - there should not be any
- Monitor consistency of global cloud cover from day to day
  - should maintain 5% consistency
- Perform regional statistics

- look for persistence in certain regions (e.g., marine stratus)

- Correlate cloud mask with independent SST and OLR determinations
  - should find good correlations

Most of the quality control indicated above will require accumulation of at least a 30 day data base. It is expected that for the first six months there will be considerable manual monitoring of the results, but that this will revert to automated monitoring as the appropriate variability in day to day cloud masks are characterized.

4.6 Development Plan

The MODIS cloud mask algorithms build on existing programs; however, much work yet remains to develop and implement the algorithms by launch Some of the approaches outlined in the document can be developed with current satellite observations, while others require modeling efforts and regional observations with theMAS.

Our research and development strategy makes use of three data sets. The first is a global data set of collocated HIRS/2 and AVHRR GAC observations. The strengths of this data set are its global coverage and the fact that the collocated observations have many MODIS like bandwidths. This allows us to investigate many of the spectral tests described above The disadvantage of the data set is the large FOV (HIRS/2 FOV is 17 km at nadir) and the horizontal displacement of the HIRS/2 footprints (gaps of approximately 20 km) This data set also does not have the complete AVHRR image, only those AVHRR pixels that lie within the HIRS/2 footprint To overcome this later disadvantage we have compiled a second data set of collocated HIRS/2 and AVHRR LAC (Local Area Coverage) observations. This data set has similar spectral and spatial resolution to the future MODIS and will be important for validation and development of cloud shadow detection techniques. The disadvantages, of course, are the non-global nature and the gaps between the HIRS FOV.

The third data set is from MAS aircraft flights The initial MAS instrument recorded twelve (or eleven) spectral bands in the visible to infrared and enabled development and exploration of

some of the techniques discussed above. Since December 1994, the MAS has recorded 50 spectral channels, 19 of which are similar to the bandwidths of the future MODIS. This will be the most MODIS-like data set and will play an important role in testing and developing the mask. The validation section discusses the field programs that have flown, or will fly, the MAS.

We recognize the need to work closely with the MODIS land, ocean, and atmosphere groups in the continued development of the cloud mask. To this end we have offered to process different MAS and AVHRR data scenes for examination. We have developed the FORTRAN code to read the Goddard HDF MAS 50 channel data format and output a cloud mask similar in structure to the MODIS 48 bit cloud mask. *This code is available to MODIS science team members to test the cloud mask and assist in its development.*

4.7 Validation Plan

Validation will be approached in several ways: (i) collocation with higher resolution aircraft data, (ii) ground-based and aircraft in situ observations, and (iii) intercomparisons with other AM-1 platform instruments. Our validation approach relies heavily on the sources of the data that were used in the algorithm development, which consisted primarily of the MAS, a fifty channel visible, near-infrared, and thermal infrared imaging spectrometer with 50 m resolution at nadir (King *et al.* 1996), HIS, a 2 km resolution nadir-viewing (soon to be modified for scanning) Michelson interferometer with 0.5 cm^{-1} spectral resolution from 4 to 15 μm (Smith *et al.* 1992), and AVIRIS, a 224 band imaging spectrometer from 0.4-2.5 μm with 20 m resolution at nadir (Vane *et al.* 1993). In addition, we plan to make extensive use of the AERONET (Aerosol Robotic Network), a network of ground-based sunphotometers established and maintained by Brent Holben (Goddard Space Flight Center) that measures the spectral aerosol optical thickness and sky radiance, reporting the data via a satellite communication link from each remotely-located CIMEL sunphotometer to Goddard Space Flight Center from sunrise to sunset, 7 days a week. Finally, we plan to utilize ground-based microwave radiometer observations to derive column water vapor and liquid water path, especially over the Atmospheric Radiation Measurement

(ARM) CART (Clouds And Radiation Testbed) site in Oklahoma.

Comparison of MODIS radiances and products with those from other instruments should be made periodically (perhaps annually) in different seasons in daytime and nighttime conditions. We anticipate numerous opportunities, unspecified, in which scientists worldwide will intercompare MODIS-derived atmospheric, land, and ocean data products with local measurements of the geophysical property of interest. This wide-scale synthesis of data sets from scientists from Australia, Japan, China, Europe, South America, and Africa will greatly enhance the confidence that we place in the MODIS-derived products, and will, with time, aid our ability to assess the quality of the data products from a wide variety of climatic conditions and seasons. This would not be possible, nor appropriate, for the small MODIS Science Team to accomplish entirely on its own.

4.7.1 AIRCRAFT OBSERVATIONS OF CLOUDS

Key measurements for this validation approach will be MODIS observations collocated with measurements from the ER-2 instruments (MAS, CLS, HIS, passive microwave, multi-angle camera). The major limitation of this approach is establishing statistical significance of the case study samples. The major strength is that it provides a very complete cloud data set.

Validation will rely heavily on the source of data that helped in the algorithm development, primarily the MAS. Several field campaigns are planned with the ER-2 carrying the MAS over varying scenes and different ecosystems.

Several field programs offer opportunities for pre-launch and post-launch MODIS validation through collection and analysis of observations obtained from the MAS and HIS. These field campaigns often include the Cloud and aerosol Lidar System (CLS; Spinhirne *et al.* 1989) for verifying cloud top altitude and multi-layer clouds, the University of Washington C-131A, with the Cloud Absorption Radiometer (CAR; King *et al.* 1986) and extensive in situ cloud microphysics (liquid water content, effective radius, cloud drop size distribution), aerosol properties (size distribution, scattering and absorption coefficients), and meteorological sensors. These data will be used in validating the cloud mask algorithm

Mission	*Dates*	*Responsible Team Members*	*Primary Purpose*
SUCCESS	April-May 1996	Steve Ackerman, Si-Chee Tsay, Paul Menzel	cirrus cloud properties
TARFOX	July 1996	Didier Tanré, Yoram Kaufman, Lorraine Remer, Si-Chee Tsay	tropospheric aerosol and cirrus over the ocean; surface BRDF
FIRE III	May-June 1998	Michael King. Si-Chee Tsay, Steve Platnick, Steve Ackerman	arctic stratus clouds over sea ice
MODIS-specific validation campaigns			
WINCE	January-February 1997	Paul Menzel, Steve Ackerman, Dorothy Hall	cloud detection and properties over snow/ ice covered surfaces
ARM-1	October 1998	Paul Menzel, Steve Ackerman	periodic flights over the SGP ARM site with MAS & HIS
MOBY	January 1999	Paul Menzel, Steve Ackerman	cirrus clouds and atmospheric corrections over the ocean
ARM-2	March 1999	Michael King. Si-Chee Tsay, Steve Platnick, Steve Ackerman	periodic flights over the NSA ARM site with MAS & HIS
California	July 1999 December 1999	Michael King, Steve Platnick, Si -Chee Tsay	marine stratocumulus (July) and valley fog (December)

Mission	*Dates*	*Responsible Team Members*	*Primary Purpose*
Kalahari Desert	August-September 1999	Michael King, Yoram Kaufman, Si-Chee Tsay, Steve Platnick, Didier Tanré, Lorraine Remer	smoke, clouds and radiation from biomass burning in the Savannah marine stratocumulus off Namb-ian desert; surface BRDF
Gulf of Mexico	January 2000	Paul Menzel, Chris Moeller	clear-sky and cirrus clouds, in-cluding sediment outflow from river estuaries
California & Pacific North-west	September 2000	Yoram Kaufman, Lorraine Remer, Elaine Prins, Didier Tanré	fire detection and smoke aerosol properties

4.7.2 COMPARISON WITH SURFACE REMOTE SENSING SITES (E.G., ARM)

Results of the cloud mask will be compared to ground based measurements such as lidar, ra-dar, passive microwave and optical radiometers. The advantage is that comparisons could be conducted throughout the lifetime of the MODIS and thus provide proper sampling for statistical analysis. The disadvantage is that the ground based sites will not represent all climate regimes. This could be improved by comparing the MODIS cloud mask with surface observer cloud fra-tion and/or ceilometer cloud base altitude. While this later comparison provides global land co-verage, the accuracy and quality of routine cloud observations is less than that of field programs such as ARM. Periodic experiments, such as with the aircraft, could improve this sample.

In addition to the airborne campaigns in which MODIS team members are directly planning to participate, we expect to make use of selected ground-based networks as follows:

Measurement	*Location*	*Responsible Investigators*	*Primary Purpose*
AERONET	multiple locations in US, Japan, South America, Africa, & Europe	Brent Holben, Yoram Kaufman, Didier Tanré	aerosol optical thickness and columnar size distribution
ARM	Oklahoma, North Slope of Alaska, Western Tropical Pacific	Paul Menzel, Si-Chee Tsay	cloud base height (micropulse lidar), temperature and moisture profiles, sky radiance (visible and IR)
AEROCE	multiple island locations worldwide	Joe Prospero, Yoram Kaufman, Didier Tanré	aerosol hydroscopicity, scattering and absorption coefficients, size dependent chemical composition

The ground-based measurements will be obtained on a continuous basis as well as during intensive field experiments. All of these validation opportunities, as well as intercomparison of data derived from MODIS with other sensors on AM-1 and other spacecraft, will be discussed in detail below.

Validation will also be conducted through comparison with independent analysis of other satellite data. For example, MODIS cloud retrievals will be compared to analyses of other instruments such as MISR and ASTER. This comparison provides global coverage.

4.7.3 INTERCOMPARISONS WITH OTHER AM-1 PLATFORM INSTRUMENTS

Comparisons with products from other platforms are also planned Cloud masks will be compared with those from AVHRR and HIRS/2 data, ASTER and MISR (also on the AM-1 platform), and CERES. Timing, coverage and resolution will vary from one instrument to another; for example with ASTER, comparisons will be possible for selected swaths (60 km wide with 30 m resolution) that are available for different (and selected) ecosystems no more than once every 16 days. The ASTER product will include a classification for each pixel poleward of 60°N or 60°S using a bit map with the following bit flags: unknown, ice cloud, water cloud, shadow, land, ice, wet ice, and water. The high spatial resolution of the ASTER data (30 m at nadir) will

help to ensure that sub-pixel effects are properly accounted for in the MODIS data.

The MODIS Cloud Mask product will be compared to the CERES Single Satellite Footprint (SSF) and Single Satellite Gridded products that include cloud top pressure and temperature, cloud optical thickness, effective radius and phase, and cloud category (lower, lower-middle, upper-middle, high). CERES is heavily dependent on MODIS observations for cloud detection, so it will be important to ensure that the MODIS and CERES-derived cloud products are consistent.

The MODIS Cloud Mask products will be compared to the MISR Top-of-Atmosphere/Cloud Product. The components of the MISR product that will be used are Reflecting-Level Reference Altitude (retrieved using MISR stereo imagery), Angle-by-angle cloud masks, Cloud shadow mask, and Altitude-binned cloud fraction. The MODIS and MISR Cloud Masks will be compared to ensure consistency of cloud identification, and the MISR stereo cloud heights will be compared with the MODIS cloud top heights to geometrically validate the MODIS radiometrically derived cloud height data. We have begun this work using MODIS data collected during the SUCCESS.

Since the MODIS cloud mask algorithms will also be developed using data sets of collocated AVHRR and HIRS/2 data, intercomparison of the cloud masks from these data will also be done. The disparity of the resolution will render these intercomparisons somewhat less useful; however, global averages of cloud conditions and their variability from day to day will provide useful guidelines for quality control and validation.

An additional validation test for cloud masking is the accuracy and internal consistency of clear-sky data products. This includes checks of SST, as well as land reflectance and surface temperature. This is an information feedback loop between cloud data products and land/ocean data products. The major limitation is that it is based on indirect inferences and may be difficult to unambiguously deduce cause and effect.

4.7.4 PRE-LAUNCH ACTIVITIES

Pre-launch validation will be accomplished using MAS and AVIRIS data already gathered in various field campaigns. Especially valuable are data taken in combination with nearly coincident airborne in situ microphysical data as well as data from ground-based instrumentation (both remotely sensed and in situ). A sampling of data sets already in-hand, along with key sensors and responsible investigators are:

Field Campaign	*Principal Sensors*	*Responsible Team Members*	*Primary Purpose*
ASTEX	MAS, CLS, CAR, microphysics probes	Michael King, Si-Chee Tsay	marine stratocumulus clouds over the ocean
TOGA-COARE	MAS, CLS, microphysics	Paul Menzel, Steve Ackerman, Liam Gumley	tropical cirrus clouds and multi-layer clouds over ocean regions
SCAR-A	MAS, CAR, CLS, AVIRIS, aerosol microphysics, AERONET	Yoram Kaufman, Lorraine Remer, Michael King, Si-Chee Tsay, Paul Menzel	aerosol properties in the polluted East coast region; surface bidirectional reflectance properties
MAST	MAS, CLS, CAR, cloud microphysics	Steve Platnick, Michael King, Si-Chee Tsay	marine stratocumulus clouds over the ocean, including the effect of aerosol on clouds (ship tracks)
SCAR-C	AVIRIS, MAS, AERONET, in situ aerosol probes	Yoram Kaufman, Lorraine Remer, Elaine Prins	smoke, clouds and radiation interactions resulting from forest fires in the U. S.
ARMCAS	MAS, AVIRIS, CLS, CAR, microphysics	Si-Chee Tsay, Michael King, Steve Platnick, Steve Ackerman	arctic stratus clouds over sea ice; multi-layer clouds, surface bidirectional reflectance (sea ice & tundra)
SCAR-B	MAS, AVIRIS, CLS, CAR, microphysics, aerosol properties,	Yoram Kaufman, Lorraine Remer, Michael King, Si-Chee Tsay,	smoke, clouds and radiation from biomass burning in the cerrado, Pantanal, and Amazon rainforest; BRDF

	AERONET	Elaine Prins	
SUCCESS	MAS, CLS, HIS, AERI	Steve Ackerman, Paul Menzel, Si-Chee Tsay	mid-latitude cirrus clouds over continents
TARFOX	MAS, LASE, CAR, aerosol properties, AERONET	Didier Tanré, Yoram Kaufman, Lorraine Remer, Si-Chee Tsay	sulfate aerosols, water vapor, and radiative forcing of aerosols in the ocean-atmosphere system; surface BRDF
WINCE	MAS, HIS, CLS	Paul Menzel, Steve Ackerman, Chris Moeller, Dorothy Hall	cloud detection and properties over snow/ice covered land and lakes

In addition, numerous data sets obtained with the CAR of the internal scattered radiation field in smoke (Kuwait oil fires), clouds (FIRE I marine stratocumulus experiment, MAST, ASTEX, ARMCAS), and many additional measurements of the bidirectional reflectance function of natural surfaces such as tundra, sea ice, oceans, smoke, cerrado, rainforests, and the Great Dismal Swamp, add immeasurably to a data set on the surface reflectance characteristics of natural surfaces. The analyses of these data sets are being conducted by Michael King, Si-Chee Tsay, and Jason Li.

Limited validation will also be carried out using collocated HIRS and AVHRR data sets by Paul Menzel and Steve Ackerman, focusing on surface emissivity effects. This data set has the advantage of global coverage, but the spatial scale is far removed from that of MODIS, with spectral bandwidths that are much wider and off-center from those of MODIS.

In the foreseeable future, prior to the launch of AM-1 in late June 1998, we anticipate collecting the following additional data set:

Field Campaign	***Principal Sensors***	***Responsible Team Members***	***Primary Purpose***
FIRE III	MAS, CLS, CAR, AERONET, microphysics probes	Michael King, Si-Chee Tsay, Steve Platnick, Steve Ackerman	arctic stratus clouds over sea ice, surface BRDF (tundra & sea ice)

The Subsonic Aircraft Contrail and Cloud Effects Special Study(SUCCESS) field experiment was conducted in April-May 1996, with the goal of determining the radiative properties of cirrus contrails, and of contrasting them with naturally occurring cirrus. To assess the radiative impact of these clouds required a well-calibrated set of radiation measurements and"ground (or in situ) truth" observations. We acquired MAS and HIS multispectral observations along with CLS cloud height measurements from the NASA ER-2 aircraft by coordinating over flights of the ER-2 with in situ aircraft and ground based measurements. The MAS and HIS measurements were employed to address the very important relationship between cirrus radiative properties and the thermodynamic environment (atmospheric temperature and moisture conditions) wherein cirrus clouds form and are maintained. The HIS provided accurate measurements of the thermodynamical properties supporting the cirrus life cycle and the MAS measured the cirrus areal extent and radiative properties. Additional emphasiswas placed on developing and validating methods of detecting upper tropospheric clouds and defining their areal extent with infrared (e.g, 13.9 μm) and near infrared (e.g., 1.88 μm) channels; these being similar to the MODIS channels andhence the MAS cirrus detection, thereby having direct relevance to the MODIS cloud mask algorithm. The CLS data were used to validate MAS upper tropospheric clouds.

The Tropospheric Aerosol Radiative Forcing Observational Experiment (TARFOX, 10-31 July 1996) campaign measured atmospheric aerosols emanating from industrial centers in North America transported over the Atlantic Ocean. Their extent, radiative properties, and transport mechanisms were studied from satellite, aircraft, ship, and ground-based sensors. The MAS on the NASA ER-2 aircraft and the GOES Imager on GOES-8 were the primary sensors of interest to the atmosphere group (Didier Tanré, Yoram Kaufman, Paul Menzel) The monitoring effort focused on the corridor extending from Wallops Island, Virginia to Bermuda. In situ aircraft (UK Meteorological Office C-130H, University of WashingtonConvair C-131A, Naval Postgraduate School Pelican, and NASA ER-2), ground measurements (Lidar, AEROCE, AERONET), and satellite observations (AVHRR, ATSR-2, GOES) were used to measure the direct effects of tropospheric aerosols on regional radiation budgets of the cloud-free ocean-atmosphere system,

while simultaneously measuring the chemical, physical, and optical properties of the predominant aerosols. The suite of measurements made during TARFOX and subsequent collaborative analyses will provide a better understanding of the impact of these aerosols over the US eastern seaboard and western Atlantic Ocean and will be used to assess the degree of closure (consistency) between aerosol radiative forcing calculations and various measurements of aerosol properties and other satellite-derived parameters. This study provided a means to validate current and future satellite remote sensing methods and products (aerosol optical thickness τ_a, aerosol size distribution $n_c(r)$, and earth radiation budgets).

The Winter Cloud Experiment (WINCE; January-February 1997) investigated the difficulties in detecting clouds and estimating their properties in winter conditions(Steve Ackerman, Paul Menzel, Chris Moeller). The field campaign was conducted from Madison, WI. Cirrus and thin clouds over frozen tundra and lakes in the northern US and Canada were measured with the MAS, HIS, and CLS (along with the GOES-8 and AVHRR). One of the missions investigated the product stability under nighttime conditions(infrared only). In addition, two ground sites in New England measured snow and ice cover during MAS/HIS overflights in clear sky condition (in collaboration with Dorothy Hall and George Riggs working on the MODIS snow/ice product). Examples of the MAS cloud mask will be distributed to science team members so that they can determine its effect on their MODIS products.

FIRE, the First ISCCP (International Satellite Cloud Climatology Project) Regional Experiment, has previously conducted four successful field missions focused on cloud remote sensing and modeling studies as they relate to climate. FIRE Phase III will be conducted in the Arctic over an 8 week period or longer with a serial deployment of low- to mid-level aircraft, together with a 3 week period of high-altitude ER-2 overflights. During this component of FIRE III, we anticipate utilizing the University of Washington CV-580 and, to a lesser extent, the NCAR C-130Q. Both of these aircraft will be equipped with an extensive set of PMS cloud microphysics probes, a Gerber PVM-100A liquid water content and effective radius probe, Johnson-Williams and King hot wire probes, a Nd:YAG lidar, thermodynamic state variable measurements, and as-

lected chemistry instrumentation. In addition, the ER-2 will participate as the upper level aircraft from May 15-June 7, 1998, with the MAS, CLS, a scanning HIS, a multispectral along-track scanning radiometer (AirMISR), and a microwave imaging radiometer (MIR). The primary sensors of interest to Goddard Space Flight Center (Michael King, Si-Chee Tsay, Steve Platnick) are the MAS, CLS, and scanning HIS on the ER-2, the CAR on the CV-580, and numerous in situ microphysics probes that will be invaluable in accessing the accuracy of cloud retrievals of the microphysical and radiative properties of Arctic stratus clouds over a bright (sea ice) surface. This valuable data set will also be of interest to the University of Wisconsin for testing the cloud mask algorithm for readiness at-launch. The suite of measurements made during FIRE III and subsequent collaborative analyses will provide a means to validate current and future satellite remote sensing methods and products (cloud optical thickness τ_c, effective radius r_e, and single scattering albedo ω_0).

Operational surface networks

Data from various surface observing networks are incorporated into pre-launch validation activities, as well as selected data from the ARM site. These are collected and archived daily at the University of Wisconsinon the Man-computer Interactive Data Access System (McIDAS), which is connected to Paul Menzel's Science Computing Facility (SCF). In addition, data from the AERONET are archived at Goddard Space Flight Center by Brent Holben and are invaluable to the aerosol pre-launch validation activities of Yoram Kaufman and Didier Tanré.

Existing satellite data

All of the MODIS pre-launch studies at the University of Wisconsin (Paul Menzel) rely on AVHRR, HIRS, and GOES data for field experiment support and validation. These data are archived at the University of Wisconsin and accessible on McIDAS. Additional AVHRR data collected in support of MAST, ARMCAS, and various other pre-launch validation activities are available to Goddard Space Flight Center through the archive appropriate to that experiment

(Langley Research Center DAAC, Goddard Space Flight Center DAAC, or the Naval Postgraduate School). Finally, pre-launch activities that are coordinated with Landsat-TM data sets are archived at Goddard by Yoram Kaufman.

4.7.5 POST-LAUNCH ACTIVITIES

New EOS-Targeted Coordinated Field Campaigns

In the first two years following the launch of EOS AM-1 (June 1998), we anticipate collecting the following data sets for the purpose of validating MODIS algorithms and data products through direct intercomparisons of MODIS data with in situ and airborne remote sensing data sets. These campaigns will be EOS-targeted campaigns of direct relevance to assuring the accuracy of MODIS-derived data products:

The first EOS-targeted campaign after the MODIS launch will be coordinated with measurements taken at the Southern Great Plains (SGP) ARM site in Oklahoma, probably in October 1998. The ER-2 with MAS, HIS, and CLS will be deployed to synchronize with the MODIS overflight; the ARM site suite of ground-based measurements (class-sonde, AERI, tower measurements of temperature and moisture at various elevations, microwave moisture measurements, lidar and radar observations, whole sky imagers) will be collected simultaneously. These combined air and ground measurements will be used to validate MODIS radiance measurements. Results will be used to adjust the infrared calibration coefficients as necessary. In addition, the ARM ground-based measurements can be used to validate geophysical parameters as well. Lidar and radar observations of cloud boundaries over the ARM sites will be used to validate the presence of a cloud as well as its cloud top pressure altitude. Whole sky imagers are also available at the site, and can be used to compare satellite and ground-based estimates of cloud amount. Finally, optical depth measurements derived from lidar will aid in specifying the limit of thin cirrus detection in the cloud mask algorithm.

EOS-Targeted Field Campaign	*Principal Sensors*	*Responsible Team Members*	*Primary Purpose*
ARM overflights (SGP & NSA)	MAS, HIS, CLS, AERI, surface lidar & microwave sensors	Steve Ackerman, Paul Menzel, Bo-Cai Gao, Si-Chee Tsay	mid-latitude cirrus clouds over continents, Arctic stratus over sea ice and tundra
MOBY	MAS, HIS, MOBY, AERONET	Paul Menzel, Chris Moeller	cirrus clouds and atmospheric correction over the ocean
California	MAS, CLS, AirMISR	Michael King, Steve Platnick, Si-Chee Tsay	marine stratocumulus and valley fog
Kalahari Desert	MAS, AirMISR, CLS, in situ microphysics, AERONET	Michael King, Yoram Kaufman, Si-Chee Tsay, Steve Platnick, Didier Tanré, Lorraine Remer	smoke and radiation from biomass burning in the Savannah; marine stratocumulus off Nambian desert; surface BRDF
Gulf of Mexico	MAS, HIS, surface ship, M-AERI	Paul Menzel, Chris Moeller	clear-sky and cirrus clouds, including sediment outflow from river estuaries
California & Pacific Northwest	MAS, AirMISR, AVIRIS, CLS, CAR, in situ microphysics, AERONET	Yoram Kaufman, Lorraine Remer, Elaine Prins, Didier Tanré	fire detection and smoke aerosol

The MOBY (Marine Optical Buoy) positioned near Lanai, Hawaii will be used in January 1999 to investigate MAS and HIS infrared-derived sea surface temperatures, visible/near-infrared water-leaving radiances (using the recently added 0.47 μm channel on MAS), and radiometric calibration of the MAS measurements. The SST and water-leaving radiance data will aid in evaluating the results of several cloud mask spectral tests by providing accurate information on background radiance conditions. The effect of elevated water leaving radiances (caused by suspended materials or sub-aqueous bottom reflectance) on the cloud mask results will be investigated using MAS cloud mask results with MOBY water leaving radiances. MOBY data will also

help assess temporal variability of water leaving radiance. MAS visible/near infrared calibration will be assessed by combining MOBY data with model-generated atmospheric scattered radiance. Well calibrated data are important for setting meaningful cloud mask test thresholds.

An independent ground validation campaign of MODIS cloud heights will be undertaken six months after the MODIS launch (Fall 1998) through comparisons with stereo determinations of cloud heights (using the two GOES satellites over the U. S. and the University of Chicago ground all sky cameras), aircraft reports of cirrus cloud heights (from the ACARS), and lidar estimates of cirrus heights (using the University of Wisconsin lidar). These intercomparisons will be conducted in concert with a field campaign of the MAS on the ER-2 after the MODIS launch (probably at the time of the ARM overflights described above) Validation of the MODIS cloud emissivity will be attempted through comparison with the lidar determinations. Pre-launch validations will come from cloud top property determinations with MAS data from several field campaigns that will include stereo and lidar measurements as well.

Once the MODIS is in orbit and returning regular data, we envision two focused periods of ER-2 overflights, to be coordinated with the EOS AM-1 orbit, in California (the first one over marine stratocumulus clouds located over the ocean between Monterey and San Diego in July 1999, and the second over valley fog in the central valley of California in December 1999). These experiments would entail ER-2 flights from home base in California (Dryden Flight Research Center), and would consist, once again, of the MAS and CLS, together with coordinated underflights by the University of Washington CV-580 with its in situ microphysics probes. This data set, of special interest to Goddard Space Flight Center (Michael King, Steve Platnick, Si-Chee Tsay) would help to validate the cloud optical thickness and effective radius between MODIS and the smaller spatial resolution airborne sensors on the ER-2.

In collaboration with the MODIS Land Group as well as MISR, CERES and ASTER, we plan to conduct a 4 week experiment on biomass burning in the Savannah region of southern Africa (near the Kalahari Desert of Namibia). Biomass burning occurs in August-September, as in South America, so we plan to conduct this experiment in August-September 1999, well after the

launch of AM-1. Opportunities to study Namibian marine stratus or other cloud types may also be available. This experiment, like SCAR-B in 1995, will entail both the NASA ER-2 aircraft as well as the University of Washington CV-580. Primary instruments of interest for the ER-2 are the MAS, scanning HIS, CLS, AirMISR, SSFR, and RAMS. The latter two instruments are to characterize spectral and broadband flux of particular relevance to CERES objectives. As in Brazil (SCAR-B), we will coordinate the ER-2 with in situ aerosol and chemistry measurements on the CV-580 and overfly numerous AERONET locations in Namibia, South Africa, and Zimbabwe.

The field experiment in the Pacific Northwest is designed to measure aerosol in smoke from prescribed fires which is a fresh organic aerosol with black carbon and strong coagulation downwind. Experiments investigating dust effects (such as Sahelian outbreaks from Africa) will be planned later on, though some opportunity may present itself on transit to and from the Kalahari Desert region of southern Africa. In the Pacific Northwest we plan to observe the relationship between aerosol emission and properties of the fires that cause these emissions. In addition to the ER-2 aircraft with the MAS, AirMISR, CLS, and AVIRIS, we plan to collaborate with in situ measurements and ground-based characterization of both aerosol and water vapor properties. This validation campaign is of interest to Yoram Kaufman, Didier Tanré, Lorraine Remer, and Bo-Cai Gao, and will be useful in validating both aerosol optical and microphysical properties, total column water vapor, and fires.

Finally, the Gulf of Mexico campaign involving the ER-2 aircraft and surface ships is similar to previous campaigns conducted by Paul Menzel and Chris Moeller. Here the focus is on characterizing the MODIS-derived sea surface temperature and sediment outflow from river estuaries, and in characterizing cirrus clouds over a well characterized ocean surface. The skill of the MODIS cloud mask over very turbid (caused by suspended materials fromthe Mississippi River tributary system) coastal waters will also be assessed. The primary sensors of interest are the MAS and scanning HIS from the ER-2, and a dipping-bucket sea surface temperature instrument and M-AERI instrument from a well-coordinated surface ship (Peter Minnett and Otis Brown,

University of Miami).

Other satellite data

MODIS retrievals will be compared to those determined from in situ radiosonde measurements, the NOAA HIRS operational retrievals, the GOES sounder operational retrievals, NCEP analysis of all available data, and retrievals from the Atmospheric Infrared Sounder (AIRS) on the EOS PM-1 platform. Total ozone will be compared to Total Ozone Mapping Spectrometer (TOMS) measurements as well as the operational NOAA ozone estimates from HIRS. In addition, MODIS aerosol retrievals will be compared to POLDER and ILAS on ADEOS. ADEOS is one of several platforms that will carry the TOMS instrument in the 1998 time period.

To assure that cloud, aerosol and water vapor products are properly derived from our satellite-based data processing algorithms, it is necessary to coordinate the above-specified airborne campaigns with in situ cloud microphysics, aerosol sampling, and meteorological sampling with the satellite overpasses.

4.7.6 Implementation of Validation Results

The MODIS atmosphere algorithms for the cloud mask, cloud properties, aerosol properties, precipitable water, and atmospheric profiles will evolve in the first year after MODIS is launched in accordance with seasonal changes and validation results. Thereafter, algorithm changes will be restrained to occur once per year as needed. We anticipate assessing the performance of the MODIS algorithms initially by processing one month per season (October, January, April, July), as well as specific time periods with validation experiments of special relevance, as outlined above. After initially looking at one year's data, consistency checks, quality assurance flags, validation campaigns, as appropriate, and intercomparisons with other instruments (especially on AM-1), we will begin whole-scale reprocessing, including every month. The duration of this initial stage may be in excess of one year, during which time the MODIS calibration algorithm will likely undergo additional refinement. Continual refinement of the MODIS "operational" alg-

rithms will largely be conducted at the Team Members SCF as well as at the Team Leader Computing Facility (TLCF), as many of the algorithms are dependent on results from other algorithms (like calibration). Only periodically (after say 1.5 years following launch), the first reprocessing at the DAAC will be initiated.

5.0 References

Ackerman, S. A., 1997: Remote sensing aerosols from satellite infrared observations. *J. Geophys. Res.*, **102**, 17069-17079, 1997.

Ackerman, S. A., 1996: Global satellite observations of negative brightness temperature difference between 11 and 6.7 μm. *J. Atmos. Sci.*, **53**, 2803-2812.

Ackerman, S. A., W. L. Smith, A. D. Collard, X. L. Ma, H. E. Revercomb and R. O. Knuteson, 1995: Cirrus cloud properties derived from high-spectral resolution infrared spectrometry during FIRE II, Part II: Aircraft HIS results. *Jour. Atmos Sci.* **52**, 4246-4263.

Ackerman, S. A., W. L. Smith and H. E. Revercomb, 1990: The 27-28 October 1986 FIRE IFO cirrus case study: Spectral properties of cirrus clouds in the 8-12 micron window. *Mon. Wea. Rev.*, **118**, 2377-2388.

Ben-Dor, E., 1994: A precaution regarding cirrus cloud detection from airborne imaging spectrometer data using the 1.38 μm water vapor band. *Remote Sens. Environ.*, **50**, 346-350.

Coakley, J. A. and F. P. Bretherton, 1982: Cloud cover from high-resolution scanner data: Detecting and allowing for partially filled fields of view *J. Geophys. Res.*, **87**, 4917-4932.

Frey, R. A., S. A. Ackerman, and B. J. Soden, 1995: Climate parameters from satellite spectral measurements. Part I: Collocated AVHRR and HIRS/2 observations of the spectral greenhouse parameter. *Jour. Clim.* **9**, 327-344.

Gao, B. C., A. F. H. Goetz, and W. J. Wiscombe, 1993: Cirrus cloud detection from airborne imaging spectrometer data using the 1.38 micron water vapor band. *Geophys. Res. Lett.*, **20**, 301-304.

Gao, B. C., and A. F. H. Goetz, 1991: Cloud area determination from AVIRIS data using water vapor channels near 1 μm. *J. Geophys. Res.*, **96**, 2857-2864.

Gesell, G., 1989: An algorithm for snow and ice detection using AVHRR data: An extension to the APOLLO software package. *Int. J. Remote Sensing*, **10**, 897-905.

Hall, D. K., G. A. Riggs, and V. V. Salomonson, 1995: Development of methods for mapping

global snow cover using Moderate Resolution Imaging Spectroradiometer data. *Remote Sens. Env.*, **54,** 127-140.

Hutchison, K. D., and K. R. Hardy, 1995: Threshold functions for automated cloud analyses of global meteorological satelitte imagery. *Int. J. Remote Sens.*, **16**, 3665-3680.

Inoue, T., 1987: A cloud type classification with NOAA 7 split window measurements. *J. Geophys. Res.*, **92**, 3991-4000.

King, M. D., M. G. Strange, P. Leone and L. R. Blaine, 1986: Multiwavelength scanning radometer for airborne measurements of scattered radiation within clouds. *J. Atmos. Oceanic Technol.,* **3**, 513-522.

King, M. D., W. P. Menzel, P. S. Grant, J. S. Myers, G. T. Arnold, S. E. Platnick, L. E. Gumley, S. C. Tsay, C. C. Moeller, M. Fitzgerald, K. S. Brown and F. G. Osterwisch, 1996: Airborne scanning spectrometer for remote sensing of cloud, aerosol, water vapor and surface properties. *J. Atmos. Oceanic Technol.*, **13**, 777-794.

Kriebel, K. T., 1978: Measured spectral bidirectional reflection properties of four vegetated surfaces. *Appl. Opt.*, **17**, 253-259.

Kriebel, K. T., and R. W. Saunders, 1988: An improved method for detecting clear sky and cloudy radiances from AVHRR data. *Int. J. Remote Sens.*, **9**, 123-150.

Kriebel, K.T., R.W.Saunders, G.Gesell, 1989: Optical properties of clouds derived from fully cloudy pixels. *Contr. Phys. Atmos.*, **62**, 165-171.

Leprieur, C., Y. H. Kerr, and J. M. Pichon, 1996: Critical assessment of vegetation indices from AVHRR in a semi-arid environmnet.*Int. J. Remote Sensing*, **17**, 2549-2563.

Liou, K. N., 1973: A numerical experiment on Chandrasekhar's discrete-ordinate method for radiative transfer: Applications to cloudy and hazy atmospheres. *J. Atmos. Sci.*, **30**, 1303-1326.

Matthews, E., and W. B. Rossow, 1987: Regional and seasonal variations of surface reflectance from satellite observations at 0.6 μm. *J. Climate Appl. Meteor.*, **26**, 170-202.

McClain, E. P., 1993: Evaluation of CLAVR Phase-I algorithm performance: Final Report, U. S.

Department of Commerce/NOAA/NESDIS, Report 40-AANE-201-424.

Menzel, W. P., D. P. Wylie, and K. I. Strabala, 1993: Trends in global cirrus inferred from four years of HIRS data. *Technical Proceedings of the Seventh International TOVS Study Conference*, 10-16 February, Igls, Austria.

Minnis, P. and E. F. Harrison, 1984a: Diurnal variability of regional cloud and clear sky radiative parameters derived from GOES data. Part I: Analysis method. *J. Climate Appl. Meteor.*, **23**, 993-1011.

Minnis, P., and E. F. Harrison, 1984b: Diurnal variability of regional cloud and clear-sky radiative parameters derived from GOES data. Part III: November 1978 radiative parameters. *J. Climate Appl. Meteor.*, **23**, 1032-1051.

Rizzi, C. Serio, G. Kelly, V. Tramutoli, A. McNally and V. Cuomo 1994: Cloud clearing of infrared sounder radiances. *J. Appl. Meteor.*, **33**, 179-194.

Pinty, B., and Verstraete, M. M., 1992: GEMI: A non-linear index to monitor global vegetation from satelites. *Vegetation*, **101**, 15-20.

Penaloza, M. A., R. M. Welch, 1996: Feature selection for classification of polar regions using a fuzzy expert system. *Remote Sens. Environ.*, **58**, 81-100.

Prabhakara, C., J.-M., Yoo, D. P. Kratz, and G. Dalu, 1993: Boundary layer stratus clouds: inferred from satellite infrared spectral measurements over oceans. *J. Quant. Spectrosc. Radiat. Transfer*, **49,** 559-607.

Rossow, W. B., 1989: Measuring cloud properties from space. A review. *J. Climate*, **2**, 201-213.

Rossow, W. B., and L. C. Garder, 1993: Cloud detection using satellite measurements of infrared and visible radiances for ISCCP. *J. Climate*, **6**, 2341-2369.

Rossow, W. B., L. C. Garder and A. A. Lacis, 1989: Global, seasonal cloud variations from satellite radiance measurements. Part I: Sensitivity of analysis.*J. Climate*, **2**, 419–458.

Rossow, W. B., A. W. Walker, and L. C. Garder, 1993: Comparison of ISCCP and other cloud amounts. *J. Climate*, **6**, 2394-2418.

Saunders, R. W. and K. T. Kriebel, 1988: An improved method for detecting clear sky and cloudy radiances from AVHRR data. *Int. J. Remote Sens.*, **9**, 123-150.

Sèze, G., and W. B. Rossow, 1991a: Time-cumulated visible and infrared radiance histograms used as descriptors of surface and cloud variations. *Int. J. Remote Sens.*, **12**, 877-920.

Sèze, G., and W. B. Rossow, 1991b: Effects of satellite data resolution on measuring the space-time variations of surfaces and clouds. *Int. J. Remote Sens.*, **12**, 921-952.

Simpson, J. J., 1992: Image masking using polygon fill and morphological operations.*Remote Sens. Environ.*, **40**, 161-183.

Simpson, J. J., and R. H. Keller, 1995: An improved fuzzy logic segmentation of sea ice, clouds, and ocean in remotely sensed arctic imagery. *Remote Sens. Environ.*, **54**, 290-312.

Smith, W. L, 1968: An improved method for calculating tropospheric temperature and moisture profiles from satellite radiometer measurements. *Mon. Wea. Rev.*, **96**, 387.

Smith, W. L. and C. M. R. Platt, 1978: Comparison of satellite-deduced cloud heights with indications from radiosonde and ground-based laser measurements. *J. Appl. Meteor.*, **17**, 1796-1802.

Smith, W. L., X. L. Ma, S. A. Ackerman, H. E. Revercomb, and R. O. Knuteson, 1992: Remote Sensing Cloud Properties from High Spectral Resolution Infrared Observations,*J. Atmos. Sci.*, **50**, 1708-1720.

Smith. W. L., and R. Frey, 1990: On cloud altitude determinations from High Resolution Interferometer Sounder (HIS) observations. *J. Appl. Meteor.*, **29**, 658-662.

Soden, B. J. and F. P. Bretherton, 1993: Upper tropospheric relative humidity from the GOES 6.7 μm channel: Method and climatology for July 1987. *J. Geo. Res.*, **98**, 16669-16688.

Spinhirne, J. D., W. D. Hart and D. L. Hlavka, 1996: Cirrus infrared parameters and shortwave reflectance relations from observations. *J. Atmos. Sci.*, **53**, 1438- 1458.

Spinhirne, J. D., and T. Nakajima, 1994: Glory of clouds in the near infrared. Appl. Optics, 33, 4652-4662.

Spinhirne, J. D., and W. D. Hart, 1990: Cirrus structure and radiative parameters from airborne

lidar and spectral radiometer observations,*Mon. Wea. Rev.*, **118**, 2329-2343.

Spinhirne, J. D., R. Boers and W. D. Hart, 1989: Cloud top liquid water from lidar observations of marine stratocumulus. *J. Appl. Meteor.*, **28**, 81–90.

Stamnes, K., and R. A. Swanson, 1981: A new look at the discrete ordinate method for radiative transfer calculations in anisotropically scattering atmospheres. *J. Atmos. Sci.*, **38**, 387-399.

Stearns, C. R., L. M. Keller, G. A. Weidner and M. Sievers, 1993: Monthly mean climatic data for Antarctic automatic weather stations. *Antarctic Met. and Climat.*, **61** 1-21.

Stowe, L. L., E. P. McClain, R. Carey, P. Pellegrino, G. Gutman, P. Davis, C. Long, and S. Hart, 1991: Global distribution of cloud cover derived from NOAA/AVHRR operational satellite data. *Adv. Space Res.*, **11**, 51-54.

Stowe, L. L., S. K. Vemury, and A. V. Rao, 1994: AVHRR clear sky radiation data sets at NOAA/NESDIS. *Adv. Space Res.*, **14**, 113-116.

Stowe, L. L., P. Davis, and E. P. McClain, 1995: Evaluating the CLAVR (Clouds from AVHRR) Phase I cloud cover experimental product. *Adv. in Space Res.*, **16**, 21-24.

Strabala, K. I., S. A. Ackerman, and W. P. Menzel, 1994: Cloud properties inferred from 8-12 μm data. *J. Appl. Meteor.*, **33**, 212-229.

Suttles, J. T., R. N. Green, P. Minnis, G. L. Smith, W. F. Staylor, B.A. Wielicki, I. J. Walker, D. F. Young, V. R. Taylor, and L. L. Stowe, 1988: Angular radiation models for Earth-atmosphere system: Volume I - Shortwave radiation. NASA RP 1184, 144 pp.

Tarpley, J. D., 1979: Estimating incident solar radiation at the surface from geostationary satellite data. *J. Appl. Meteor.*, **18**, 1172-1181.

Tsonis, A. A., 1984: On the separability of various classes from GOES visible and infrared data*J. Clim. Appl. Meteor.*, **23** 1393-1410.

Vane, G., R. O. Green, T. G. Chrien, H. T. Enmark, E. G. Hansen, and W. M. Porter, 1993: The Airborne Visible/Infrared Imaging Spectrometer (AVIRIS). *Remote Sens. Environ.*, **44**, 127–143.

Wielicki, B. A, J. T. Suttles, A. J. Heymsfield, R. W. Welch, J. D. Spinhirne, M. L. Wu, D. O'C

Starr, L. Parker, and R. F. Arduini, 1990: The 27-28 October 1986 FIRE cirrus case study: Comparison of radiative transfer theory with observations by satellite and aircraft. *Mon. Wea. Rev.* **118**, 2356-2376.

Wu, X., J. J. Bates and S. Singh khalsa, 1993: A climatology of the water vapor band brightness temperatures for NOAA operational satellites. *J. Climate*, **7**, 1282-1300.

Wylie, D. P., and W. P. Menzel, 1989: Two years of cloud cover statistics using VAS. *J. Climate Appl. Meteor.*, **2**, 380-392.

Wylie, D. P., W. P. Menzel, H. M. Woolf, and K. I. Strabala, 1994: Four years of global cirrus cloud statistics using HIRS. *J. Climate*, **7**, 1972-1986.

Yamanouchi, T., K. Suzuki, and S. Kawaguci, 1987: Detection of clouds in Antarctica from infrared multispectral data of AVHRR. *J. Meteor. Soc. Japan*, **65**, 949-962.

Appendix A. Example Code for reading Cloud Mask Output

This is an example FORTRAN program to read the MODIS cloud mask The code picks out the first byte of data from the six byte product, and returns -1 in the CldMsk data array (one scan cube) if the product is not defined at a certain pixel, a 1 if it is clear and a 0 if cloudy This particuliar version just passes a binary (0 or 1) value for cloud or clear, where clear is defined by this user to be anything greater than 66% probability of clear It also returns the value of the land sea flag from the 2 bit product in the cloud mask product (0-3) to the LandSea_Flag variable This is a good example of how a user can design what they extract out of the cloud mask file based upon their needs. It also includes the appropriate MAPI and SDP toolkit calls used in Version 1.

========== Begin Example Cloud Mask Reader ==========

```
      SUBROUTINE Read_CldMsk(Modfil,Scan_No,
     &                 Dim1_CM,Dim1_QA,Dim2,Dim3,
     &                 DS_Dim1_CM,DS_Dim1_QA,DS_Dim2,DS_Dim3,
     &                 CM,QA,Error_Flag)


C-------------------------------------------------------------------
C !F77
C
C !DESCRIPTION:
C
C  Read_CldMsk retrieves one scan of MODIS Cloud Mask and Cloud Mask
C  QA data from the MOD35 HDF product file.  It is assumed that the
C  spatial dimensions (number of frames and lines) of the HDF Cloud
C  Mask and QA SDSs are equal (See Design Notes below).
C
C !INPUT PARAMETERS:
```

```
C  INTEGER  Modfil     M-API file handle structure for HDF files
C
C  INTEGER  Scan_No     1-based instrument scan number
C
C  INTEGER  Dim1_CM     Size of dimension 1 of Cloud Mask buffer as
C                      dimensioned in calling program
C
C  INTEGER  Dim1_QA     Size of dimension 1 of Cloud Mask QA buffer
C                      as dimensioned in calling program
C
C  INTEGER  Dim2/Dim3   Size of dimensions 2 and 3 of Cloud Mask and
C                      Cloud Mask QA buffers as dimensioned in the
C                      calling program.
C
C !OUTPUT PARAMETERS:
C  BYTE     CM         Three dimensional (3-D) array for passing
C                      cloud mask data.  Index 1 is byte number,
C                      index 2 is (1-km) frame number, and index 3 is
C                      relative (1-km) line number within scan.
C
C  BYTE     QA         Three dimensional (3-D) array for passing cloud
C                      mask quality assurance data.  Index 1 is QA byte
C                      number, index 2 is (1-km) frame number, and
C                      index 3 is relative (1-km) line number within
C                      scan.
C
C  INTEGER  DS_Dim1_CM  Size of retrieved Cloud Mask data block along
```

```
C               dimension 1 of output buffer.  It is as large
C               as the byte dimension of the HDF Cloud Mask
C               SDS
C
C  INTEGER  DS_Dim1_QA  Size of retrieved Cloud Mask QA data block
C               along dimension 1 of output buffer.  It is
C               as large as the byte dimension of the HDF Cloud
C               Mask SDS
C
C  INTEGER  DS_Dim2     Size of retrieved Cloud Mask and QA data
C               blocks along dimension 2 of output buffers.
C               It is as large as the frame (across track)
C               dimension of the HDF Cloud Mask and QA SDS
C               data arrays, which are assumed equal.
C
C  INTEGER  DS_Dim3     Size of retrieved Cloud Mask and QA data
C               blocks along dimension 3 of output buffers.
C               It is equal to 10, the number of 1-km
C               detector lines in a MODIS instrument scan.
C
C  LOGICAL  Error_Flag  variable that is set to .TRUE. if an error is
C               detected. It is set to .FALSE. if no errors
C               are identified.
C
C !REVISION HISTORY:
C  $Log$
C !TEAM-UNIQUE HEADER:
```

```
C
C   This software is developed by the MODIS Science Data Support
C   Team for the National Aeronautics and Space Administration,
C   Goddard Space Flight Center, under contract NAS5-32373.
C
C !REFERENCES AND CREDITS
C
C   Written by Vicky Lin        May 1997
C   Research and Data systems Corporation
C   SAIC/GSC MODIS Science Data Support Office
C   7501 Forbes Blvd, Seabrook MD 20706
C
C   vlin@ltpmail.gsfc.nasa.gov
C
C !DESIGN NOTES:
C
C   Subroutine Read_CldMsk checks the return status of all internal
C   function calls.  If any call returns a fail indicator, Read_CldMsk
C   reports an error message to the LogStatus file, and sets the output
C   argument Error_Flag to .TRUE..  Additional checks on Scan_No
C   and comparision of the dimension sizes of the 'Cloud_Mask' and
C   'Quality_Assurance' arrays are made.  If incompatibilities are
C   found, Error_Flag = .TRUE. will be returned
C
C   If all function calls are successful and no other discrepancies
C   in the input parameters and dimensions size are found,
C   Read_CldMsk runs to completion and returns Error_Flag = .FALSE..
```

```
C
C
C Externals:
C  Function:
C    GMAR                (libmapi.a)
C    GMARDM              (libmapi.a)
C
C  Named Constant:
C    P_SDID, P_ACCESS    (mapic.inc)
C    DFACC_READ          (hdf.inc: included in "mapic.inc")
C    MAPIOK              (mapi.inc: included in "mapic.inc")
C    MODIS_W_GENERIC     (MODIS_39500.f)
C
C Internals:
C  Variables:
C    arrnam      SDS array name
C    grpnm       SDS group name
C    Edge(3)     Array specifying the number of data value to read.
C    Start(3)    Array specifying the starting location of data.
C    Max_QA_Bytes Maximum number of Cloud Mask QA bytes
C    Max_Frames  Maximum number of frames per scan line.
C    Max_Lines   Maximum number of 1-km lines per scan cube.
C    Rank        Number of dimensions in an array
C    MaxScan_No  Total Swath Number
C    count       A temporary buffer for data of the target array.
C    LinesPerScan Number of lines per scan cube
C    fbyte       Byte location of 1st nonblank character of the input
```

```
C               string.
C   lbyte       Byte location of the last nonblank character of the
C               input string.
C
C   Subroutines:
C    MODIS_SMF_SETDYNAMICMSG
C    STRING_LOC
C
C !END
C--------------------------------------------------------------------------

    IMPLICIT NONE

    INCLUDE 'mapic.inc'
    INCLUDE 'PGS_MODIS_39500.f'

C Function argument declarations
    INTEGER Modfil(*),Scan_No, Dim1_CM, Dim1_QA, Dim2, Dim3,
   *       DS_Dim1_CM, DS_Dim1_QA, DS_Dim2, DS_Dim3

    BYTE    CM(Dim1_CM,Dim2,Dim3), QA(Dim1_QA,Dim2,Dim3)

    LOGICAL Error_Flag

C Local variable declarations
    CHARACTER*4  msg4
    CHARACTER*13 data_type
```

```
      CHARACTER*25 msg25
      CHARACTER*80 arrnm, grpnm
      CHARACTER*255 msgbuf

      CHARACTER*(*) NAME_CM_SDS, NAME_QA_SDS
      PARAMETER ( NAME_CM_SDS='Cloud_Mask',
     *          NAME_QA_SDS='Quality_Assurance' )

      INTEGER LinesPerScan, Max_Frames, Max_Lines, Max_QA_Bytes
      PARAMETER (LinesPerScan=10, Max_QA_Bytes=10, Max_Frames=1500,
     *          Max_Lines=10)

      BYTE count(Max_Frames*Max_Lines*Max_QA_Bytes)

      INTEGER Dim_Size_CM(3), Dim_Size_QA(3), Edge(3), fbyte, i,
     *       indx, j, k, lbyte, MaxScan_No, Rank, rtn, Start(3)
      INTEGER STRING_LOC


C Initialization
      Error_Flag = .FALSE.
      grpnm = ' '
      Rank = 3


C Check for valid file and access mode
      IF (Modfil(P_SDID).le.0 .or. Modfil(P_ACCESS).ne.DFACC_READ) THEN
```

```
      CALL MODIS_SMF_SETDYNAMICMSG(MODIS_E_GENERIC,
     *  'Invalid SD_ID or file access type','Read_CldMsk')
      Error_Flag = .TRUE.
      RETURN
     End If


C Retrieve dimensions of SDS array "Cloud_Mask"
     arrnm = NAME_CM_SDS

     rtn = GMARDM(Modfil, arrnm, grpnm, data_type, Rank, Dim_Size_CM)

     IF (rtn .NE. MAPIOK) then
      CALL MODIS_SMF_SETDYNAMICMSG(MODIS_E_GENERIC,
     *  'GMARDM failed during access to Cloud_Mask array',
     *  'Read_CldMsk')
      Error_Flag = .TRUE.
     ENDIF


C Retrieve dimensions of SDS array "Quality_Assurance"
     arrnm = NAME_QA_SDS

     rtn = GMARDM(Modfil, arrnm, grpnm, data_type, Rank, Dim_Size_QA)

     IF (rtn .NE. MAPIOK) THEN
```

```
      CALL MODIS_SMF_SETDYNAMICMSG(MODIS_E_GENERIC,
     *     'GMARDM for Quality_Assurance failed','Read_CldMsk')
      Error_Flag = .TRUE.
     ENDIF

     If (Error_Flag) Return


     DS_Dim1_CM = Dim_Size_CM(3)
     DS_Dim1_QA = Dim_Size_QA(1)
     DS_Dim2 = Dim_Size_CM(1)
     DS_Dim3 = LinesPerScan

C Compare line and frame dimension sizes of "Quality_Assurance"
C and "Cloud_Mask" arrays.  First compare frames, then lines.

     IF (Dim_Size_CM(1) .NE. Dim_Size_QA(2)) THEN
      WRITE(msg25, '(2(2x, I6))') Dim_Size_CM(1), Dim_Size_QA(2)
      rtn = STRING_LOC(msg25,fbyte,lbyte)
      msgbuf = 'Cloud_Mask and Quality_Assurance ' //
     *         'frame dimension sizes do not match: '
     *         // msg25(fbyte:lbyte)
      CALL MODIS_SMF_SETDYNAMICMSG(MODIS_E_GENERIC,msgbuf,
     *     'Read_CldMsk')
      Error_Flag = .TRUE.
     End If
```

```
      IF ( Dim_Size_CM(2) .NE. Dim_Size_QA(3) ) THEN
        WRITE(msg25, '(2(2x, I6))') Dim_Size_CM(2), Dim_Size_QA(3)
        rtn = STRING_LOC(msg25,fbyte,lbyte)
        msgbuf = 'Cloud_Mask and Quality_Assurance ' //
     *          'line dimension sizes do not match: '
     *          // msg25(fbyte:lbyte)
        CALL MODIS_SMF_SETDYNAMICMSG(MODIS_E_GENERIC,msgbuf,
     *       'Read_CldMsk')
        Error_Flag = .TRUE.
      End If

      IF (Error_Flag) Return


C Check for valid input value for variable "Scan_No"
      MaxScan_No=Dim_Size_CM(2)/LinesPerScan

      IF (Scan_No .LT. 1 .OR. Scan_No .GT. MaxScan_No) THEN
        WRITE(msg4,'(i4)') MaxScan_No
        WRITE(msg25,'(i15)') Scan_No
        rtn = STRING_LOC(msg25,fbyte,lbyte)
        msgbuf = 'Scan_No out of bounds.  It should be in range 1 -'
     *          // msg4 // CHAR(10) // 'Scan_No = '
     *          // msg25(fbyte:lbyte)

        CALL MODIS_SMF_SETDYNAMICMSG(MODIS_E_GENERIC,msgbuf,
```

```
*       'Read_CldMsk')
        Error_Flag = .TRUE.
      ENDIF


C Check for adequate output buffer size to store a scan of
C Cloud_Mask data.

      IF ( Dim1_CM .LT. Dim_Size_CM(3)) THEN
        WRITE(msg25, '(i15)') Dim1_CM
        rtn = STRING_LOC(msg25,fbyte,lbyte)
        msgbuf = '1st dimension of output buffer too small' //
*           ' to hold Cloud_Mask array'
*       // CHAR(10) // 'Dim1_CM = ' // msg25(fbyte:lbyte)
        CALL MODIS_SMF_SETDYNAMICMSG(MODIS_E_GENERIC,msgbuf,
*       'Read_CldMsk')
        Error_Flag = .TRUE.
      END IF

      IF (Dim2 .LT. Dim_Size_CM(1)) THEN
        WRITE(msg25,'(i15)') Dim2
        rtn = STRING_LOC(msg25,fbyte,lbyte)
        msgbuf = '2nd dimension of output buffer too small' //
*           ' to hold Cloud_Mask array'
*       // CHAR(10) // 'Dim2 = ' // msg25(fbyte:lbyte)
        CALL MODIS_SMF_SETDYNAMICMSG(MODIS_E_GENERIC,msgbuf,
```

```
*       'Read_CldMsk')
        Error_Flag = .TRUE.
      END IF

      IF (Dim3 .LT. LinesPerScan) THEN
        WRITE(msg25,'(i15)') Dim3
        rtn = STRING_LOC(msg25,fbyte,lbyte)
        msgbuf = '3rd dimension of output buffer too small' //
*           ' to hold Cloud_Mask array'
*     // CHAR(10) // 'Dim3 = ' // msg25(fbyte:lbyte)
        CALL MODIS_SMF_SETDYNAMICMSG(MODIS_E_GENERIC,msgbuf,
*       'Read_CldMsk')
        Error_Flag = .TRUE.
      END IF

      IF (Error_Flag) RETURN



C Retrieve SDS "Cloud_Mask" data
      arrnm = NAME_CM_SDS
      Start(1) = 0
      Start(2) = (Scan_No-1)*LinesPerScan
      Start(3) = 0
      Edge(1) = Dim_Size_CM(1)
      Edge(2) = LinesPerScan
      Edge(3) = Dim_Size_CM(3)
```

```
      rtn = GMAR(Modfil, arrnm, grpnm, Start, Edge, count)


      IF (rtn .NE. MAPIOK) THEN
        write(msg25,'(3(2x,I6))') Start
        rtn = STRING_LOC(msg25,fbyte,lbyte)
        msgbuf = 'GMAR failed during access to Cloud_Mask array'
*           // CHAR(10) // 'Read Dimension Offsets = '
*           // msg25(fbyte:lbyte)
        CALL MODIS_SMF_SETDYNAMICMSG(MODIS_E_GENERIC,msgbuf,
*   'Read_CldMsk')
        Error_Flag = .TRUE.
        RETURN
      ENDIF

C Rebuffer 3-dimension cloud mask data with byte dimension
C varying most rapidly.


      Do 30 k=1,Edge(3)
      Do 30 j=1,Edge(2)
      Do 30 i=1,Edge(1)
        indx = (k-1)*Edge(1)*Edge(2) + (j-1)*Edge(1) + i
        CM(k,i,j) = count(indx)
   30 continue
```

```
C Check for adequate output buffer size to store a scan of
C Quality_Assurance data.

      IF (Dim1_QA .LT. Dim_Size_QA(1)) THEN
        WRITE(msg25,'(i15)') Dim1_QA
        rtn = STRING_LOC(msg25,fbyte,lbyte)
        msgbuf = '1st dimension of output buffer too small' //
     *           ' to hold Quality_Assurance array'
     *     // CHAR(10) // 'Dim1_QA = ' // msg25(fbyte:lbyte)
        CALL MODIS_SMF_SETDYNAMICMSG(MODIS_E_GENERIC,msgbuf,
     *       'Read_CldMsk')
        Error_Flag = .TRUE.
      END IF

      IF (Error_Flag) RETURN


C Retrieve SDS "Quality_Assurance" data
      arrnm = NAME_QA_SDS
      Start(1) = 0
      Start(2) = 0
      Start(3) = (Scan_No-1)*LinesPerScan
      Edge(1) = Dim_Size_QA(1)
      Edge(2) = Dim_Size_QA(2)
      Edge(3) = LinesPerScan
```

```
      rtn = GMAR(Modfil, arrnm, grpnm, Start, Edge, count)

      IF (rtn .NE. MAPIOK) THEN
        write(msg25,'(3(2x,I6))') Start
        msgbuf = 'GMAR failed during access to Cloud Mask QA array'
     *          // CHAR(10) // 'Read Dimension Offsets = '
     *          // msg25
        CALL MODIS_SMF_SETDYNAMICMSG(MODIS_E_GENERIC,msgbuf,
     *  'Read_CldMsk')

        Error_Flag = .TRUE.
        RETURN
      ENDIF

C Move scan of QA data from work to output buffer.
      Do 40 k = 1, Edge(3)
      Do 40 j = 1, Edge(2)
      Do 40 i = 1, Edge(1)
        indx = (k-1)*Edge(1)*Edge(2) + (j-1)*Edge(1) + i
        QA(i,j,k) = count(indx)
   40 Continue


      RETURN
      END
================== End Example Cloud Mask Reader ====================
```

Appendix B. Acronyms

ACARS	ARINC (Aeronautical Radio Inc.) Communications, Addressing and Repoting System
AERI	Atmospheric Emitted Radiation Interferometer
AEROCE	Aerosol/Ocean Chemistry Experiment
AERONET	Aerosol Robotic Network
AirMISR	Airborne MISR
AIRS	Atmospheric Infrared Sounder
AMSU	Advanced Microwave Sounding Unit
APOLLO	AVHRR (Advanced Very High Resolution Radiometer) Processing scheme Over cLoud Land and Ocean
ARM	Atmospheric Radiation Measurement Program
ARMCAS	Arctic Radiation Measurements in Column Atmosphere-surface System (Beaufort Sea, Alaska, June 1995)
ASTEX	Atlantic Stratocumulus Transition Experiment (Azores, June 1992)
ASTER	Advanced Spaceborne Thermal Emission and Reflection adiometer
AVHRR	Advanced Very High Resolution Radiometer
AVIRIS	Airborne Visible/Infrared Imaging Spectrometer
BRDF	Bidirectional Reflectance Distribution Function
CAR	Cloud Absorption Radiometer
CART	Clouds and Radiation Testbed
CEPEX	Central Equatorial Pacific Experiment (Fiji, February-March 1993)
CERES	Clouds and the Earth's Radiant Energy System
CHAPS	Collocated HIRS/2 and AVHRR Processing Scheme
CLAVR	Cloud Advanced Very High Resolution Radiometer
CLS	Cloud Lidar System

COARE	Coupled Ocean-Atmosphere Response Experiment
DAO	Data Assimilation Office (Goddard Space Flight Center)
EOS	Earth Observing System
EOSDIS	EOS Data and Information System
FIRE	First ISCCP Regional Experiment (California, June-July 1987, Beaufort Sea, Alaska, April-June, August 1998)
FOV	Field of View
GAC	Global Area Coverage
GLAS	Geoscience Laser Altimeter System
GLI	Global Imager
GOES	Geostationary Operational Environmental Satellite
HIS	High-spectral resolution Interferometer Sounder
HIRS	High Resolution Infrared Radiation Sounder
HSB	Humidity Sounder from Brazil
ILAS	Improved Limb Atmospheric Spectrometer
ISCCP	International Satellite Cloud Climatology Project
LASE	Lidar Atmospheric Sensing Experiment
LBA	Large Scale Biosphere-Atmosphere Experiment inAmazonia
M-AERI	Marine-Atmospheric Emitted Radiation Interferometer
MAS	MODIS Airborne Simulator
MAST	Monterey Area Ship Tracks Experiment (Monterey and nearby Pacific Ocean, June 1994)
McIDAS	Man-computer Interactive Data Access System
MISR	Multi-angle Imaging Spectro-Radiometer
MOBY	Marine Optical Buoy
MODIS	Moderate Resolution Imaging Spectroradiometer
NAST	NPOESS Aircraft Sounding Testbed

NCAR	National Center for Atmospheric Research
NDSI	Normalized Difference Snow Index
NDVI	Normalized Difference Vegetation Index
NPOESS	National Polar Orbiting Environmental Satellite System
NSA	North Slope of Alaska
POLDER	Polarization and Directionality of Earth's Reflectances
RAMS	Radiation Measurement System (NASA Ames Research Center and Scripps Institution of Oceanography)
SCAR-A	Sulfate, Clouds and Radiation–Atlantic (Delmarva Peninsula and near-by Atlantic Ocean, July 1993)
SCAR-B	Smoke, Clouds and Radiation–Brazil (Brazil, August-September 1995)
SCAR-C	Smoke, Clouds and Radiation–California (Pacific Northwest, September 1994)
SCF	Science Computing Facility
SeaWiFS	Sea-viewing Wide Field-of-view Sensor
SGP	Southern Great Plains
SHEBA	Surface Heat Budget of the Arctic Ocean
SSFR	Spectral Solar Flux Radiometer (NASA Ames Research Center)
SST	Sea Surface Temperature
SUCCESS	Subsonic Aircraft Contrail and Cloud Effects Special Study(April-May 1996)
TARFOX	Tropospheric Aerosol Radiative Forcing Observational Experiment(Delmarva Peninsula and near-by Atlantic Ocean, July 1996)
TIROS	Television and Infrared Observation Satellite
TLCF	Team Leader Computing Facility
TM	Thematic Mapper
TOGA	Tropical Ocean Global Atmosphere
TOMS	Total Ozone Mapping Spectrometer
TOVS	TIROS-N Operational Vertical Sounder

WINCE	Winter Cloud Experiment
WMO	World Meteorological Organization